Enhanced Oil Recovery by Alkaline-Surfactant-Alternated-Gas/CO_2 Flooding

Thesis submitted in partial fulfillment of the

requirements for the degree of

DOCTOR OF PHILOSOPHY

by

RANJAN PHUKAN

Department of Chemical Engineering

Indian Institute of Technology Guwahati

Guwahati – 781039

Assam, India

May 2020

Enhanced Oil Recovery by Alkaline-Surfactant-Alternated-Gas/CO_2 Flooding

Thesis submitted in partial fulfillment of the

requirements for the degree of

DOCTOR OF PHILOSOPHY

by

Ranjan Phukan

Department of Chemical Engineering

Indian Institute of Technology Guwahati

Guwahati – 781039

Assam, India

May 2020

Enhanced Oil Recovery by Alkaline-Surfactant-Alternated-Gas/CO_2 Flooding

Ranjan Phukan

DEPARTMENT OF CHEMICAL ENGINEERING
INDIAN INSTITUTE OF TECHNOLOGY GUWAHATI

STATEMENT

I do hereby declare that the contents embodied in this thesis entitled "**Enhanced Oil Recovery by Alkaline-Surfactant-Alternated-Gas/CO_2 Flooding**" are the results of the investigations carried out by me at Department of Chemical Engineering, Indian Institute of Technology, Guwahati, India, and Department of Petroleum Technology, Dibrugarh University, India under the guidance of Dr. Pankaj Tiwari and Dr. Subrata Borgohain Gogoi. In keeping with the general practice of reporting scientific observations, due acknowledgements have been made wherever the work described was based on the findings of other investigators.

Date: May 2020 Ranjan Phukan

DEPARTMENT OF CHEMICAL ENGINEERING

INDIAN INSTITUTE OF TECHNOLOGY GUWAHATI

CERTIFICATE

This is to certify that the thesis entitled "**Enhanced Oil Recovery by Alkaline-Surfactant-Alternated-Gas/CO_2 Flooding**" submitted by **Mr. Ranjan Phukan (Roll No.: 126107015)** for the award of the degree of Doctor of Philosophy has been carried out under our supervision and guidance. The work documented in this thesis has not been submitted to any other University or Institute for the award of any degree.

(**Dr. Pankaj Tiwari**)
Associate Professor
Department of Chemical Engineering
Indian Institute of Technology, Guwahati
Guwahati – 781039, India

(**Dr. Subrata Borgohain Gogoi**)
Professor
Department of Petroleum Technology
Dibrugarh University
Dibrugarh – 786004, India

Dedicated to

My Parents, Family, & Supervisors.

Acknowledgements

I would like to express my deep sense of gratitude to everyone who directly or indirectly helped me in different ways in completing this research work. Foremost, I would like to express my gratitude to my supervisors, **Dr. Pankaj Tiwari** and **Dr. Subrata Borgohain Gogoi** for giving me continuous guidance and encouragement during the course of this work. I am indebted to both of them for their constant inspiration and useful suggestions throughout the entire period.

I am grateful to **Dr. Pankaj Tiwari** for his invaluable support, continuous motivation, and insightful discussions throughout this research. I appreciate his critical comments while performing the experiments, analyzing the experimental data and writing the thesis. His uncompromised approach to complete the experiments, data analysis, writing manuscripts as well as thesis within a fixed time immensely helped me in completing the works in time. He guided me to write and improve the quality of manuscripts for journals as well as the thesis. It has been a great experience working with him.

I would like to express my profound gratitude to **Dr. Subrata Borgohain Gogoi** for providing me motivation and valuable guidance during this research work. She has been my source of inspiration and supporter throughout my research work. Her supervision, useful suggestions, and invaluable contribution enabled me to complete my work successfully. I have been greatly benefited by the useful advice given by her from time to time with regard to writing manuscript and thesis. Her knowledge and enthusiasm have provided an invaluable contribution to this research.

I must also thank my doctoral committee members **Dr. Ramgopal V. S. Uppaluri**, **Dr. Pallab Ghosh,** Department of Chemical Engineering, **Dr. Lalit Mohan Pandey**,

Biosciences and Bioengineering, Department for their valuable suggestions and contributions towards my research work.

I must also thank the faculty members of the Department of Chemical Engineering for their kind cooperation during my stay in the department. I am also thankful to all the staff members and scientific officers of the Chemical Engineering Department for their genuine help during my entire research period. I am thankful to all faculty and staff members of the Department of Petroleum Technology, Dibrugarh University for their kind help and cooperation during the course of my research work.

I also extend my special thanks to my mates Dr. Rahul Saha, Mr. Bhargava Baruah, Dr. Pallab Das, Dr. Bhaskarjyoti Medhi, Mr. Pankaj Baruah, and Mr. Sombir Pannu for their cooperation and assistance in my research work.

Last but not least, I would like to express my deep sense of gratitude to parents and family members. Their constant inspiration, care, and love kept me focused and motivated. I appreciate the courage, understanding and dedicated support shown by all of them despite many testing times at their end.

Abstract

CO_2-water alternating gas (CO_2-WAG) injection is the most widely used technique for controlling the mobility and conformance control issues of CO_2 flooding. To achieve better performance through the synergic combination of gas and chemicals, the WAG process was modified by injecting chemical solutions (instead of just water) alternately with gas. The technique is called alkaline-surfactant-alternated-gas/CO_2 (ASAG) flooding when gas and alkali-surfactant slugs are alternately injected into the reservoir. The ASAG flooding is a relatively new technique and limited experimental works have been reported. In the present work, the potential of the ASAG flooding for enhanced oil recovery (EOR) was investigated by lab-scale core flooding experiments, using reservoir cores and crude oil of an oil field of Upper Assam Basin, India. Additionally, to design the ASAG process rationally, the key parameters that affect the oil recovery performance were studied and fine-tuned for optimal performance.

Characterization of reservoir rock and fluids is necessary to make a preliminary assessment of the effectiveness of any EOR process. Therefore, initial work focused on the analysis of reservoir rock, crude oil and formation water of the oilfield based on which application of ASAG flooding was judged. Routine core analysis was conducted for the measurement of porosities & permeabilities of the core plugs. The porosities of the core plugs were related to the depth of the formation from where the cores were obtained. Moreover, more porous core plugs were found to be more permeable. Further characterization of the rock was done to evaluate its mineralogy and clay content through X-ray diffraction (XRD) and field emission scanning electron microscope (FESEM) studies. The experimental results indicated the presence of quartz as the dominant mineral along with clays in the rock matrix. Additionally, the characterization of crude oil was done in detail to determine the important physicochemical properties affecting the process

of oil recovery, including API gravity, viscosity, pour point, resin and asphaltene content, wax content, and acid number. The crude oil was found to be of medium gravity, acidic nature and with enough of resin-content for asphaltene stabilization. These preliminary investigations of the crude oil properties indicated that the crude oil considered in this study was suitable for ASAG flooding. The formation water was also analyzed to determine its pH, ionic composition, and TDS. It was observed that formation water collected from the oilfield is of low salinity and contains divalent ions in small amounts.

To recover the best possible incremental oil, this work also stressed on designing optimal chemical formulations for ASAG flooding based on the foam stability, phase behavior, interfacial tension (IFT) measurement, and adsorption studies. The experimental investigations were targeted to evaluate the optimum concentrations of surfactants and alkali, and to indentify the optimal brine salinity. The objective was to design chemical slugs that will generate stable foams, achieve ultra-low oil-water IFTs and reduce surfactant loss due to adsorption onto rock surfaces. Amongst the surfactants considered in this study, sodium dodecyl sulfate (SDS) at 0.3 wt% and alpha olefin sulphonate (AOS) at 0.5 wt% provided the most stable CO_2-foam. Likewise, amongst the alkalis considered in this study, Na_2CO_3 was the preferred choice as the oil-water IFT values achieved were the minimum (0.0068 mN/m and 0.0087 mN/m respectively) with this alkali when combined with the optimum surfactant concentrations. Additionally, the optimal brine salinity was found at 70% of formation salinity (2400 ppm) which corresponded to the occurrence of maximum type III microemulsion and lowest IFT value. Further, it was evaluated that preflushing with black liquor (BL) can reduce the adsorption of surfactants by core plugs and the optimum concentration of BL for preflushing was found as its CMC value.

The current work finally addresses the potential of ASAG flooding for EOR by performing a series of lab-scale core flooding experiments on core plugs under different

operating conditions. The performance of different core flooding experiments was evaluated on the basis of oil recovery and the extent of mobility control. The mobility reduction factor (MRF) or average pressure drop was determined to ascertain the extent of mobility control during the flooding process. While ASAG flooding was of particular concern, other EOR processes such as tertiary continuous gas injection (CGI), CO_2-water alternating gas (WAG), surfactant alternated gas (SAG), and alkali-surfactant (AS) flooding have also been studied for comparative assessment purpose. It was observed that due to the synergic effect of in-situ foam generation and ultra-low IFT conditions during ASAG flooding, the oil recovery efficiency was the highest among all the EOR processes considered in the study.

The last section of the thesis was devoted to study the effect of key operational parameters on the performance of ASAG flooding. The critical parameters investigated were slug ratio, slug size, injection scheme, gas injection rate, total fluid volume injected, and tapering of slug. It was evaluated that selective mobility reduction effect could be exhibited by foam generated in the reservoir rock by ASAG injection. This was supported by the core flooding results indicating higher oil recovery due to stronger foam formation in higher porosity/permeability core plugs than in the lower porosity/permeability core plugs. Additionally, the effect of change in brine salinity during ASAG flooding was also investigated. The experimental results indicated that the application of salinity gradient during ASAG flooding resulted in better oil recovery due to the lowest oil-water IFT environment and generation of the most stable foam. The experimental investigations were also targeted to evaluate the use of a less costly natural surfactant black liquor (BL) for preflushing prior to ASAG injection. It was observed that preflushing can improve displacement efficiency by minimizing surfactant adsorption and better foam stability. The

results indicated that by combining all the favorable operating parameters, oil recovery up to 31 %OOIP could be obtained by the immiscible ASAG flooding.

Thus, the present work highlighted that the synergic combination of alkali, surfactant, and CO_2 gas injection in the form of ASAG flooding has the potential to improve oil recovery in sandstone oil reservoirs producing medium gravity crude oil. The laboratory approach adopted for designing the optimal chemical slug may help screening chemicals suitable for candidate oilfields. Additionally, the key operational parameters influencing the ASAG flooding process efficiency are defined and optimum conditions are determined for assisting successful implementation at pilot and field scale.

Table of Contents

List of Tables

Chapter 2

Chapter 3

Chapter 4

Chapter 5

Chapter 6

Appendix

List of Figures

Chapter 1

Chapter 2

Chapter 3

Chapter 4

Chapter 5

Chapter 6

Acronyms and Nomenclature

ϕ	Porosity, %
μ	Viscosity, cP
AN	Acid number, mg KOH/g
AOS	Apha olefin sulphonate
API	American petroleum institute
AS	Alkaline surfactant
ASAG	Alkaline-surfactant-alternated-gas/CO_2
ASP	Alkaline surfactant polymer
ASTM	American society for testing and materials
B	Temkin constant
BL	Black liquor
BV	Bulk volume
CAG	Chemical alternated gas
C_e	Equilibrium concentrations of surfactants, mg/l
CGI	Continuous gas injection
CMC	Critical micelle concentration
C_o	Initial concentrations of surfactants, mg/l
E_{do}	Microscopic displacement efficiency
EOR	Enhanced oil recovery
E_{ro}	Oil recovery efficiency
E_{vo}	Volumetric sweep efficiency
EWF	Extended water flooding
FESEM	Field emission scanning electron microscope
FTIR	Fourier transform infra-red spectrometry
FW	Formation water

GAC	Gas alternated chemical
GV	Grain volume
IFT	Interfacial tension
K	Permeability
K_{abs}	Absolute permeability, md
K_e	Effective permeability, md
K_H	Linear isothermal model constant
K_L	Langmuir constant
K_T	Temkin constant
M	Mobility ratio
MFC	Mass flow controller
MMP	Minimum miscibility pressure
MRF	Mobility reduction factor
N_{cap}	Capillary number
n	Freundlich constant
OOIP	Original oil in place
PV	Pore volume
q	Flow rate, ml/min
q_e	Adsorption at equilibrium time (µg/g)
q_{max}	Langmuir adsorption capacity (µg/g)
R/A	Resin/asphaltene
R_L	Non-dimensional Langmuir constant
R^2	Regression coefficient
ROIP	Residual oil in place
SAG	Surfactant alternating gas
SDBS	Sodium dodecyl benzene sulfonate

SDS	Sodium dodecyl sulfate
SFB	Synthetic formation brine
SMR	Selective mobility reduction
S_{oi}	Initial oil saturation
S_{or}	Residual oil saturation
S_{wc}	Connate water saturation
$t_{1/2}$	Half-decay time
TDS	Total dissolved solids
TX-100	Triton X-100
V_{foam}	Volume of foam, ml
WAG	Water alternating gas
WF	Water flooding
XRD	X-ray diffraction
γ	Kinematic viscosity, cSt
ΔP	Pressure drop, psi
$\Delta\rho$	Density difference between the oleic and aqueous phases, g/cm^3
λ	Interfacial tension, mN/m
ω	Angular velocity, rad/s

CHAPTER 1

Introduction and Literature Review

Enhanced oil recovery

CO_2 flooding

Different forms of WAG injection

ASAG flooding

Objectives

Thesis organization

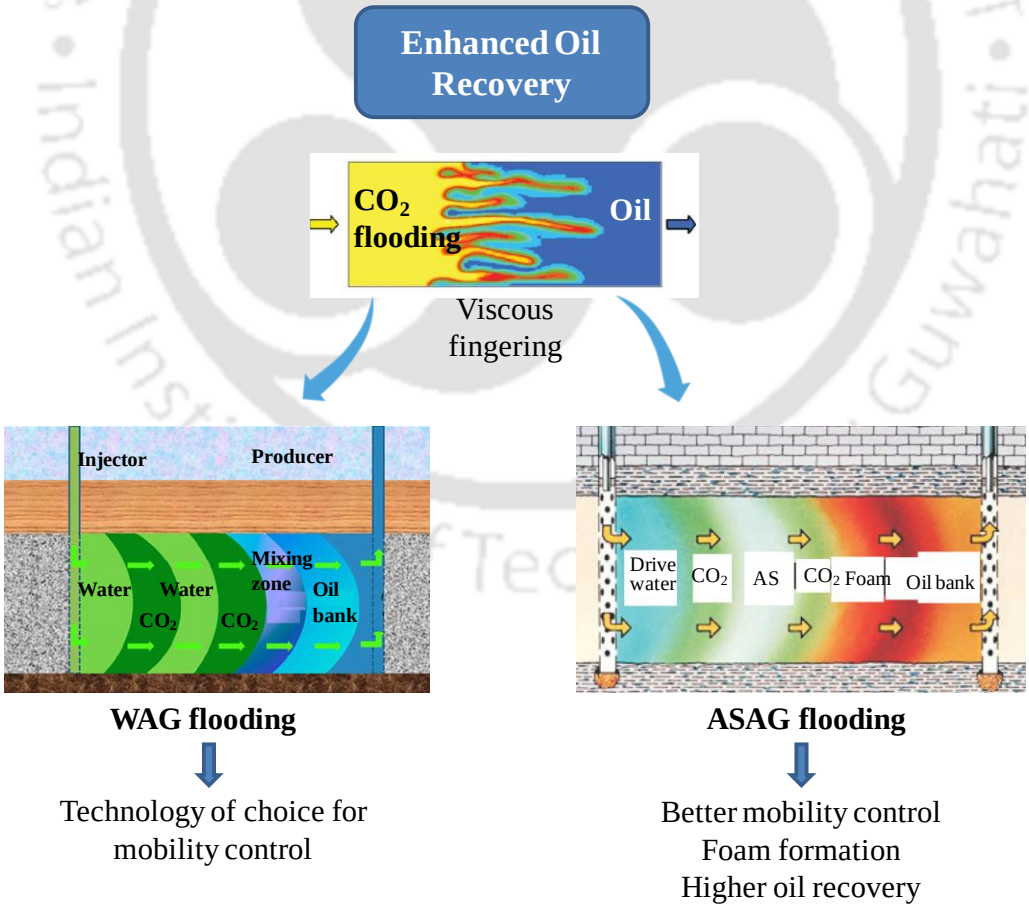

Chapter 1

Introduction and Literature Review

This chapter presents a brief summary of the gas injection-based enhanced oil recovery (EOR) methods and with special reference to CO_2 flooding. The problems associated with CO_2 flooding and the techniques employed to overcome the CO_2 mobility and conformance control issues have been discussed briefly. It describes the water-alternating-gas (WAG) and alkaline-surfactant-alternated-gas/CO_2 (ASAG) flooding processes. It also presents the literature review on the methods related to ASAG flooding. The importance and objectives of the present work are also highlighted. Finally, the organization of the thesis has been presented.

1.1 Introduction

Energy is an essential element in our everyday life and a prerequisite for economic development. The main source of energy comes from fossil fuels. As per the report of ExxonMobil 2017, oil would continue to remain as the world's most consumed energy source [1]. With population and economic growth, the demand for oil is rising steeply and will continue to do so in the future. The global crude oil demand has already crossed the symbolic figure of 100 million barrels per day (mbd) and is expected to rise to about 110 mbd by in the mid-2030s [2, 3]. According to the International Energy Agency (IEA, 2018), the total oil production worldwide in 2018 was averaged 80 mbd. Thus, the global oil supply lag demand and the gap is expected to further widen after 2020 unless new projects are implemented. Moreover, there has been an appreciable decline in hydrocarbon reservoirs discovery in the past few decades [4]. So, in order to meet the increasing crude

oil demand focused efforts are required to recover remaining oil from known reservoirs. In this regard, enhanced oil recovery (EOR) methods are becoming increasingly important as a means of maximizing the recovery of oil in place.

Basically, the recovery of crude oil starts with the primary recovery which uses the natural energy of the reservoir to produce about 5 -10 % original oil in place (OOIP). As the reservoir pressure depletes, water and/or natural gas are injected to boost the reservoir pressure and displace the oil during the secondary recovery. Producing this way, an additional 15 to 20 %OOIP can be recovered. The average recovery factor after the conventional primary and secondary recovery methods is reported to be around 35% OOIP [5-8]. Thus, a significant portion of the oil is left behind in the reservoir and is still waiting for extraction when conventional methods become uneconomical. This residual oil is the target of the EOR methods [9]. Depending on the type of fluid injected and injection schemes adopted, the EOR methods may be thermal process, chemical flooding, gas injection, microbial methods or their combinations.

Thermal EOR methods involve adding heat to the reservoir to recover the oil by reducing the oil viscosity. This EOR method is most suitable for heavy oil reservoirs and includes: (a) Steam drive which involves continuous injection of steam through injection wells, driving the oil towards the producing wells; (b) Huff 'n' Puff, which involves alternate steam injection and oil production from the same well; (c) In-situ combustion, which involves partial combustion of oil in place to reduce the oil viscosity and sometimes followed by the injection of water to recover the heat from the rock behind the front.

Chemical methods are based on the injection of water containing chemical additives. This category includes: (a) Polymer flooding where polymers are added to water to increase water viscosity and to reduce mobility ratio; (b) Surfactant flooding where surfactant solutions are injected to mobilize the residual oil through reduction of the

interfacial tension (IFT) between oil and water; (c) Alkaline flooding where alkaline solutions are injected to enhance the recovery factor through several mechanisms such as IFT reduction, emulsification, and wettability alteration. However, alkaline-surfactant-polymer (ASP) is considered as the most promising chemical method because it integrates the advantages of alkali, surfactant, and polymer. Due to the synergy, ASP has the ability to improve microscopic displacement as well as the volumetric sweep efficiencies during the displacement process [10].

Gas Injection is the second most widely used EOR process, only next to thermal processes. In gas injection, the displacement of oil is achieved by non-aqueous injection of hydrocarbon solvents, lean hydrocarbon gases or high-pressure non-hydrocarbon gases like CO_2, N_2 or flue gases. However, CO_2 injection is preferred over other gases because it is cheaper, has higher density, and offers environmental benefits by providing for CO_2 sequestration in the reservoir [11, 12].

Other EOR methods include the microbial-based EOR by in-situ and ex-situ methods. The in-situ MEOR utilizes microbial growth and metabolism inside the reservoir, while ex-situ scheme involves direct injection of desired active products produced by microbes on the surface [13]. Lazar et al. [14] reported oil recovery up to 50% of residual oil through the application of microbial EOR methods. The hybrid EOR methods which are combinations of two or more EOR methods are also developed to increase oil recovery, lower operational costs, and overcome challenges [15]. One of the hybrid EOR methods that is gaining popularity recently is the low salinity water flooding (LSW). LSW changes the brine salinity or ionic composition of the injected water for improving oil recovery. The mechanism of oil recovery by LSW depends on a number of factors that are related to the composition of brine injected like fine clay mineral migration, alteration of wettability, formation of emulsion, pH control, and reduction of IFT [16]. The addition of other

materials like nanoparticles, polymer, surfactant, gas in LSW has also shown promising results for EOR.

1.2 Concepts of EOR Processes

The main aim of the EOR processes is to improve the overall oil recovery efficiency (E_{ro}), which is product of the macroscopic or volumetric sweep efficiency (E_{vo}) and the microscopic displacement efficiency (E_{do}):

$$E_{ro} = E_{vo} \times E_{do} = E_a \times E_v \times E_{do} \tag{1.1}$$

where E_a and E_v are the areal sweep efficiency and vertical invasion efficiency respectively [17]. E_a is the fraction of the total pattern area that is swept by the displacing fluid and E_v the fraction of the pay zone's vertical section that is swept by injected fluids. Both E_a and E_v are influenced by fluid mobilities, reservoir heterogeneity, and total volume of fluid injected [18]. Microscopic displacement efficiency (E_{do}) is defined as the fraction of oil displaced in the pores within the volume of the reservoir that has been flooded. It can be expressed as

$$E_{do} = \frac{S_{oi} - S_{or}}{S_{oi}} \tag{1.2}$$

where S_{oi} is the initial oil saturation, and S_{or} is the remaining oil saturation. The E_{do} depends on fluid viscosity, reservoir dip, capillary pressures, rock wettability, and IFT value. Experiences have shown that it is not possible to produce all the oil from the swept region of the reservoir due to the trapping of the oil droplets by capillary forces caused by the high IFT value between oil and water. The displacement efficiency can be increased by reducing capillary forces or IFT value as is done in miscible gas flooding and chemical flooding, or by decreasing oil viscosity as in thermal flooding or gas flooding. Both,

microscopic displacement and macroscopic sweep efficiencies are strongly dependent on the mobility ratio (M).

Mobility ratio (M) is defined as the ratio of the mobility of the displacing fluid to the mobility of the displaced fluid.

$$M = \frac{\text{Mobility of the displacing fluid}}{\text{Mobility of the displaced fluid}} = \frac{K_{rdisplacing} / \mu_{displacing}}{K_{rdisplaced} / \mu_{displaced}} \quad (1.3)$$

where 'K_r' represents the relative permeability and 'μ' the viscosity. Both E_{do} and E_{vo} values increase as the M decreases. Thus, for efficient displacement, mobility of the displacing fluid should be less than the mobility of the displaced fluid i.e. $M < 1$ which is considered to be favorable, while $M > 1$ is unfavorable. A large viscosity difference between the displacing and displaced fluid makes the M unfavorable promoting viscous fingering to reduce oil recovery. $M < 1$ can be achieved by increasing the viscosity of displacing fluid, decreasing the μ of the displaced fluid, and by improving the K_r of the displaced fluid (oil).

Oil recovery efficiency is greatly influenced by the capillary forces which are responsible for trapping residual oil in the small pore spaces of the reservoir rock. A very important parameter considered in EOR is the capillary number. This is a dimensionless parameter and defined as the ratio of viscous to interfacial forces, neglecting the gravitational forces. The viscous forces help to mobilize oil, while the capillary forces cause oil retention [19].

$$N_{cap} = \frac{\text{Viscous forces}}{\text{Interfacial forces}} = \frac{\mu v}{\lambda \, Cos\theta} \quad (1.4)$$

where v is the displacing fluid pore flow velocity, μ is the viscosity of the displacing fluid, λ is the IFT between the displaced and displacing phase fluids and θ is the angle of contact.

After conventional water flooding, the value of N_{cap} is low and normally of the order of 10^{-7} to 10^{-6} due to which sufficient amount of oil is left behind in the pore spaces of the reservoir rock trapped by capillary forces [20]. Generally, three factors are responsible for the high residual oil saturation: high oil viscosity, existence of interfacial forces between oil, water and/or gas, and reservoir heterogeneities. If the N_{cap} in an EOR process is increased, the residual oil saturation can be mobilized and produced. The relationship between residual oil saturation and N_{cap} is termed as capillary desaturation curve. A large value of N_{cap} of the order of 10^{-3} is required to mobilize trapped oil and to reduce the residual oil saturation to about zero [21]. N_{cap} can be increased by increasing pressure gradient, increasing the displacing fluid viscosity or by decreasing the IFT. The most convenient way to increase the N_{cap} is to lower the IFT value. Most of the chemical and gas EOR methods are designed to lower the IFT value so that the N_{cap} can be increased for better oil recovery.

1.3 CO_2 Flooding

CO_2 flooding as an EOR method was first implemented way back in 1930, however, most of its development took place in the 1970s [11]. It is a well established EOR method and considered to be the most effective for light and medium oil reservoirs This process has the capability to extend the field's production life by 15-20 years and can recover an additional 15 to 25% of OOIP [22]. Along with oil recovery, CO_2 flooding has also been recognized as a carbon sequestration method [23, 24]. The concentrations of the primary greenhouse gases (CO_2 and methane) have substantially increased since the 1700s due to human activities [25]. These gases are currently emitted to the atmosphere more quickly than the capacity of the natural system to remove/absorb them resulting in the accumulation of these gases in the atmosphere. Global warming which is the result of such

accumulation adversely affects the ecosystem and climate. By injecting CO_2 gas into the underground reservoir for oil recovery, the sequestration of CO_2 takes place reducing the emission of the greenhouse gas. Fig. 1.1 shows the schematic representation of oil recovery by CO_2 flooding.

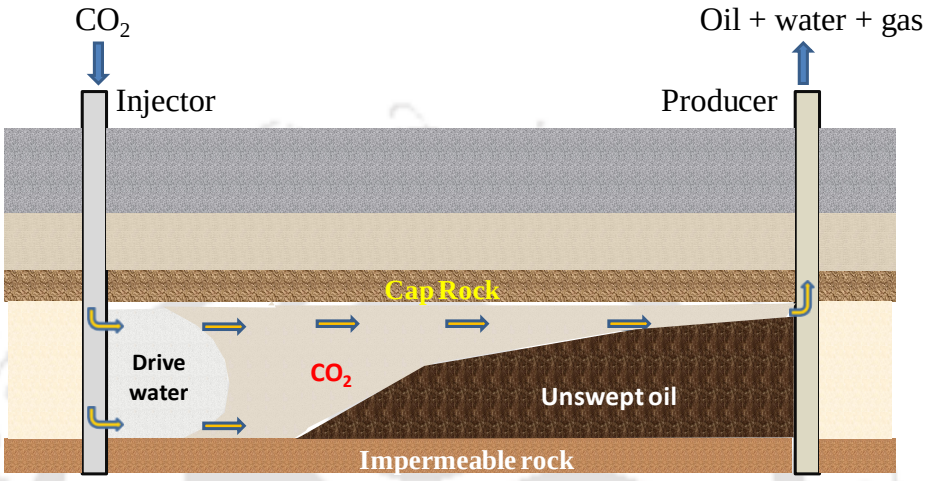

Fig. 1.1: Schematic representation of continuous CO_2 flooding showing early injection gas breakthrough [[26], modified]

Depending upon the operating pressure, the injected CO_2 can develop miscible or immiscible conditions with oil in the reservoir. However, miscible or near-miscible flooding is the preferred method due to its potential to achieve improved oil recovery. In miscible flooding, the increase in oil recovery occurs through the mobilization of lighter oil components, reduction of oil viscosity, swelling of oil, and reduction of IFT [27, 28]. This process occurs when the operating pressure of the reservoir is above the minimum miscibility pressures (MMP) of the crude oil when CO_2 becomes miscible with oil through multi-contact or dynamic miscibility. The injected CO_2 gas vaporizes the intermediate components of crude oil (vaporizing gas drive method) and develops complete miscibility due to the mutual mass transfer between the two phases [29]. Miscibility causes the lowering of IFT thereby eliminating the capillary pressure and the result is literally 0%

residual oil saturation [30]. Although the miscible process is more efficient for EOR, achieving miscibility is not always possible under various reservoir conditions and fluids properties due to technical and safety considerations. Conversely, in immiscible displacement the operating pressures is below the MMP, so less mutual interchange of components takes place between the injected gas and the crude oil. The main driving mechanisms of immiscible CO_2 flooding are oil swelling, oil viscosity reduction, solution gas drive, and reduction of IFT or a combination of these mechanisms which assists in mobilizing a part of the residual oil to improve oil recovery [31].

In the immiscible flooding method, CO_2 gas is injected at subcritical pressures which not only provides energy to the reservoir to assist the flow of oil but also produces additional oil [32]. Injected CO_2 dissolves in the crude oil to reduce oil viscosity which in turn improves the mobility ratio resulting in better E_V. Moreover, CO_2 gas upon contact with crude oil causes oil swelling by a process of dissolution. Swelling causes the discontinuous residual oil droplets to combine with the flowing oil phase, and the result is a lower residual oil saturation [33]. Fig. 1.2 illustrates the saturation pressure, oil viscosity and swelling factor dependence on CO_2 solubility in crude oil. Saturation pressure increases as CO_2 solubility increases, as shown in Fig 1.2 (a) which can be explained by the fact that higher pressure is required to gasify oil with higher fraction of dissolved CO_2 gas [34]. Fig. 1.2 (b) shows that the viscosity of crude oil decreases with an increase in CO_2 solubility in crude oil. This is the primary mechanism of heavy oil recovery by CO_2 flooding as the viscosity of heavy oil can be reduced considerably by CO_2 dissolution as a lower pressure [35]. Swelling factor is also observed to increase with CO_2 dissolution as depicted in Fig 1.2 (c). Although miscibility between crude oil and CO_2 is not significant in immiscible flooding, still CO_2 will dissolve in the oil phase to cause a reduction of IFT and improve the oil relative permeability. Additionally, the oil is displaced towards the

production well by the injected CO_2 gas. However, oil swelling and viscosity reduction are the prominent effects of the immiscible CO_2 EOR process contributing towards additional remaining oil recovery from the reservoir. Literature reports that CO_2 immiscible flooding could recover an additional 4.7 to 12.5 %OOIP [36].

According to the IEA, the total numbers of worldwide CO_2-EOR projects were 166 in 2017 with more number of miscible CO_2-EOR projects compared to the immiscible projects. The largest miscible CO_2 flooding in the world was developed in 1972 in Texas by Chevon in the SACROC (Scurry Area Canyon Reef Operators Committee) unit of the Permian Basin, which was also the first miscible CO_2 flooding project. CO_2 is recovered from flues gas of four gas plants and after dehydration is transported 220 miles to SACROC for injection [37]. The Bati Raman project in Turkey is acknowledged as the world's largest application of the immiscible CO_2-EOR project [38]. Started in 1986 after successful lab tests added by the availability of a large amount of CO_2 gas in a neighboring field about 55 miles away, the project is producing 7,000 bpd [39]. CO_2 required for injection can be obtained from either natural or anthropogenic sources. In the U.S, the principal source of CO_2 comes from natural CO_2 reservoirs. CO_2 gas from these sources is mainly injected in the Permian Basin CO_2-EOR projects [40]. Nonetheless, CO_2 from anthropogenic sources is steadily gaining importance due to the benefit derived from CO_2 sequestration. One of the biggest global CO_2-EOR projects using anthropogenic CO_2 was reported to be the Weyburn project in Canada [41]. The source of the CO_2 gas was the large gasification plant situated in North Dakota from where the gas is transported. About 1,600 x 10^3 ton/year of CO_2 is sequestered which was equivalent to 67% of injected gas amount.

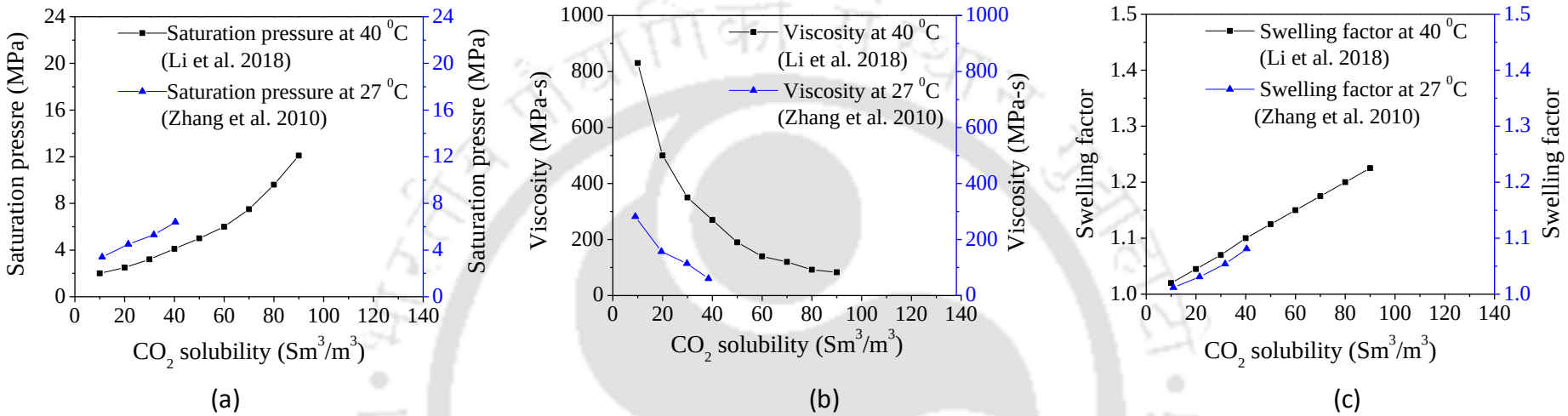

Fig. 1.2: CO_2 solubility in crude oils with respect to (a) Saturation pressure, (b) Viscosity, and (c) Swelling factor [34, 42]

As far as India is concerned, Oil and Natural Gas Corporation (ONGC) is mainly involved in studying the feasibility of CO_2-EOR application in Indian oilfields. One CO_2-EOR pilot project was planned in the Ankleshwar oil field of Western India, where experimental and modeling studies had given encouraging results. These studies indicated that CO_2-EOR is technically feasible in this field and recovery could be expected to improve by approximately 4% in the project life of 35 years. The anthropogenic CO_2 for injection would be supplied from an adjacent gas processing plant in Hazira. The CO_2 gas of the plant is being vented to the atmosphere and by injecting into the oilfield it is expected to sequester 5 to 10 million tons of CO_2 [43, 44].

1.4 Problems Associated with CO_2 Flooding

Although CO_2 flooding is considered a successful EOR technique, a large part (35%–65%) of the oil in place remains unrecovered even after a sufficient volume of CO_2 injection. Miscible CO_2 flooding typically recovers 10%–20% OOIP through the injection of dense CO_2 equivalent to nearly 80% of the hydrocarbon pore volume (HCPV), while immiscible CO_2 flooding can recover only 5%–10% OOIP because of the non-zero IFT between the CO_2 and crude oil [45]. The primary reason for the lower oil recovery of CO_2 flooding is related to its density and viscosity. The low density relative to oil leads to gravity overriding/segregation, a situation where CO_2 migrates toward the upper part of the pay zone. As a result, the lower portions of the formation remain unswept by CO_2 lowering E_{vo} and consequently significant amount of oil is left behind. Moreover, mobility ratio in CO_2 flooding is unfavorable due to the much lower viscosity of the injected CO_2 gas compared to crude oil under reservoir conditions. The high mobility ratio promotes viscous fingering and excessive flow in high permeability

layers. The resultant effect is early gas breakthrough, reduced E_{vo}, and high residual oil saturation.

The other problems associated with CO_2 flooding that reduce the process-efficiency are corrosion and asphaltene precipitation. When CO_2 reacts with formation water carbonic acid form making the formation water acidic. The acidic environment may corrode the downhole tubular and production equipment increasing the risk of leaks. Moreover, the acidic water may dissolve harmful elements affecting drinking water sources. Another dominant problem that may occur during CO_2 flooding is the possibility of asphaltene precipitation. Asphaltenes tend to remain in solution under reservoir temperature and pressure conditions stabilized by resins adsorbed on their surface. Asphaltenes may start to precipitate if the stability of crude oil is destabilized due to changes in temperature and/or pressure during primary depletion. Asphaltenes may also become unstable as a result of the mixing of fluids as well as during gas injection for EOR operations [46]. During CO_2 flooding, the interaction of the CO_2 and crude oil may cause the asphaltene-to-resin ratio of crude oil to altered leading to asphaltene precipitation and thereby its deposition [47]. In the reservoir, the precipitation may obscure the movement of CO_2 into the portions of the reservoir containing residual oil and thereby lower E_{vo}. Resins have the effect of keeping asphaltenes in solution. A high resin to asphaltene ratio (R/A) indicates that asphaltenes are less likely to come out of solution [48]. Leontaritis and Mansoori [49] presented a condition for asphaltene stability as follows: $R/A > 3.0$ as steady-state, $2.0 < R/A < 3.0$ as meta-steady state and $R/A < 2.0$ as unsteady state. However, among all the complications of CO_2 flooding, unfavorable mobility ratio and conformance issues are considered the most dominant ones affecting the process.

The techniques commonly employed to overcome CO_2 mobility and conformance control problems are summarized below:

(a) Water-alternating-gas (WAG): This is the technology of choice for CO_2 mobility control where instead of continuous injection, CO_2 is alternately injected with water into the reservoir as short slugs so as to provide better E_{vo} and reduce CO2 consumption. This technique lowers the relative permeability to CO_2 through increased water saturation and lower CO_2 gas saturation in the pore spaces of the reservoir rock. The mobility of gas is controlled and early gas breakthrough is alleviated through WAG injection which improves the displacement efficiency of the process [50, 51]. The first reported WAG field application was a pilot study in the North Pembina oil field in Alberta, Canada in 1957 [52, 53]. The obvious advantage of WAG lies in the fact that both the injected fluids are available in large volumes and so less costly. The schematic representation of the CO_2-WAG process is shown in Fig. 1.3.

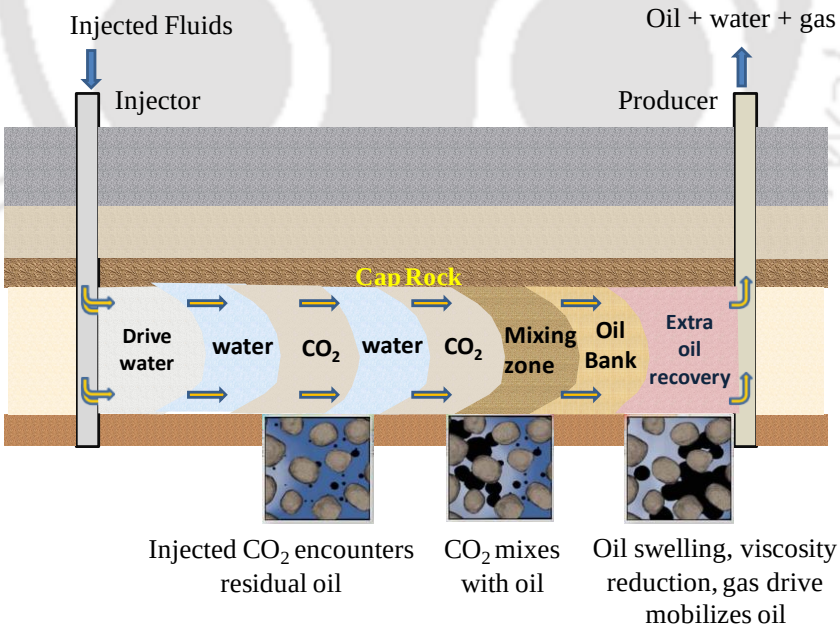

Fig. 1. 3: Schematic representation of CO_2-WAG flooding showing the alternated CO_2 and water injection cycles[[54], modified]

(b) *Direct Thickener*: The use of direct thickeners like soluble polymers that significantly increase CO_2 viscosity is sometimes used for mobility control during CO_2 flooding. The thickened CO_2 gas injected without water improves the displacement efficiency without the water blocking problems and corrosion issues associated with WAG.

(c) *CO_2-foams*: Foam has been used to control gas mobility and improve oil recovery during gas EOR processes. Foam exhibits various favorable attributes which makes it an attractive method for improving oil recovery. Foam reduces the apparent viscosity of the gas and lowers the relative permeability of the liquid, making the mobility ratio favorable. Additionally, foam reduces CO_2 mobility by a greater fraction in high-permeability cores than in lower-permeability cores [55, 56]. This unique property of foam is termed as selective mobility reduction which assists in smoothening heterogeneities [57]. The stronger foam generated in the high-permeability zones behaves like a more viscous fluid which diverts fluid to low-permeability zones of the reservoir, thus providing better mobility control to improve E_{vo} [58]. The presence of surfactant during foam flooding, on the other hand, helps to mobilize residual oil by lowering the oil-water IFT value.

1.5 Different Types of WAG Flooding

Although WAG is the most widely used technique for mobility control in CO_2 flooding, the process still leaves behind about 33% to 67% of the oil unrecovered by secondary water flooding. The improvement of oil recovery by WAG injection is around 10 % OOIP [52, 59, 60]. This low recovery is primarily due to the water blocking effect. Water blocking occurs when the injected water separates the residual oil from coming into contact with the CO_2 gas. Water itself cannot remove the capillary

held residual oil due to the high oil-water IFT and consequently, the microscopic displacement efficiency is low. Moreover, in the case of viscous oil reservoirs due to the unfavorable mobility ratio, viscous fingering of injected water and early injection gas breakthrough occurs. Thus, major areas of the reservoir with residual oil remain unswept by the injected fluids resulting in low oil recovery [61]. Other concerns associated with CO_2-WAG injection are difficulty in controlling gas/CO_2 breakthrough as the WAG process matures, huge volumes of water injection delay the project duration, corrosion, and water injectivity loss.

Various studies to improve the performance of CO_2-WAG and overcome its limitations have led to the development of the chemically-enhanced-water alternated gas (CEWAG) method. This method combines the benefits of both gas and chemical EOR methods. Different types of chemicals like surfactants, alkalis, co-surfactants, salts, polymers, co-solvents, and nanoparticles are used based on the specific application [57, 62]. The mechanism is referred to as surfactant-alternated-gas (SAG) flooding when surfactants are added to water during the WAG injection process resulting in foam formation in the pore spaces of the reservoir rock [63, 64]. Previous studies have reported improvement in E_{vo} and significant increase in oil recovery by SAG flooding compared to continuous CO_2 injection and CO_2-WAG injection [65-68]. The higher oil recovery obtained by SAG injection can be attributed to a number of factors like the reduction of oil-water IFT due to the presence of surfactants, better mobility control due to foam formation, and mutual mass transfer between the fluids. Foam increases the apparent viscosity of CO_2 gas thereby reducing its mobility. Thus channeling and viscous fingering problems are alleviated significantly. Additionally, foam also decreases the permeability to water due to the higher trapped gas saturation in pore spaces of the reservoir rock [69]. Although foam can be formed in the reservoir by

the co-injection or alternate injection of gas and surfactant solutions, the alternate method is preferred over co-injection due to its characteristic advantages [66, 70, 71]. SAG minimizes contact between the water and gas/CO_2 in the surface facilities and pipelines reducing corrosion. SAG injection also increases gas injectivity due to changing saturation near the well-bore [72]. Additionally, SAG injection can reduce gravity override problems without increasing injection well pressures that cannot be done with continuous co-injection method [73].

However. surfactants injected with CO_2 during the SAG process are susceptible to be adsorbed by the clay minerals in the rock matrix which reduces the efficiency of the foam process [74]. Traditionally, alkali has been used to decrease the adsorption of anionic surfactants onto the reservoir rock. Alkali acts as a sacrificial agent for anionic surfactants by fixing the surface charge to negative values. The negative charge of the surface causes electrostatic repulsion between the rock surface and the surfactant, leading to a significant decrease in adsorption of surfactant [75]. Adding alkali also assists in converting the naturally occurring naphthenic acids in crude oils to produce in situ surfactant (soaps). The combination of injected surfactants and in-situ soaps generated helps to form microemulsion, which exhibits ultra-low oil-water IFT (<0.01 mN/m) thereby mobilizing capillary held residual oil for increasing oil recovery. In association with the CO_2 gas, the alkali-surfactant (AS) combination in the chemical slug results in the formation of strong/ stable in-situ foam in the reservoir. This process of alternate injection of gas/CO_2 and AS slug is variably referred to as alkaline-surfactant-foam (ASF) flooding, low tension gas (LTG) process, alkali surfactant gas (ASG) injection and alkaline-surfactant-alternated-gas/CO_2 (ASAG) flooding in the literature [76-81]. Fig. 1.4 shows a schematic representation of the displacement process in continuous gas injection (CGI), WAG, SAG, and ASAG flooding.

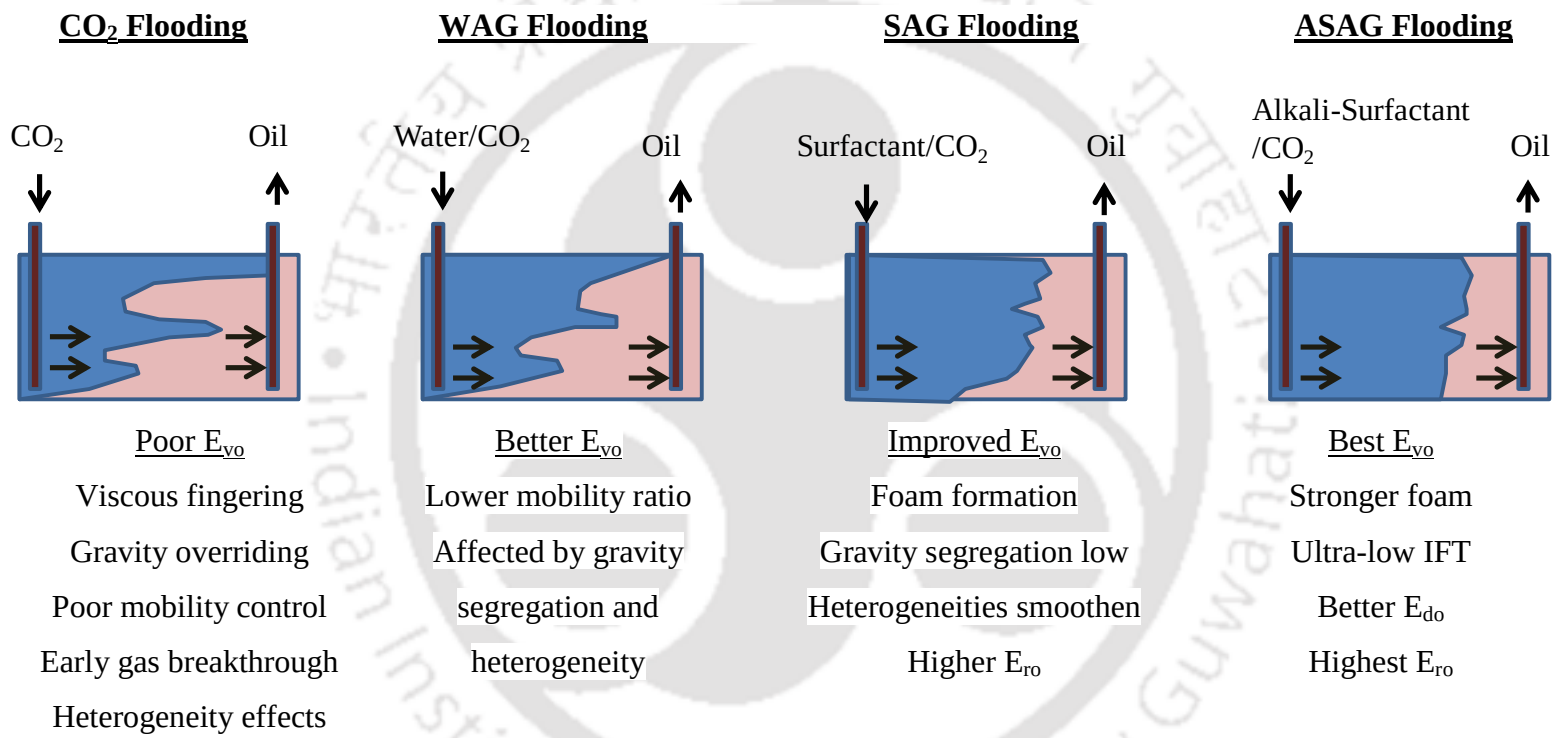

Fig. 1.4: Schematic representation of the displacement process in CGI, WAG, SAG, and ASAG injection scheme [[82], modified]

1.6 Alkaline-Surfactant-Alternated-Gas/CO_2 (ASAG) Flooding

ASAG flooding is, in essence, a modification of the CO_2-WAG process designed to overcome the limitations associated with WAG. This is a relatively new EOR method compared to alkali surfactant polymer (ASP) and gas flooding, and only limited experimental works have been reported. ASAG flooding involves the alternate injection of AS slug and gas/CO_2 in the reservoir leading to the formation of in-situ foam, due to the alternating imbibition/drainage cycles, which helps to control the gas mobility (Fig. 1.5). The combination of alkali-surfactant in the chemical slug assists in the attainment of ultra-low oil-water IFT, which in turn increases the N_{cap} high enough to mobilize the residual oil held by capillary forces [81]. Studies have reported that the displacement efficiencies obtained from ASAG flooding are comparable to those of ASP flooding for core flooding experiments carried out under similar conditions [78, 83]. In fact, ASAG flooding is reported to be an attractive alternative solution to ASP for reservoir under harsh conditions like high salinity, high temperature, and also for tight rock [79, 84]. Currently, ASP flooding is the most promising chemical EOR method but the use of polymers carries various limitations. Polymers, for example, may cause plugging of low permeability rocks, can be unstable under high salinity and high reservoir temperatures and maybe mechanically degraded due to high flow rate [85]. For these harsh salinity and reservoir conditions, polymers in ASP can be successfully replaced by gas/CO_2 as in ASAG flooding. Foam formation during ASAG flooding provides the required mobility control through an increase in the apparent viscosity of gas and reduction of the relative permeability of the aqueous phase. The result is the improvement of both the E_{vo} as well as the E_{do} during ASAG flooding. With these favorable attributes, ASAG flooding is considered to be a viable EOR method and as a potential alternative to ASP flooding for oilfield applications.

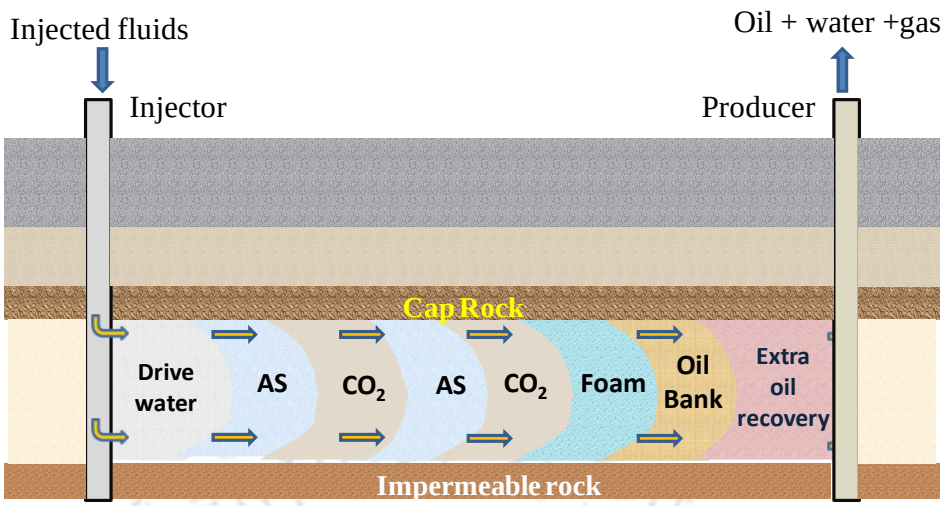

Fig. 1.5: Schematic representation of ASAG flooding showing the alternate injection of alkali-surfactant (AS) slug and gas/CO_2 injection

1.7 Oil Recovery Mechanisms of Other EOR Methods

ASAG process was designed to integrate the favorable attributes of chemical (alkaline and surfactant) and gas /CO_2 flooding, which in turn makes the oil recovery mechanism quite complex. The oil recovery mechanisms of alkaline and surfactant chemical EOR processes are summarized below:

1.7.1 Alkaline Flooding

In this EOR method, alkaline solutions are injected into an oil reservoir during or post waterflooding. The oil recovery mechanisms of alkaline flooding primarily include reduction of oil-water IFT, wettability reversal, and emulsification with entrapment of oil [6, 86-90]. Depending on the nature of the crude oil and the reservoir rock, each of the mechanisms may play more or less important roles when alkaline solutions are injected under different reservoir conditions. Alkaline flooding is not recommended for carbonate reservoirs because the alkali solution reacts with calcium ions causing hydroxide precipitation which leads to formation damage [91].

Crude oils with acid number greater than 0.5mg KOH/g in crude oil are known as acidic crudes are suitable for alkaline EOR [92]. The mechanism of alkali-crude oil

reaction in alkaline flooding is shown in Fig. 1.6. Sheng [93] reported that a highly oil-soluble single pseudo-acid component (HA) is assumed to be present in oil. This pseudo-acid component partitions into the aqueous phases upon contact with water i.e.

$$HA_o \leftrightarrow HA_w \tag{1.4}$$

where HA_o and HA_w are the acid species, A is long organic chain and subscript 'o' and 'w' represents oleic and aqueous phase respectively. HA_w dissociates into its components as:

$$HA_w \leftrightarrow H^+ + A^- \tag{1.5}$$

Further, upon alkali (Na_2CO_3) hydrolysis OH^- ions are produced which react with HA_w to form oil soaps NaA (which acts as a soluble anionic surfactant). The overall reaction is:

$$HA_w + Na_2CO_3 \leftrightarrow NaA + H_2O \tag{1.6}$$

Another important oil recovery mechanism of alkaline flooding is wettability reversal. In oil-wet reservoirs, the addition of alkali increases the pH of injected water which causes the rock wettability reversal from oil-wet to water-wet. As a result, the water-oil relative permeability ratio and the water-oil mobility ratio are reduced, that improves the oil displacement efficiency [94, 95]. In the case of water-wet reservoirs, the non-wetting residual oil in discontinuous form can be converted to a continuous wetting phase through wettability reversal under specific conditions of pH, salinity and reservoir temperature. Moreover, water droplets in the continuous oil phase increase the pressure gradient of the flow. Thus, the capillary held residual oil is mobilized and higher recovery is obtained [86].

The commonly used alkalis are NaOH, Na_2CO_3, Na_4O_4Si, BNaO, $(NH_4)_2CO_3$, and NH_4OH. Na_2CO_3 has been reported to be a better candidate for alkaline flooding. Alkali consumption during flooding can be reduced by the use of Na_2CO_3 and breakthrough times are also minimized. With Na_2CO_3, the mineral dissolution and ion exchange are also considerably lower compared with NaOH and Na_4O_4Si [96]. Cheng [97] reported that

formation damage by precipitates of CO_3 is less severe due to their smaller sizes compared to SiO_4 and OH precipitates. Moreover, Na_2CO_3 has also been found to be less corrosive when compared to NaOH and Na_4O_4Si for sandstone reservoirs [98].

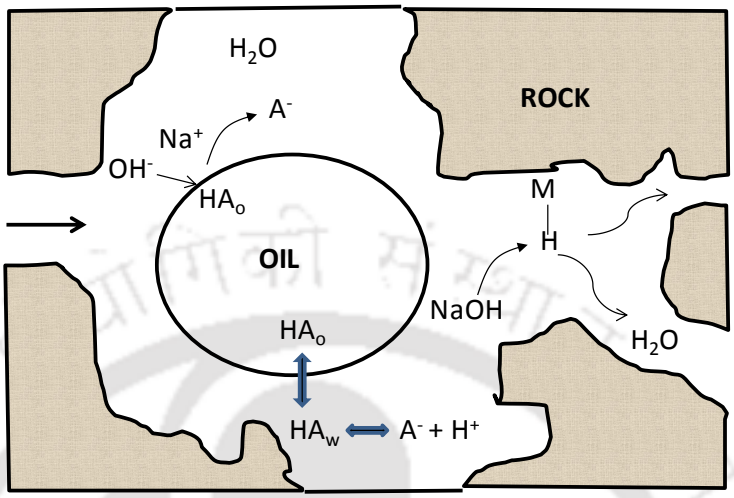

Fig. 1.6: Schematic diagram of alkaline flooding mechanism illustrating the reaction between alkali (NaOH) and acid component of crude oil [99]

1.7.2 Surfactant Flooding

In surfactant flooding, solutions containing surface-active agents are injected into the reservoir for the purpose of mobilizing trapped residual oil [100]. The primary oil recovery mechanism of surfactant flooding are lowering of oil-water IFT due to the adsorption of surfactants on the liquid-liquid interface and changing the reservoir rock wettability [101]. IFT reduction plays a very important role in surfactant flooding and is affected by many factors like the type of surfactants and their concentrations, solvents, salinity, composition of crude oil and reservoir conditions [102]. A correctly designed surfactant system interacts with brine and crude oil to form microemulsions at the interface of oil and water reducing IFT to ultra-low value [103]. In this respect, the phase behavior study of microemulsion is very important in surfactant-based EOR application to evaluate surfactant formulations and as an indicator of ultra-low IFT. Microemulsion phase

behavior can be described by Winsor type I, type II, and type III. A change in the phase behavior can be brought about by changing the variable such as salinity, surfactant structure, temperature, and pressure [104]. For an ionic surfactant, microemulsion phase behavior is particularly affected by the salinity or concentration of electrolyte [87].

At low salinity, type I or oil-in-water microemulsions occur and are characterized by coexistence with nearly pure excess oil phase. Whereas, at very high salinity, type II or water-in-oil microemulsions are formed, which are characterized by coexistence with an excess brine phase. In between the type I and type II regions, a narrow intermediate salinity range exists in which oil and water microemulsions are formed as a middle phase and coexist with both excess oil and excess water phases. These are referred to as type III microemulsions and the salinity as optimal salinity. Type III microemulsion and optimal salinity are of great importance in surfactant flooding because of the existence of ultra-low IFT [105, 106]. With low IFT, the residual oil droplets are able to easily flow through the pore throats as the capillary trapping is reduced (Fig. 1.7). These oil droplets travel forward and merge with the oil down the stream leading to the formation of the oil bank [102]. Additionally, surfactant solutions also cause the altering of reservoir rock wettability to more water-wet condition by increasing the spontaneous imbibition of water into matrix blocks, which helps to increase the oil recovery [107]. The wettability mechanism is more prominent in carbonate reservoirs which are likely to be oil-wet.

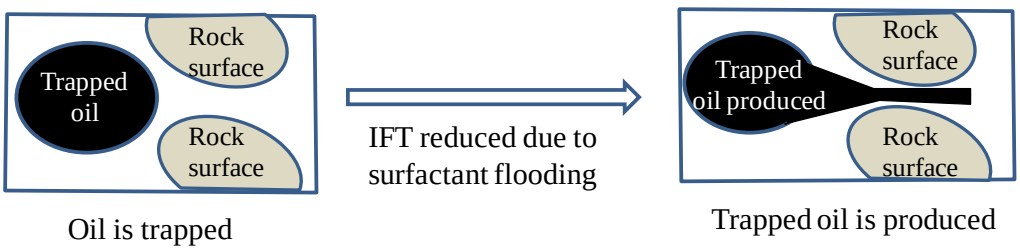

Fig. 1.7: Mechanism of oil recovery by surfactant flooding illustrating the effect of low IFT on residual oil [[108], modified]

1.8 Foams Concepts

Foams are dispersions of gas in liquid where liquid containing surfactant forms the external or continuous phase, whereas gas forms the internal or discontinuous phase separated by thin liquid films called lamellae [57]. The role of the surfactant is to stabilize the lamellae against rapture thus providing stability to foam. The border where the lamellae join or meet a solid surface is known as the plateau border. In wet foam, the liquid exists mainly in the plateau borders. A 2-D view of foams in general is shown in Fig. 1.8.

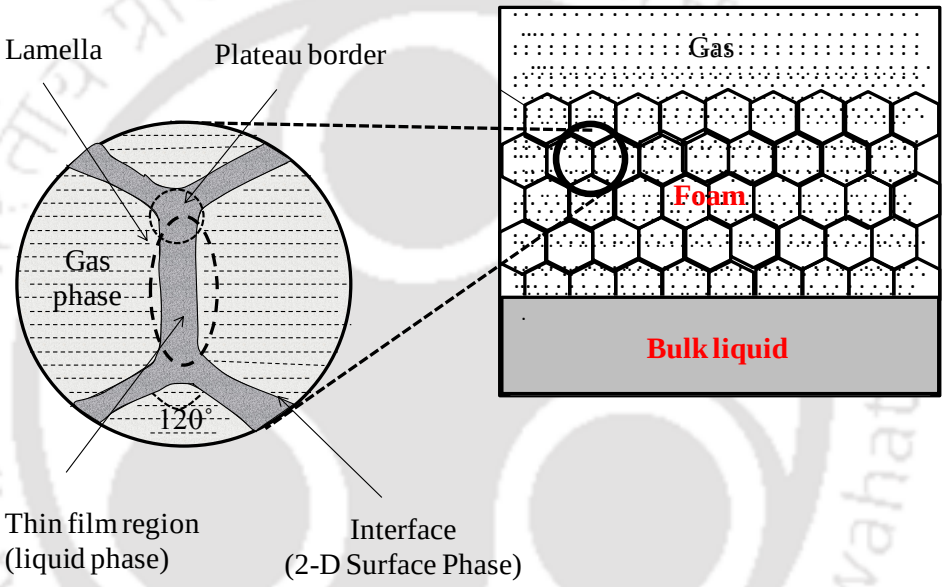

Fig. 1.8: Schematic representation of a general foam system showing the lamella and plateau borders [109]

Foam has a wide range of applications in the oil industry. During drilling, foams can be used to carry the rock cuttings to the surface. In well-stimulation treatments, foams can cause diversion of acids to improve the acid-injection profile. In EOR, foams are popularly used for gas mobility control. Broadly, foams can be grouped as bulk foam and foam in reservoir rock. Foam with bubble sizes much smaller than the pores or volume of the container is termed as bulk foam. On the other hand, foam in reservoir rock has bubble size larger than the pore size so that energy is required to force the bubbles through the

pore constriction [110]. The behavior of foam in reservoir rock is influenced by pore size and pore throat distribution. Foam in porous media does not exist as continuous interconnected gas bubbles but as discrete gas bubbles separated by liquid lamellae. These gas bubbles are in contact with the pore walls through the wetting phase fluid. Foam travels as bubble train in porous media with each bubble separated from the next by liquid lamellae film.

When foam flow through reservoir rocks, gas can exist as trapped gas, continuous gas, or discontinuous but moving gas. The continuous gas flows in interconnected channels without any lamellae. Discontinuous but moving gas is separated by lamellae. The moving lamellae senses drag force while moving along the pore walls. Thus, the moving gas experiences resistance to flow which is like the effect of increasing gas viscosity. The actual gas viscosity is not increased by foam but gas experiences increased resistance to flow due to lamellae presence, so foam is said to increase apparent gas viscosity. Discontinuous foams are stronger foam, which are formed when gas and surfactant are co-injected or alternately injected under proper conditions. Trapped gases that are not mobile reduces the pore volume available for flow and changes gas flow paths. This causes a reduction in the effective permeability of gas flowing through the porous rocks [111]. Foam thus reduces gas mobility by increasing the apparent viscosity of gas and decreasing the gas effective permeability. Reducing gas mobility in the porous rock increases gas saturation and consequently decreases the liquid saturation. The lower value of liquid saturation, in turn, decreases the liquid relative permeability.

During the flow of foam through the pore spaces of the reservoir rock, the lamellae creation and decaying takes place continuously during the flooding process. But the rate of lamellae creation should be greater than or equal to the rate of decaying for better mobility control. There are three generally accepted mechanisms of foam generation: leave-behind,

lamella division, and snap-off. When gas enters liquid saturated reservoir rock, lamellae is left behind in the pore throats between the pore spaces. Foam generated by the leave behind mechanism is considered weak. The lamella formed can get transported and multiply by lamella division mechanism. Lamella division occurs by subdivision of pre-existing lamellae in the reservoir rock when the pressure gradient is sufficient to move the lamellae through the pore throats. Snap-off is an important mechanism of foam generation in the reservoir rock. This is a mechanical process where the liquid wetting phase forms collars in the pore throat that snaps off the gas bubble as it moves through the pore throat. For snap-off to occur the pore throat to pore body ratio should be 1:2.67. Both lamellae division and snap-off mechanisms generate discontinuous gas foams which are considered as strong foam [112].

1.9 Foam Stability

Foams are not thermodynamically stable and ultimately collapse in due course of time. Foam stability is dependent on many factors concerning the bulk solution and interfacial properties such as gravity drainage, capillary drainage, surface elasticity, disjoining pressure, and gas diffusion.

1.9.1 Gravity and Capillary Drainage

Foam stability depends on the liquid drainage from the inside of lamellae which causes film thinning and eventually rapture. Foam drainage is driven by two forces: gravity and capillarity. Gravity causes the liquid in the lamellae to drain causing the gas bubbles to collide and collapse unless the liquid film is thick. Liquid drainage due to capillary pressure occurs when the lamella is thin. Capillary pressure is measured as the difference of pressure between the gas and the liquid phase. As shown in Fig. 1.8, gas-liquid interface along the thin-film regions are flat or larger radii, while at the plateau borders are curved or smaller radii. Since capillary pressure is inversely proportional to the interface-radius (as

per the Young-Laplace equation), there exists a difference of pressure between the thin-regions and plateau borders. This pressure difference causes the liquid out of the lamella towards the plateau borders, thus reducing film thickness and eventually rapture [113].

1.9.2 Marangoni Effect

For foam to be stable, the thin films should be elastic to withstand deformations without collapsing. If the liquid film in the foam system undergoes a sudden expansion, the adsorbed surfactant concentration decreases in the expanded area of the film. This causes an increase in the local surface tension gradient. As a result, liquid flow into the film takes place from the low-tension area to the high-tension area. The liquid flow opposes the thinning of liquid film which helps to stabilize the foam system. When equilibrium surfactant concentration is reached, the liquid flow stops. This effect is known as surface elasticity or Marangoni effect [109].

1.9.3 Disjoining Pressure

The disjoining pressure arises from the overlap of molecular interactions between interfacial layers and is the total effect of forces which are of different nature. It is the difference of pressure between the gas and the liquid phases within a film, and is dependent on the film's thickness. There are three components of the disjoining pressure: attractive Van der Waals force, repulsive electrostatic potentials, and steric/hydration forces. The Van der Waals force results from the interactions of neutral molecules across the film and results in film thinning. This is because these forces are present when surfactant is absent making disjoining pressure negative and so lamellae rapture quickly. When the ionic surfactant is added, the surfactant molecules are adsorbed on the gas-liquid interface creating an electrical double-layer, which is the source of the repulsive forces that stabilize the lamella. Thus, the ionic strength of the aqueous solution also determines the

degree of lamella stabilization [114]. The steric forces which are repulsive in nature also prevent lamella thinning [85].

1.9.4 Gas Diffusion

In a foam system, the gas bubbles do not have a uniform size distribution. The smaller gas bubbles are at a higher pressure than the larger bubbles. This gives rise to a chemical potential difference, which causes diffusion of gas through the liquid from the smaller to larger bubbles. The result is smaller bubbles shrinks while the larger bubbles grow by coalescence [105].

1.10 Literature Review of ASAG Process

The use of foam to reduce the mobility of gas-phase was proposed as early as in the late 1950s when Bond and Holbrook [115] patented the alternate injection of surfactants solutions (1 wt% sodium dioctylsulfosuccinate) with foaming properties and gas in sand packed glass tubes. Their experiments showed that the SAG process could recover 70% OOIP compared to 40% OOIP by WAG flooding which demonstrated the usefulness of employing surfactant solutions in conjunction with gas-drive. The formation of foam front at the interface of the injected gas and surfactant solution increased the displacement of the gas drive and improved oil recovery.

Kamal and Marsden [116] experimentally studied the displacement process of foam in glass tubes packed with sands. The 0.05 and 0.1 PV micellar slug was used to displace the crude oil in secondary and tertiary recovery mode. Foam was formed in a foam generator from 0.2 wt% Triton X-100 and was used to displace a micellar slug. Similar experiments were carried out with polymer thickened water (500 ppm polyacrylamide) in place of foam to compare the results. Their results demonstrated that additional oil recovery can be obtained by injecting micellar slug followed by foam drive. Foam could effectively displace micellar slugs to obtain oil recovery. Although ultimate oil recoveries

by micellar slug displaced by foam and polymer solution were comparable, much lesser amount foaming agent than polymer was required. Consequently, foam displacement process was shown to be more cost-effective than polymer.

Bernard et al. [117] reported experimental works to enhance the performance of CO_2 flooding by controlling gas mobility through alternated CO_2 and surfactant solution injection into the reservoir. They performed these tests on Berea sandstones and carbonate cores and with all three types of surfactants namely anionic, non-ionic and cationic. The results of their study indicated that the efficiency of the WAG injection increased when surfactant was added to the water due to the reduction of CO_2 mobility by about 50%. With the increase in surfactant concentration from 0.1 to 1 wt%, the CO_2 mobility could be reduced from 60 to 5 md/cp. Foams generated reduced CO_2 flow through cores and a lesser amount of CO_2 was required for the same oil recovery. Moreover, surfactant slug followed by continuous CO_2 injection resulted in the same oil recovery as alternated CO_2 and surfactant slug injection.

Julio and Emanuel [118] performed core flooding experiments on unconsolidated sandstone cores using heavy California oil (14 ^{0}API) to tested the mobility-control ability of foam during immiscible CO_2 flooding. Foam formed by the co-injection of CO_2 and 0.5 wt% surfactant solution (Chevron's CRSO 85/66) was able to recover an extra 33.6 % OOIP compared to waterflooding and WAG flooding. The increase in oil recovery was a result of mobility control and diversion of CO_2 to lower permeability zones unswept by waterflooding and WAG.

Lawson and Reisberg [119] studied a technique for mobility control during chemical flooding by injecting alternate slugs of inert gas (N_2) and surfactant solution on Berea sandstone, Ottawa sand packs, and Indiana limestone. They observed that foam formation could successfully provide mobility control, which was comparable with

mobility control by water-soluble polymers. Their experimental results also indicated that the use of alkali (borax) in the chemical slug and preflood could reduce surfactant adsorption in carbonate rocks.

Demin et al. [120] reported the first field pilot test of ASP foam (ASPF) carried out in the northern part of Daqing oilfield, China by adding natural gas to the ASP slug . The chemical slug comprising of 0.3 wt% surfactant, 1.2 wt% NaOH and 1200 mg/l PAM was coinjected with natural gas. ASPF flooding increased oil recovery by 30% and 10% OOIP beyond water flooding and ASP flooding respectively. Higher recovery was attributed to improvement in the volumetric sweep efficiency due to foam formation.

Srivastava et al. [83] used foam as a gas/CO_2 mobility control agent, formed by co-injecting and alternate injecting of gas/CO_2 and chemical slug in Berea sandstone and Silurian dolomite cores. The process was termed as alkaline-surfactant-gas (ASG) injection. The ASG slug consisted of high-performance chemicals (surfactants, alkali, co-solvents having the ability to lower oil-water IFT to ultra-low) and gas/CO_2. The ASG drive which followed the ASG slug consisted of aqueous phase of low surfactant concentration and gas. The authors observed an increase in oil recovery during ASG flooding due to the synergic effect of ultra-low IFT conditions and foam generation. ASG process could successfully recover incremental oil up to a maximum of 90 % of remaining oil after waterflood. Alkali presence increased the efficiency of the ASG flooding due to in-situ soap generation and surfactant adsorption reduction. Comparable oil recoveries and pressure responses were observed both for ASG and ASP flooding performed under similar experimental conditions.

Zhang et al. [42] studied the chemical alternating gas (CAG) process in cores packed with Ottawa sands. The ASP slug was followed CO_2 or flue gas (70% N_2 in the CO_2 stream) and finally extended water flooding. They observed that CO_2 dissolved easily

into Saskatchewan heavy oil at moderate pressures (3.4–6.4MPa), causing viscosity reduction (45–88%) and oil swelling (1.2–8.1%). Their core flooding results indicated that higher oil recovery could be obtained by CO_2-CAG compared to CO_2-WAG (27.43% versus 9.43% OOIP).

Srivastava et al. [121] investigated the feasibility of immiscible alkaline-surfactant-alternate-gas (ASAG) injection at a laboratory scale performed with crude oil Limbodara oilfield India with Berea core sandstone core. The authors reported that displacement efficiencies of ASAG core flooding experiments were comparable to ASP experiments carried out under similar conditions. The incremental oil recovery obtained beyond waterflooding with a single ASAG cycle and two ASAG cycles were 27.79% OOIP and 29.01% OOIP respectively indicating the potential of the ASAG injection for EOR.

Pei et al. [122] studied the foam flooding for heavy oil of Shengli oilfield by co-injecting alkali-surfactant solutions with N_2 gas in cores and sand packs. They observed that tertiary oil recovery by polymer-enhanced foam flooding was 11% higher than that of ASP flooding. The results showed that tertiary oil recovery by foam flooding improved with the increase in gas-liquid ratio and slug size.

Guo et al. [123] investigated the alkaline/surfactant/foam (ASF) process by coinjection AS slug (1.0 wt% Na_2CO_3 + 0.5 wt% IOS) and N_2 gas in Bentheimer sandstone cores with or without AS preflush. The designed AS slug had well-defined optimum salinity which reduced the IFT to ultra-low value and also displayed good mobility control. Oil recovery by AS flooding and ASF flooding without AS preflush were 43% and 47% residual oil in place (ROIP) respectively. ASF with AS preflush was far better with the recovery.

Cottin et al. [79] studied the effect of gas co-injected with AS slug in Middle East carbonate core under harsh salinity and temperature conditions. They reported cumulative

oil recovery of 48% OOIP and 76% OOIP from surfactant-gas (SG) and ASG flooding respectively. Addition of alkali (Na_2CO_3 at 10000 ppm) to the chemical slug was able to increase the pH of the slug before injection from 7.5 to 11 and thus reduce surfactant adsorption by changing the charge on the rock surface.

Luo et al. [124] evaluated the effectiveness of the chemical-augmented WAG process through an integrated process comprising of IFT and rheology measurements, phase behavior studies, and core flooding experiments on sand packs. The authors observed that reservoir oil viscosity reduced by 89% when 40.39 mol% CO_2 was dissolved at saturation pressure. Oil recovery by CO_2 injection was more than flue gas of (30% CO_2 + 70% N_2) injection in the WAG mode. Immiscible WAG with CO_2 gas could favorably recover residual oil from heavy oil reservoirs. Chemically enhanced WAG could increase oil recovery by almost 3 times than CO_2-WAG.

Zhang et al. [125] developed a foaming agent through the combination of 0.3% Cocoamido propyl betaine + 0.2% coconut diethanol amide + 1600 ppm HPAM + N_2, which displayed good foaming ability and could lower IFT to ultra-low value. The operating parameters of foam injection like co-injection, direct injection, WAG and gas-liquid ratio were studied through core flooding experiments performed on cores of Shengli oilfield. The authors observed that ultralow IFT foam flooding could recover 21.55% more heavy oil than the conventional direct foam injection indicating its effectiveness in heavy oil recovery. The ultra-low IFT foam flooding had a stronger blocking effect in high permeability zones of heterogeneous reservoirs which resulted in better sweep efficiency and higher oil recovery.

Majidaie et al. [61] investigated the chemically enhanced water alternating gas (CWAG) injection process through the injection of three WAG cycles followed by ASP slug and finally followed by two more WAG cycles. The core flooding results performed

on Berea sandstone cores indicated that CWAG method recovers more than twice the additional oil recovered by WAG. The authors reported that the CWAG process reduces the IFT to ultra-low value which minimizes the water blocking effect.

Lashgari et al. [80] used the four-phase chemical flooding reservoir simulator (UTCHEM) to assess the performance of the low-tension surfactant-gas flooding using the coreflood data generated experimentally and extension to the field scale reservoir pilot. The history matching and reservoir simulation results indicated that IFT reduction, displacement of oil by gas, and mobility control of gas were the main mechanisms of increasing oil production. The laboratory coreflood reported the recovery of 91 %OOIP, while numerical models in reservoir scale showed oil recovery between 65 – 88 % of residual oil.

Jong et al. [84] performed core flooding experiments in high permeability Berea sandstones to investigate the effect of salinity gradient on the low tension gas (LTG) flooding and the interaction between microemulsion phase behavior and foam stability. Their results showed that decreasing slug salinity leads to better foam stability, good mobility control, and increase oil recovery by 15% ROIP, compared to slug injected at optimum salinity.

Nasab and Zitha [81] evaluated the properties of the chemical slug for alkali–surfactant–foam (ASF) flooding through microemulsion phase behavior, interfacial properties, and foam stability characterization. Their results demonstrated that an ultra-low IFT environment can improve both E_{vo} and E_{do} of foam flooding. Their core flooding displacement experiments on Bentheimer sandstone cores showed that using a blend of surfactants along with gas resulted in the residual oil recovery of 33 % OOIP with maximum clean oil and minimal emulsion.

1.11 Techno-economic Feasibility, Challenges, and Screening Criteria of ASAG flooding

Previous studies have established the potential of combined chemical-gas flooding for EOR and confirmed that the process can lead to higher residual oil recovery compared to the individual processes [122, 126-128]. However, the successful planning of the EOR project requires careful consideration of all aspects involved in the process, with the most important one being the economics of the project. The economic evaluation of the project encompasses the operating expenses, price of injection fluids, capital expenditures, cumulative oil production, and other related financial matters. The economic feasibility of an EOR process is sensitive to the crude oil price, project lifetime, discount rate, and tax policy. The techno-economical advantage of ASAG flooding arises due to the alternate injection of chemicals and gas/CO_2 in short slugs into the reservoir instead of only gas flooding or chemical flooding. For an EOR process like ASAG flooding, the financial feasibility of application in a particular reservoir for enhancing oil recovery will depend greatly on the availability, transportation, injection, and separation costs of CO_2 gas. Furthermore, the proper selection of chemical slug that reduces the retention and increases the efficiency of the injected chemicals can undoubtedly better the techno-economical aspect of the ASAG process. The economics of the process can also be improved through accurate screening of candidate reservoirs and sound reservoir management. High oil prices, short project life-time, low CO_2 cost, low tax policy, and extra incentives can significantly increase the net income and encourage enterprises to employ ASAG flooding projects. Along with EOR, the ASAG flooding has the added benefit of carbon dioxide sequestration in the underground oil reservoirs reducing the greenhouse gas effect. However, for utilizing the anthropogenic CO_2 to increase oil recovery more advanced technologies are required for CO_2 capture and transportation to the oil fields.

Although there are many advantages associated with ASAG flooding, the process still has some major concerns. Due to the presence of both CO_2 and water containing chemicals in the injection side carbonic acid forms creating an acidic environment that may corrode pipelines, tubing, and other surface or sub-surface equipment. The remedial measures include the use of corrosion inhibitors, protective coatings, high-quality materials, and adequate corrosion monitoring. Another serious concern that may arise during ASAG flooding is the likelihood of hydrate formation and asphaltene precipitation that leads to possible deposition and consequently production delays. Hydrate formation may occur in the well when the near well temperature drops causing blockage of the injection well. In order to control hydrate formation, chemicals like alcohols (methanol, ethanol, and glycol) and salts are injected into the fluid stream [129]. However, alcohols are expensive and pollute the effluents making their recovery difficult. The deposition of asphaltene, on the other hand, causes formation damage and prevents the flow of injected fluids into the zones containing residual oil. Asphaltene problem can be solved by solvent washes and treatment with dispersant agents. Of these methods, the use of aromatic solvents is the most effective but is a costly method [130]. Application of ASAG flooding also produces a significant amount of water that may contain a large number of salts, chemicals, and toxic heavy metals. The oilfield produced water should be properly disposed of by injecting back into the underground formation to prevent contamination of drinking water source, agriculture and the environment. Apart from these major issues, some other operational challenges of ASAG flooding are premature breakthrough, tubular failures, gas transportation and storage problems, downhole pump malfunctioning, high cost of chemicals, foam propagation issues, and sudden drop in oil price.

Screening criteria of different EOR methods are reported in the literature by various authors [131-134]. Screening criteria are used in many field applications, laboratory and

simulation studies to choose the best and most feasible EOR method for any candidate reservoir before implementation of any EOR projects [135]. Aladasani [136] updated the EOR criteria published by Taber et al. [131] including new EOR categories considering projects reported between 1998 to 2010. Immiscible CO_2 flooding, WAG, hydrocarbon-WAG, surfactant-polymer/alkali were among the newly added EOR categories. Manrique et al. [137] suggested screening criteria for WAG projects on the basis of rock and fluid properties. They proposed the best candidates for WAG injection should have oil viscosity less than 2 cP, oil API^o gravity 30-45, viscosity ratio 1-30, net formation thickness less than 100, and average permeability less than 100. Reservoir depth, temperature and formation type were not considered to be critical for WAG flooding. Sheng [138] proposed screening criteria for AS flooding based on the criteria for both alkaline flooding and surfactant flooding. Typically, the minimum acid number for the crude to be effective for alkaline and AS flooding is 0.3 mg KOH/gm of oil [139]. Moreover surfactant systems are sensitive to high temperatures, so to prevent degradation of surfactants reservoir temperatures requires to be typically less than 200 °F [140]. But, in CO_2 flooding possibility of viscous fingering of the injected gas increases with increases of oil viscosity and consequently CO_2 flooding has been applied mainly in reservoirs having oil viscosity less than or equal to 3 [141]. As ASAG technique is a combination of immiscible CO_2-WAG and chemical (alkali-surfactant) methods, the suggested screening criteria should suit both AS flooding, CO_2 flooding, and WAG injection. However, the synergetic effect should also be contemplated in the suggested criteria of ASAG flooding.

1.12 Importance and Objectives of the Research

Despite its potential as a viable EOR process, the immiscible ASAG flooding has not been extensively studied and only a few investigations have been reported in the literature. So far, ASAG flooding was studied using Berea/Bentheimer cores and sand

packs. The oil recovery potential of immiscible ASAG flooding using real reservoir cores under reservoir conditions has not been reported so far. Thus, a systematic study needs to be conducted to evaluate the performance of ASAG flooding under reservoir conditions to simulate the real field situation. This would facilitate achieving results and conclusions which are more realistic and more field-like. Further, designing the ASAG process requires studying the key parameters affecting the oil recovery process and fine-tuning them for optimal performance. Studying the effects of these operating variables on the performance of ASAG flooding is essential for the rational design of the EOR process. A critical review of the literature suggests that the key operational parameters influencing the performance of ASAG flooding are not available and require investigation.

The desired utilization of the ASAG flooding for improving oil recovery from an oil reservoir requires the usage of the appropriate chemical formulations. For the consistent performance of these formulations, two primary requirements are to be met: lowering the oil-water IFT to ultra-low value and ensuring good mobility control through proper foaming in the reservoir rock. Thus, a systematic approach for formulating the optimal chemical slug for ASAG flooding needs to be followed. Moreover, designing the chemical slug and success of ASAG flooding will also depend on the reservoir rock and fluid properties which usually vary from reservoir to reservoir. Thus, characterizing the reservoir rock and the fluids is an essential prerequisite before embarking on the EOR process.

Based on the existing gaps in the literature, the present research work was undertaken with the following objectives to be fulfilled:

- Characterization of the reservoir rock and fluids:
    i. Routine core analysis of core plugs.

ii. Characterization of the reservoir rock to evaluate its mineralogy and clay content.

iii. Determination of physico-chemical properties of the crude oil for suitability of chemical and gas flooding.

iv. Evaluating the physico-chemical properties of the formation water and preparation of synthetic formation brine (SFB).

- Formulating the optimum chemical slug: This objective refers to the screening of chemicals for the design of optimum chemical formulations for ASAG flooding based foam stability, phase behavior study, IFT measurements, and adsorption study.
- Evaluating the potential of ASAG flooding for EOR through lab-scale core flooding experiments and comparative assessment with other related EOR techniques.
- Investigating the effects of key operational parameters on the performance of ASAG flooding. Thereby, the emphasis will be towards identifying the most suitable operating parameters in order to optimize the ASAG flooding for improving the process efficiency.

1.13 Organization of the Thesis

The contents of the thesis are organized in seven chapters.

Chapter 1 presents a brief introduction to CO_2 flooding for EOR along with its associated problems. It also describes the CO_2-WAG injection and ASAG injection processes. In

addition, this chapter reports the literature review of ASAG flooding and highlights the importance of the present work.

Chapter 2 elaborates upon the materials used, the experimental setup, and the procedures employed in the present study.

Chapter 3 describes the determination of the petrophysical properties and the characterization of reservoir rocks. The analysis of the physic-chemical properties of the crude oil and formation water are also addressed.

Chapter 4 presents the design of optimum chemical formulations for ASAG flooding through foam stability tests, IFT measurements, phase behavior tests, and adsorption tests.

Chapter 5 highlights the potential of ASAG flooding for EOR through lab-scale core flooding experiments. The other EOR techniques like tertiary CGI, CO_2-WAG, SAG, and AS flooding are also discussed for comparative assessment purpose.

Chapter 6 elaborates on the effect of key operating parameters on the performance of ASAG flooding. Also, the application of brine salinity change and preflushing during ASAG flooding are presented.

Chapter 7 briefly summarizes the important findings and conclusions drawn from the work followed by the scope of future research.

CHAPTER 2

Materials and Methods

Materials

Methods

Experimental procedures

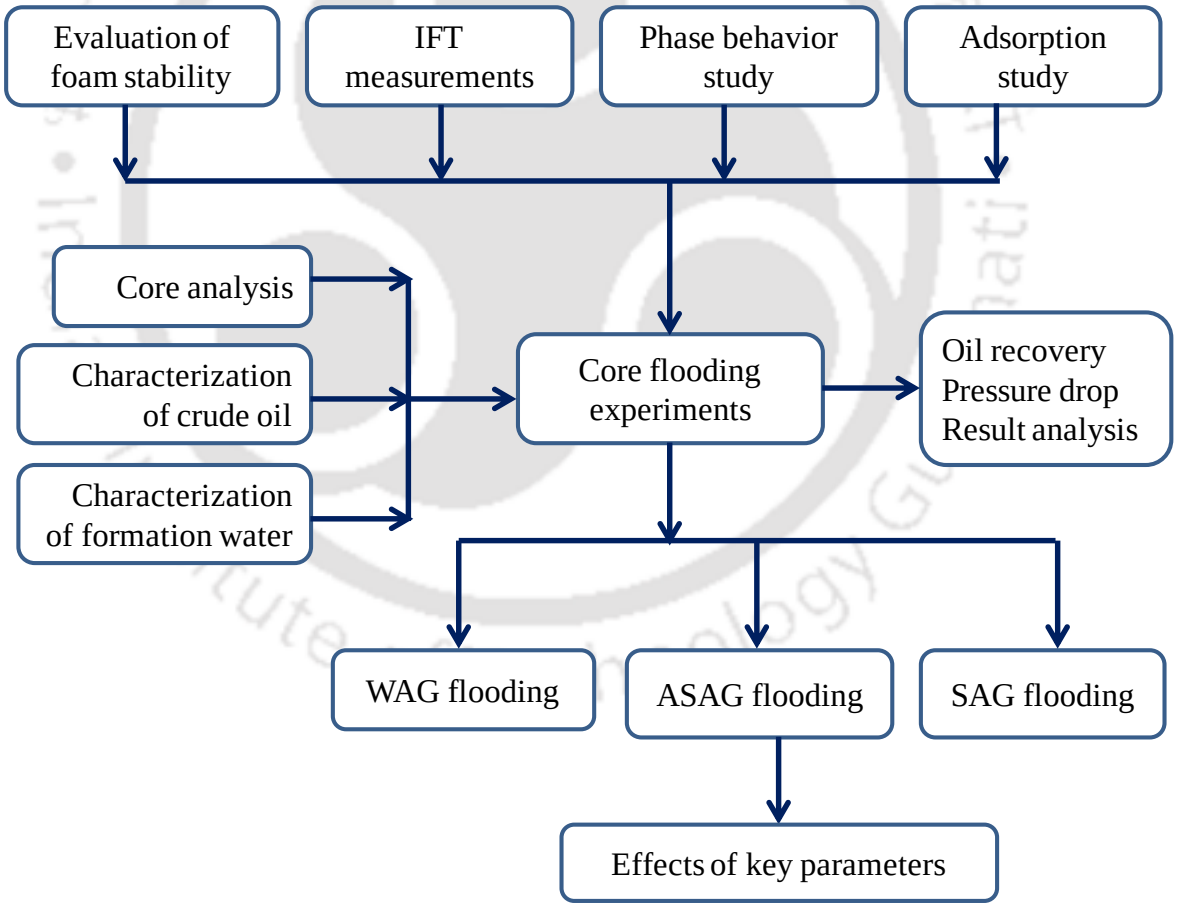

Chapter 2

Materials and Methods

This chapter consists of two sections. The first section presents the details of the chemicals, crude oil, reservoir rocks and formation water used to perform the experiments. The second section summarizes the details of the experimental setup and the procedures adopted for performing the experiments related to the study.

2.1 Materials

The oil field chosen for this study is one of the main crude oil producers of Upper Assam Basin in India, covering an area of about 25 sq km. The oilfield was discovered in the late 1960s and commercial production started from the mid-1970s. The oil-producing zones have been identified as Tipam Sand, Barail Coal Sand, and Barail Main Sand. The Tipam sand is sub-divided into six zones from where the majority of oil production takes place. The sediments are mainly sandstone together with clays and shales. The driving mechanism of the oilfield is mostly depletion drive and the reservoirs were developed through water injection. The reservoir selected for the study is the most salient and extensive one in the oilfield. The reservoir pressure initially was around 3400 psia at a depth of around 3000 meters and the formation temperature is about 70 ^{o}C. However, the present pressure has declined to approximately 1800 psia and is lower than the saturation pressure (2500 psia) of the crude oil.

Oil samples

The crude oil collected from the oilfield was chosen for the study to mimic the reservoir conditions and obtain representative results. The crude oil was separated from

water using separating funnel at a temperature of 35 ^{o}C and centrifuged before carrying out the detailed analysis.

Core samples

Core plugs (3.75 cm diameter and approximately 7 cm length), used for core analysis and core flooding, were cut parallel to bedding plane from conventional core obtained from different depths of the oilfield ranging from (2480-2486), (2925-2943) and (3940 – 3947) m. Prior to core analysis, the core plugs were completely cleaned of impurities followed by drying.

Formation water

Formation water of the same oilfield was also collected and thoroughly analyzed. Synthetic formation brine (SFB) was prepared based on the compositional analysis of the formation water.

Surfactants

As the reservoir rocks were sandstones, anionic and non-ionic categories of surfactants were selected for this study. The surfactants used are shown in Table 2.1. The surfactants SDS, AOS, SDBS and TX-100 were of industrial purity and used without any further treatment. Black liquor (BL) is an anionic water-soluble surfactant whose main constituent is sodium lignosulfonate and effluent of a paper mill of Assam, India. The detailed composition of BL is described in a previous study [142]. BL is used as a secondary (preflushing) surfactant in this study.

Alkali

The alkalis considered for preparing chemical slug along with the surfactants in this work were sodium carbonate, sodium hydroxide, and borax. The details of the alkalis are shown in Table 2.2:

Table 2. 1: Surfactants considered in the present study

Sl. No.	Name	Abbreviation	Chemical formula	Type	Procured/ brought
1.	Sodium dodecyl sulphate	SDS	$NaC_{12}H_{25}SO_4$	Anionic	Merck (India)
2.	(C_{14} – C_{16}) Alfa olefin sulphonate	AOS	R-CH=CH-(CH_2)n-SO_3Na	Anionic	Aman Enterprises, India
3.	Sodium dodecyl benzene sulfonate	SDBS	$C_{18}H_{29}NaO_3S$	Anionic	Sisco Research Laboratories Pvt. Ltd., India
4.	Black liquor	BL	$C_{20}H_{24}Na_2O_{10}S_2$	Anionic	A paper mill in Assam, India
5.	Triton X-100	TX-100	$C_{16}H_{26}O_2$	Non-ionic	Sisco Research Laboratories Pvt. Ltd., India

Table 2. 2: Alkalis considered in the present study

Sl. No.	Name	Chemical formula	Purity (%)	Procured
1.	Sodium carbonate	Na_2CO_3	99	Merck (India) & Renkem
2.	Sodium hydroxide	NaOH	97	
3.	Borax	$Na_2B_4O_7.10H_2O$	99	

Other materials

To perform the characterization of samples and other studies various analytical grade chemicals were used which are listed in Table 2.3.

Table 2. 3: Other chemicals considered in the present study

Sl. No.	Name	Chemical Formula/ Abbreviation	Purity (%)	Procured / Make & Model
1.	Sodium bicarbonate	$NaHCO_3$	99	
2.	Sodium hydroxide	NaOH	99.5	
3.	Calcium chloride	$CaCl_2$	98	
4.	Magnesium chloride	$MgCl_2$	98	
5.	Sodium chloride	NaCl	99	
6.	Potassium bromide	KBr	99.5	Merck Specialities
7.	Toluene	$C_6H_5CH_3$	99.5	Pvt Ltd., India
8.	Xylene	$C_6H_4.2CH_3$	99.5	
9.	Methanol	CH_3OH	99	
10.	Ethyl alcohol	C_2H_5OH	99	
11.	n-Heptane	C_7H_{16}	99	
12.	Potassium hydroxide pellets	KOH	99	
13.	Ethylenediaminetetraacetic acid	EDTA	99	
14.	Phenolphthalein	$C_{20}H_{14}O_4$	99	
15.	Silica gel	Si	99	
16.	Methyl ethyl ketone	$C_2H_5COCH_3$	99.5	

2.2 Experimental Procedures

2.2.1 Core Plug Preparation

The core plugs were cut from the conventional cores with the help of the Core Cutting machine and the Core Plugging machine. Thereafter, they were end faced using the End Facing machine to obtain core plugs that were exactly uniform right angle cylinders. The core plugs were required to be thoroughly cleaned of all interstitial fluids and dried before the determination of their petrophysical properties.

The cleaning of the core plugs was done in the Soxhlet apparatus for about 40 working hours. The solvents used to dissolve and extract oil/brine from the core plugs were a mixture of 50% CH_3OH + 50% C_6H_4 .$2CH_3$. The sample's cleanliness was determined from the color of the solvent that siphoned intermittently from the extractor. After cleaning in the Soxhlet apparatus, the core plugs were again cleaned in ultrasonic cleaner for 10 min, by submerging the samples in acetone solution. The core plugs are then dried at 60 ^oC to remove any moisture present in the pore spaces. Drying times varied for core plugs but usually took from 30 to 50 working hours. The plugs were weighed after a definite interval of time (every 4 hours) till a constant weight was achieved, indicating that the plugs were completely dried.

2.2.2 Determination of Porosity

The bulk volume (BV), grain volume (GV), and pore volume (PV) determination are prerequisites for the laboratory determination of porosity. The BV can be measured with the help of calipers or the Archimedes (buoyancy) principle. The pore volume can be measured by the liquid saturation method or Boyle's Law single-cell method. The grain volume can be measured from the dry weight of core plugs and sand-grain density, or by the Boyle's Law Double-Cell Method [143]. In this study, the BV of the core plugs was measured with the help of calipers and GV was determined with a Helium Porosimeter

(Make: Coretest Systems, Inc, USA; model: TPI-219) which is based on the Boyle's law double cell method. In this system, gas was allowed to flow into the reference cell of known volume (V_r) at a predetermined reference pressure (100 to 200 psig). The reference cell gas was then admitted into a connected chamber of known volume containing the core plug. The GV was calculated applying by Boyle's law using the following equation:

$$V_g = V_c - V_r\left(\frac{P_1}{P_2} - 1\right) \tag{2.1}$$

where V_g = GV of the core plug,

V_c = Sample chamber volume

V_r = Reference chamber volume

P_1 = Initial reference volume pressure

P_2 = Final lower equilibrium pressure

2.2.3 Determination of Permeability

Permeability is measured, using Darcy's equation, by passing a fluid of known viscosity through a core plug while measuring the flow rate and the pressure drop across the core plug. Darcy's equation can be expressed as [18]:

$$K = \frac{q\,\mu\,L}{A\,\Delta P} \tag{2.2}$$

where K = permeability of the rock (Darcy)

q = Volumetric flow rate (cm^3/sec)

A = Total cross-sectional of the core sample (cm^2)

L = Length of core sample (cm)

μ = Fluid viscosity (cP)

$\Delta P = P_1 - P_2$ = Pressure differential across core (atm).

The permeability measured at 100% saturation of a single-phase (liquid) is called the absolute permeability of the rock. Frequently dry gas is used in permeability determination, because its small molecules rapidly penetrate the microscopic pores, has minimum fluid-rock reaction, has high diffusivity and is convenient. However, the measurement of the permeability is mainly done in the low (laminar/viscous) flow rate region, where the pressure is proportional to the flow rate [18]. Applying the ideal gas law and Darcy's law, the gas flow equation can be expressed as:

$$K_g = \frac{2000\ \mu_g\ L\ P_b\ q_{sc}}{A\left(P_1^{\ 2} - P_2^{\ 2}\right)} \tag{2.3}$$

where K_g = Gas permeability (mD)

μ_g = Gas viscosity (cp)

P_b = Base pressure (atm)

P_1 = Inlet pressure (atm)

P_2 = Outlet pressure (atm)

q_{sc} = Gas flow rate at standard conditions (cm^3/sec).

The permeability measured by flowing gas is observed to be greater than the permeability obtained by flowing a liquid. Klinkenberg [144] postulated that the higher value was because of the greater flow rate of gas at a given ΔP and gas slippage at the sand grain surface. It was observed that for a given core plug the mean pressure (P_m) could be used to calculate the permeability.

$$P_m = \frac{P_1 + P_2}{2} \tag{2.4}$$

If measured permeability is plotted versus $1/P_m$ and extrapolated to the point where $1/P_m$ = 0 (P_m = infinity), the corresponding permeability would be approximately equal to the liquid permeability. In this work, liquid and gas permeabilities of core plugs were measured experimentally and the results were correlated. The liquid permeabilities were

measured with the Liquid Permeameter (Make: Vinci Technologies, France; Model: LiquidPerm) and the gas permeabilities with Gas Permeameter (Make: Coretest Systems, Inc., USA, Model: TKA-209). The measured gas permeability values were used to determine the liquid permeability applying the Klinkenberg principle.

2.2.4 XRD and FESEM Study

X-ray diffraction (XRD): Powder X-ray diffraction of the rock sample was conducted in a Bucker X-ray D8 advance diffractometer. Clean core samples were grounded to fine powder and X-ray diffractogram were collected for a range of Bragg angle 2θ (7^o to 90^o) with 0.03 step size and 1^o/min scanning speed. Zeiss Sigma Field Emission Scanning Electron Microscope (FESEM) was used identification of clay minerals in rock sample. The sample was prepared by gently breaking the core plug. The sample was then attached to a specimen plug and coated with gold to obtain a clear image of the rock sample. The FESEM images were obtained and compared with standard images to identify clay minerals.

2.2.5 Characterization of Crude Oil

The laboratory analysis of crude oil is necessary for characterizing a particular reservoir fluid sample and also to make a preliminary assessment of the effectiveness of EOR schemes. In this study, the crude oil was analyzed for API gravity, viscosity, asphaltene-resin content, wax content, pour point, and acid number.

Density is the mass of liquid per unit volume, while specific gravity is the ratio of the mass of a given volume of liquid at 15.5^0C to the mass of an equal volume of pure water at the same temperature. The ASTM D1298-67 [IP 150/68] hydrometer method was followed for the determination of the density of crude oil samples. The hydrometer is made of glass, graduated in units of density. The API gravity was calculated from the specific gravity by using the following equation:

$$API^0 \text{ gravity} = \frac{141.5}{\text{Sp.gr. at}15.6^0C/15.6^0C} - 131.5 \quad (2.5)$$

The dead oil viscosity of the oil samples was measured following the ASTM D445-65 method using U-tube reverse flow viscometer (type: BS/IP/RF). The selected viscometer was charged with crude oil and allowed to remain in the bath long enough to reach the test temperature. Suction pressure was used to adjust the head level of the oil sample to the first timing mark of the capillary arm of the viscometer. Allowing the sample to flow freely, the time (in sec) required for the meniscus to pass from the first timing mark to the second was recorded. The kinematic viscosity was calculated as follows:

$$\text{Kinematic viscosity (cSt)} = Ct \quad (2.6)$$

where C = Calibration constant of the viscometer (cSt/sec),

t = Flow time (sec).

From the kinematic viscosity, the dynamic viscosity was calculated as follows:

$$\text{Dynamic viscosity (cP)} = \rho\gamma \quad (2.7)$$

where ρ = Density at the same temperature as kinematic viscosity,

γ = Kinematic viscosity (cSt).

The experiments were repeated for three times and the average values are considered.

As per standard test method IP 15/67, the pour point is the lowest temperature, expressed as a multiple of 3, at which crude oil is observed to flow when cooled and examined under prescribed conditions. The oil sample was poured into a cylindrical test jar (25 mm OD and 60 mm in height). The oil was initially slightly heated in a hot water bath to ensure it flowed into test jar. The temperature of the cooling bath was maintained at 0 to 2 ^oC. The specimen was first examined at 30 ^oC. The test jar was tilted just enough to ascertain if there was movement of the specimen. If movement was noticed, the test jar was replaced in the jacket and the test repeated again at 3^0C lower. This was continued

until the point when the specimen showed no movement when the test jar was held in a horizontal position for 5 sec. The reading observed in the test thermometer was recorded. As per the method, 3 ^{o}C was to be added to the temperature recorded, which gives the pour point of the crude oil [145].

The asphaltene content of oil samples was measured by asphaltene precipitation with n-heptane (ASTM D2007-80) as reported by Bon [146]. 5 gm of the crude oil was mixed with 150 ml of n-heptane. The mixture was agitated with a stirrer for 1 hour and filtered through preweighted 125 mm No.42 Whatmann filter paper. The filtrate was used for the determination of resin content. The filter paper with solids was dried in an oven at a temperature of 60 ^{0}C until a constant weight was obtained. The solids from the filter were re-dissolved with toluene and filtered again through a new filter paper. The filter paper with solids was again dried in the oven at a temperature of 60 ^{o}C until constant weight obtained. From the measured change in weight of the filter paper, asphaltene content of the crude oil was determined accordingly. To estimate the resin content, the filtrate was mixed with 200 g of silica gel and the mixture was continuously stirred with heating for 1 hour so that the resins were adsorbed to the silica gel. After cooling for one overnight, the liquid portion was filtered. The silica gel was placed in the thimble of the soxhlet apparatus and extracted with toluene: methanol (90:10) solvent until the silica gel becomes free from resin. The solvent was evaporated in the water bath followed by drying in the oven, and eventually, the weight of the resin was determined [147].

The filtrate after removing asphaltene and resin was concentrated to about 50 ml on the water bath. The concentrate was mixed with 200 ml of methyl ethyl ketone (MEK) and cooled in a deep freezer. The mixture was kept overnight in the freezer to allow for possible wax precipitation. Finally, the mixture was filtered with Whatmann filter paper (size 42), dried in ambient temperature and weighted to determine the wax content [148].

To measure the acid number of crude oil, 1 ml of the phenolphthalein solution was added to 50 ml of C_2H_5OH in a conical flask and the mixture was heated to 40-50 ^oC. The mixture was neutralized with standard 0.1 N KOH solution. The neutralized alcohol was added to 10 gm of crude oil in a 250 ml conical flask and the mixture was heated to boiling for 5 min with agitation. Further 1 ml of phenolphthalein solution was added to the mixture and cooled to 45 ^oC. Finally, the solution was titrated quickly with the KOH solution. The acid number of the oil was calculated using the formula [145]:

$$AN = 56.1 \frac{NV}{W} \tag{2.8}$$

where, AN = Acid number in mg KOH/g of sample

V = Volume of KOH solution in ml

N = Normality of the KOH solution

W = Weight of the sample in gm.

The crude oil was also analyzed with FTIR spectrophotometer to determine the functional groups present mainly the existence of carboxylic acids. For the analysis, analytical grade potassium bromide (KBr) pellets were prepared and a small drop of the crude oil was added to the prepared KBr disc.

2.2.6 Characterization of Formation Water

The pH and total dissolved solids (TDS) values of the formation water were measured with Water Analyser (Make: Systronics; Model: 371). The density was measured with a pycnometer and viscosity using U-tube viscometer. The positive ionic compositions like Na^+, Ca^{++} and K^+ were measured with Flame Photometer (Make: Systronics, Model: 128), whereas Mg^{++} was measured by titration with EDTA. For the negative ionic compositions like Cl^- and HCO_3^-, titrations were performed with $AgNO_3$ solution and HCl acid respectively.

2.2.7 Evaluation of Foam Stability

Foamability and foam stability are two important properties of foam that influence its generation and propagation through the reservoir rocks during foam-based EOR applications. Foamability is defined as the capability of the surfactants to form foam, and foam stability is described by the changes in foam volume with respect to time, following foam generation [149]. In foam stability tests, surfactants were tested for their ability to form stable foam and to provide suitable concentration for preparation of formulation. In this work, the foam stability of different surfactants was studied to screen them and to select optimum surfactant concentrations. These optimal surfactant solutions displaying the best foaming behavior are expected to provide better mobility control during the core flooding experiments.

The foam stability tests were initially performed based on the standard shaking method [150] to determine the ability of surfactants to form strong/stable foam. A fixed amount (5 ml) of aqueous solution of surfactant was taken in test tubes and shaken in a rotary mixer (for 6 hours at a constant speed of 50 rpm) which resulted in the formation of foam above the liquid column. The foam volume was recorded by visual observation at a regular interval of time as the foam decayed at room temperature. The time taken for the foam to decay to half of the initial value was particularly noted with care. This time is taken as the half-decay time ($t_{1/2}$) which signifies foam stability. A stronger foam formation and consequently better surfactant performance are indicated by a longer half-decay time [151]. For the tests involving the presence of crude oil, 0.5 ml of crude oil (at 10 vol%) was added to the top of the 5 ml surfactant solution before the test tubes were shaken for foam generation. Particular care was taken to ensure that experimental

conditions were identical. All the experiments were performed a minimum of three times and the average values are noted.

The foam stability tests were performed with CO_2 gas in a foam column test setup (Fig. 2.1), which consisted of a visual column of toughened glass, where the 20 ml of surfactant solution along with 2 ml of crude oil (10 vol%) was placed. The visual glass column was housed inside a hot air oven where the temperature was set to reservoir temperature (70 ^{0}C). The column filled with surfactant solution and crude oil was allowed to stand inside the oven for a sufficient period of time (1 hour) so that the contents of the column attain the set temperature. Thereafter, a constant volume of CO_2 gas was injected below the surfactant solution for 5 min from a CO_2 cylinder connected to the column via a mass flow controller (MFC). This resulted in the formation of foam in the glass column. The foam volume above the liquid level with respect to time was regularly monitored and recorded. Special care was taken to record the $t_{1/2}$. Selected tests were repeated to assess the consistency of the results.

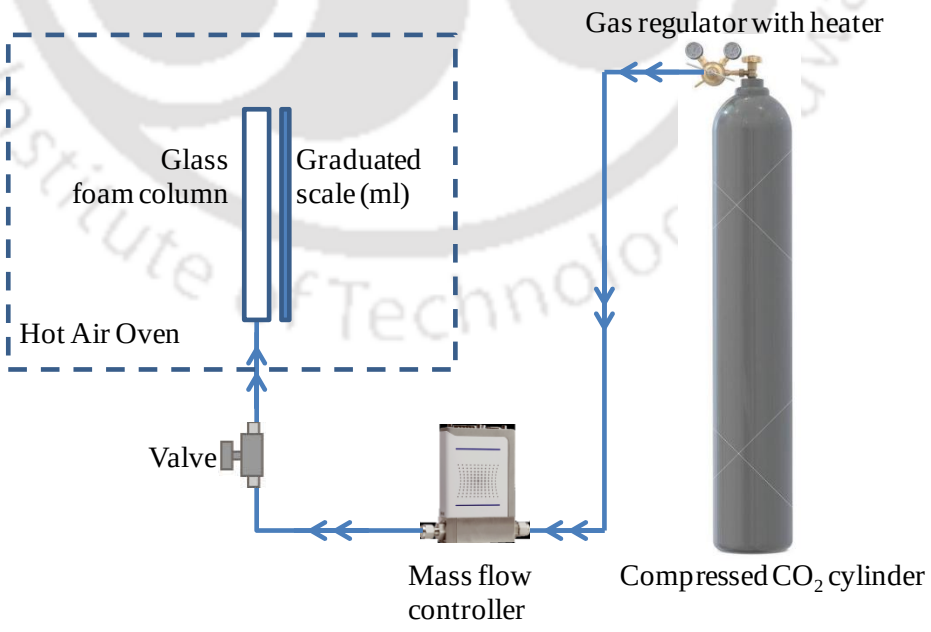

Fig. 2.1: Schematic diagram of foam column test setup [[151], modified]

2.2.8 Interfacial Tension Measurements

A spinning drop tensiometer (Make: Grace; Model: M6500) was used to measure the equilibrium IFT between crude oil (oleic phase) and AS solutions (aqueous phase) at reservoir temperature (70 ^{o}C). To achieve the required oil droplet length to diameter (L/D) ratio greater than 4, a fixed rotational speed of 6500 rpm was maintained in the experiments. From the image captured, the oil droplet diameter was measured with the Motic Images Plus 2.0 software. Finally, the equilibrium IFT was calculated by using Vonnegut's equation [152]:

$$\lambda = \frac{\Delta\rho\ \omega^2}{4}\ r^3 \qquad (2.9)$$

where λ = IFT, mN/m

$\Delta\rho$ = Density difference between the oleic and aqueous phases, g/cm^3

ω = Angular velocity, rad/s

r = Radius of the oil drop in the sample tube, cm.

2.2.9 Phase Behavior Study

Aqueous stability tests were performed to investigate the solubility and stability of chemicals in electrolyte solution. In this test, appropriate amounts of surfactants, alkali, and brine are intimately mixed together without adding oil and allowed to settle for 48 hours at reservoir temperature, to observe if any deposition, separation or cloudiness occurs.

Microemulsions are thermodynamically stable dispersion of water and oil containing a significant amount of both the phases and stabilized by a surfactant [153]. Based on the continuous and dispersed phases, microemulsions can be either water-in-oil (W/O) or oil-in-water (O/W). The phase behavior of microemulsion for oil, surfactant, and brine was first described by Winsor in 1954. Microemulsion phase behavior is a function of salinity, temperature, nature of the oil, type of the surfactant and the cosurfactant, and the water-oil ratio (WOR). In particular, brine salinity greatly influences the phase

behavior of surfactant solutions [154]. As the salinity of brine is increased, three types of microemulsions form: type I or O/W microemulsions, type II or W/O microemulsion, and type III or bicontinuous middle phase microemulsion [155]. Normally, phase behavior tests are done to determine the optimal brine salinity of surfactant solutions that have high oil and water solubilization ratios. Higher solubilization ratios will achieve ultra-low IFT (10^{-2} to 10^{-3} mN/m) as per Huh's equation [156], thus leading to higher oil recovery. In this study, solutions containing the selected concentrations of surfactant and alkali were prepared at different SFB salinities. The solution and crude oil were then mixed in small test tubes in the water-oil ratio of 2:1 and were agitated in rotary mixer at 50 rpm for 6 hours for proper mixing. Further, the test tubes were arranged in order of salinity in racks and kept in the oven (at 70 ^{o}C) to equilibrate. The fluid interfaces in the test tubes were inspected at regular intervals of 12 hours for a month to observe for Winsor type III microemulsions formation.

2.2.10 Adsorption Study

The surfactants injected during ASAG flooding are susceptible to be adsorbed due to their interaction with reservoir rocks causing the loss of valuable surfactant/foaming agent. Thus, the ability of the surfactant solutions to lower the oil-water IFT is reduced. Additionally, the generation and propagation of foam through the reservoir rock is also affected by surfactant adsorption. So, minimizing the surfactant loss during the ASAG process should be considered for economic reasons. It is mainly the solution and the solid surface properties that influence the surfactant adsorption. Both static adsorption and dynamic adsorption studies were performed to study surfactant adsorption onto the reservoir rock. Static adsorption test was done based on the depletion method [157]. In this method, the change in the surfactant concentration (depletion) after contact with crushed rock samples was measured and assumed to be adsorbed. 1 g of the rock sample (60 – 70 mesh size) was mixed with 10 ml of surfactant solution at various concentrations. The mixtures were mixed for 8 hours in a rotary mixer followed by decantation. The samples were then centrifuged at 5000 rpm for 30 minutes and then filtered by filter paper. The

UV-Vis Spectrophotometer (Make: Labman; Model: LMSP – UV 1900) was used to determine the equilibrium concentrations of the surfactant solutions. The sample preparation of the SDS surfactant was done by the method described in the literature [66, 158]. Equal volumes of SDS solution and methylene blue reagent (250 mg methylene blue, 50 gm Na_2SO_4, and 10 ml of H_2SO_4 per liter of distilled water) were mixed. The mixture was extracted with ethyl acetate which resulted in the formation of two phases. The upper liquid phase was taken and analyzed by the UV-Vis spectrophotometer after dilution. The adsorption spectra of SDS and AOS [Figure 2.2 (a) – (b)] showed the maximum adsorption (λ_{max}) at wavelengths of 655 nm and 216 nm respectively. The calibration curves of surfactants were obtained by plotting absorbance versus concentration and fitting the best straight line through the points. The standard calibration curves of SDS and AOS are shown in Fig. 2.3 (a) – (b) respectively. The amount of surfactant adsorbed on the rock sample (in mg/g) was calculated by the following relation [157]

$$\text{Amount of surfactant adsorbed} = \left(C_o - C_e\right)\frac{V}{m} \tag{2.10}$$

where C_o and C_e are the initial and equilibrium concentrations of surfactants (mg/l) respectively, V is the volume of the surfactant solution (l), and m is the weight of the rock samples (g). The adsorption isotherms were determined at a constant temperature from the relationship between the amount of surfactant adsorbed per unit mass and the equilibrium surfactant concentration. The dynamic adsorption of surfactant (AOS) onto the core plug was performed in a core flooding apparatus at reservoir temperature (70 ^{o}C). Before placing in the Hassler core holder, the core plug was saturated with SFB. Thereafter, several pore volume (PV) of SFB was injected at constant pressure until equilibrium conditions were achieved. This was followed by 10 PV of surfactant solution (at 0.5 wt% concentration) injection through the core plug at a constant pressure. The injection of 10 PVs was sufficient to achieve an equilibrium state. The effluents produced from the core plug outlet were collected in measuring cylinders for every PV, and their concentrations were analyzed [159]. The amount of surfactant adsorbed was determined as follows [160]

$$\text{Adsorption (mg/g)} = \frac{\sum_{i=1}^{N} (C_{in} - C_{out}) \text{ x } V_i}{W} \quad (2.11)$$

where C_{in} is the concentration of surfactant injected (mg/g), C_{out} is the concentration of surfactant solution coming out of the core plug at each PV (mg/g), N is the number of the PV of surfactant solution injected, V_i is the total volume of surfactant solution injected, and W is the dry weight of the core plug (g).

2.2.11 Core Flooding Experiments

A lab-scale core flooding apparatus was used to perform the core flooding experiments (Fig. 2.4). Core plugs were thoroughly cleaned (using the procedure described in Section 2.2.1) and dried prior to placing in the core holder. Three hydraulic pumps were used to displace brine, crude oil, and chemical solution. Another hydraulic pump was connected to the Hassler core holder for supplying the confining pressure, which was always maintained 500 – 700 psi higher than the upstream injection pressure. CO_2 gas was supplied from a cylinder connected with regulator-preheater assembly and MFC. In the downstream side of the core holder, a back pressure regulator (BPR) was used to maintain a constant back pressure of 300 psi [122]. A hot air blower was used to heat the chamber housing the core holder and maintain a constant reservoir temperature (70 ^{o}C). The temperature inside the core holder was monitored using Pt100 RTD temperature sensor. The probe end of the sensor was terminated in a connection head located on the end plug of the core holder. To read the temperature, the RTD element was connected to the digital temperature controller installed in the scanner where the output temperature reading was displayed. The inlet, outlet and confining pressures of the core holder were measured by using pressure transducer and stored automatically in a computer at regular time intervals. The presetting of the time interval was done through the control panel of the core flooding apparatus. Additionally, a 3-way Tee joint connecting gas cylinder, pumps and upstream end of the core holder, facilitated the alternate injection of liquids and gas.

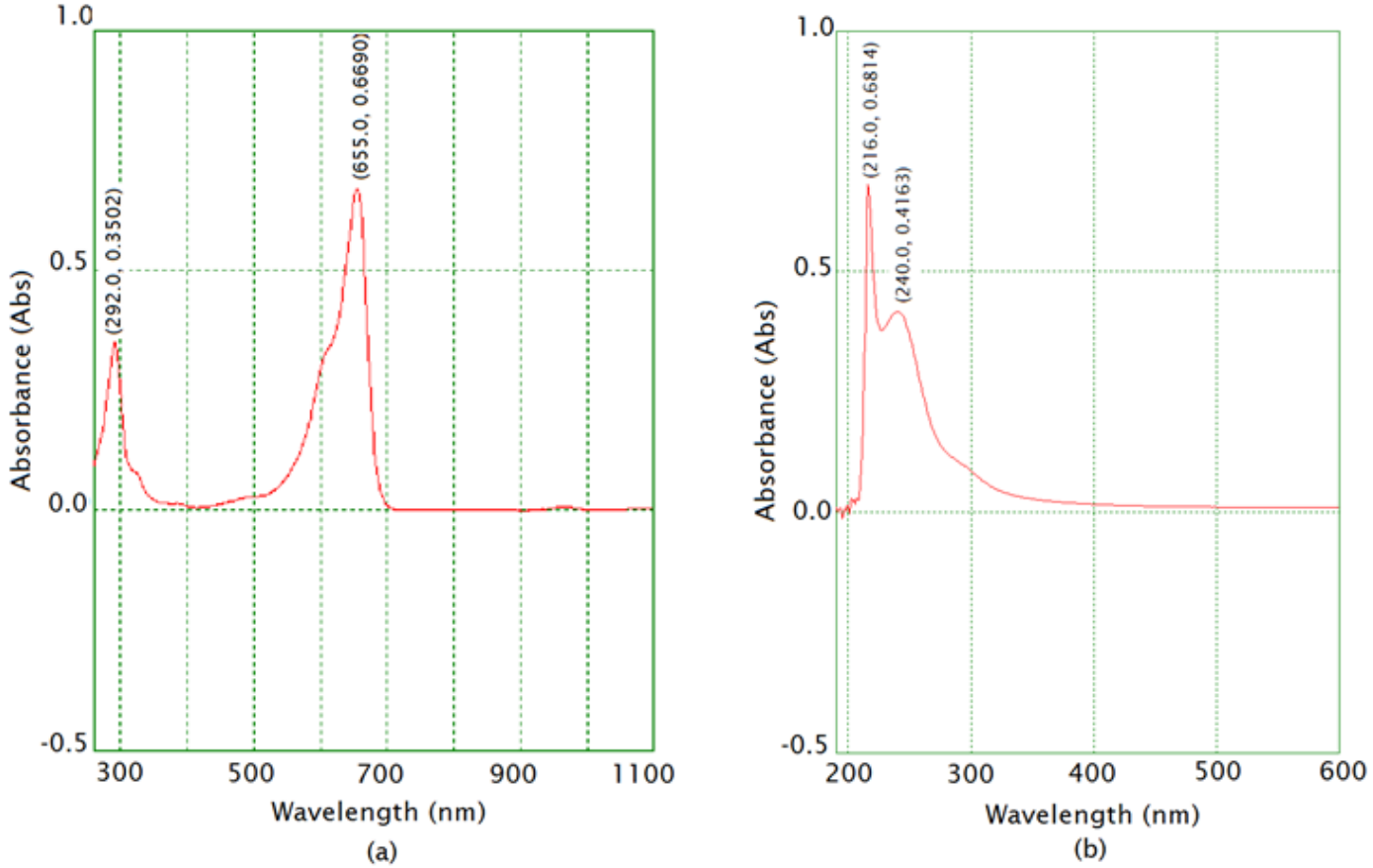

Fig. 2.2: UV-Vis adsorption spectra of the surfactants: (a) SDS and (b) AOS

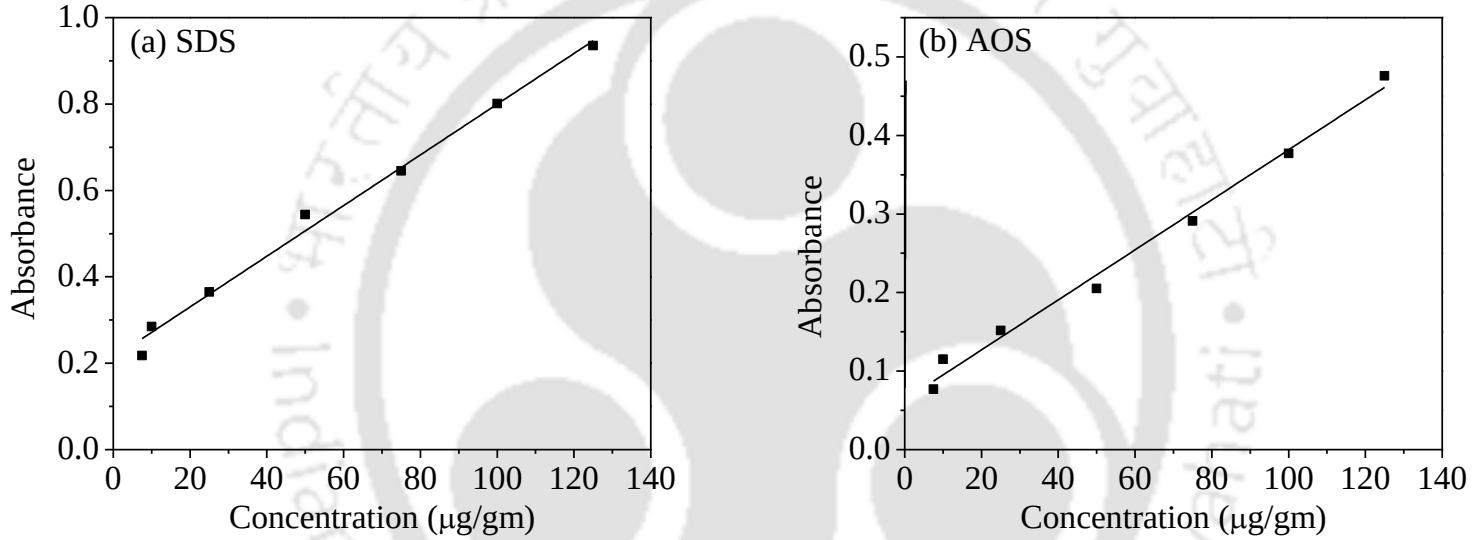

Fig. 2.3: Calibration curves of the surfactants: (a) SDS and (b) AOS

In the first step, air was removed from the core plug and flow lines by flushing CO_2 for 30 minutes. Then, CO_2 was removed from the system by vacuuming for 6 hours. Brine saturation was done by injecting several PVs of SFB at a constant rate to fully saturate the core plug at room temperature (28 ^oC) and to achieve steady-state flow conditions. After that, they were flooded in the core holder (as shown in figure 1) by formation brine at various pore volumes to ensure that all pores were fully saturated with the brine.

The absolute permeability (K_{abs}) of the core plug to SFB was calculated by applying the standard Darcy's equation by injecting SFB at different pressures. In the next step, crude oil was injected at constant pressure through the brine-saturated core plug until pressure drop (ΔP) was stable and no more water was produced. This indicated that connate water saturation was reached. The irreducible water saturation (S_{wc}) and original oil in place (OOIP) were calculated considering the water produced and the net change in weight of the core plug. Thereafter, the oil-saturated core plug was kept in the oven at 70 ^oC for 24 hours for allowing the system to equilibrate. During secondary water flooding, SFB was injected at a constant pressure to recover the crude oil from the core plug at reservoir temperature (70 ^oC). The water flooding was stopped after 4 PVs of SFB injection when no more oil was recovered, and only water was produced. Subsequent to secondary water flooding, the residual oil in the core plug was recovered by applying different EOR injection schemes. During WAG injection, liquids and gas/CO_2 were alternately injected in small slugs with a total fluid injection of 2 PV. The liquid was injected at constant pressure (~ 500 psi) and the volumetric injection rate of gas was maintained constant (0.2 ml/min) through the mass flow controller (MFC). The EOR scheme was followed by the extended water flooding (EWF) where 4 PVs of SFB were further injected to produce any remaining residual oil in the core plug. The produced fluids were collected in measuring cylinders every 0.25 PV and then centrifuged for separating the oil and the water phases.

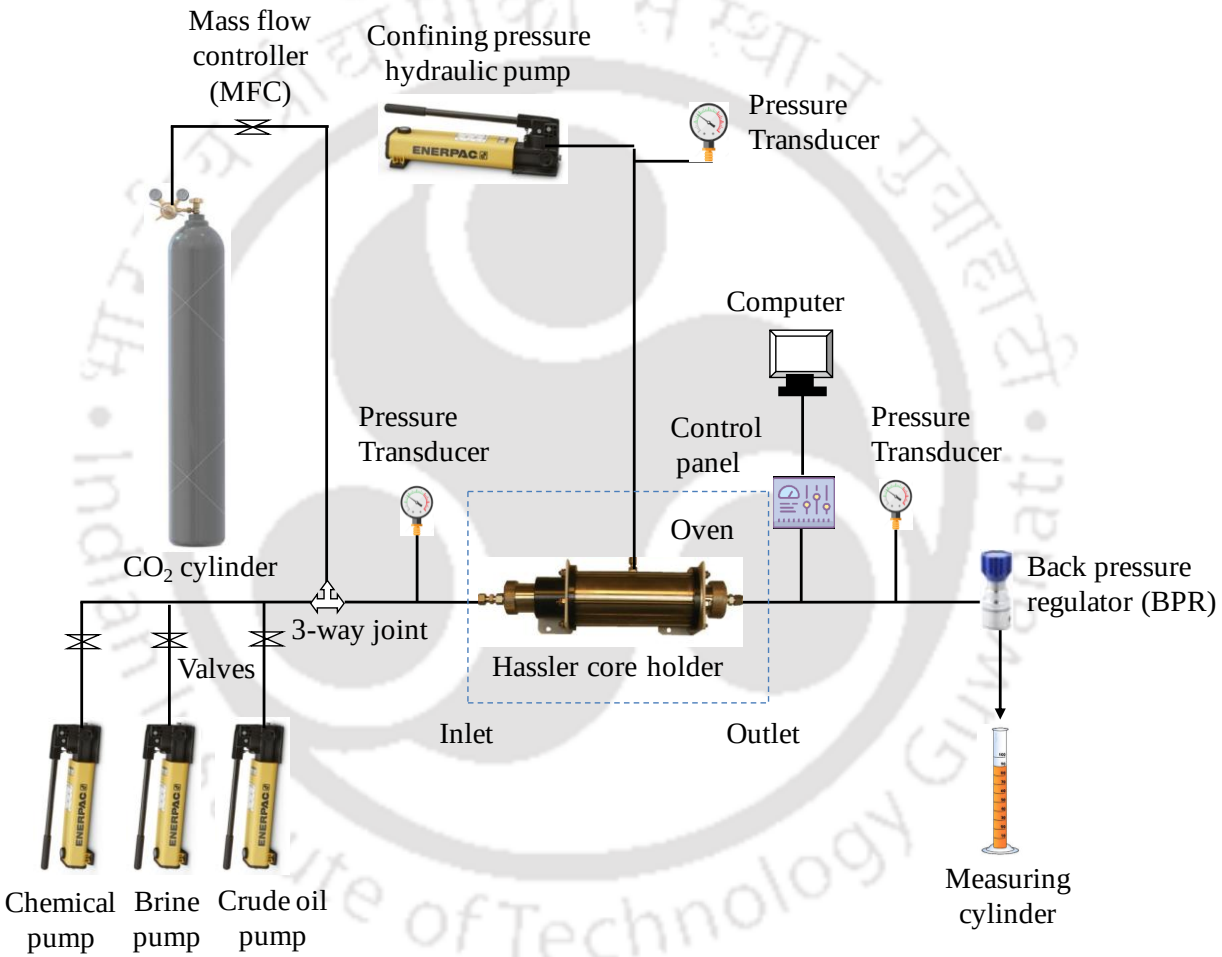

Fig. 2.4: Schematic representation of core flooding apparatus

CHAPTER 3

Reservoir Rock and Fluid Analyses

Porosity and permeability of core plugs

Type of crude oil

Synthetic formation brine

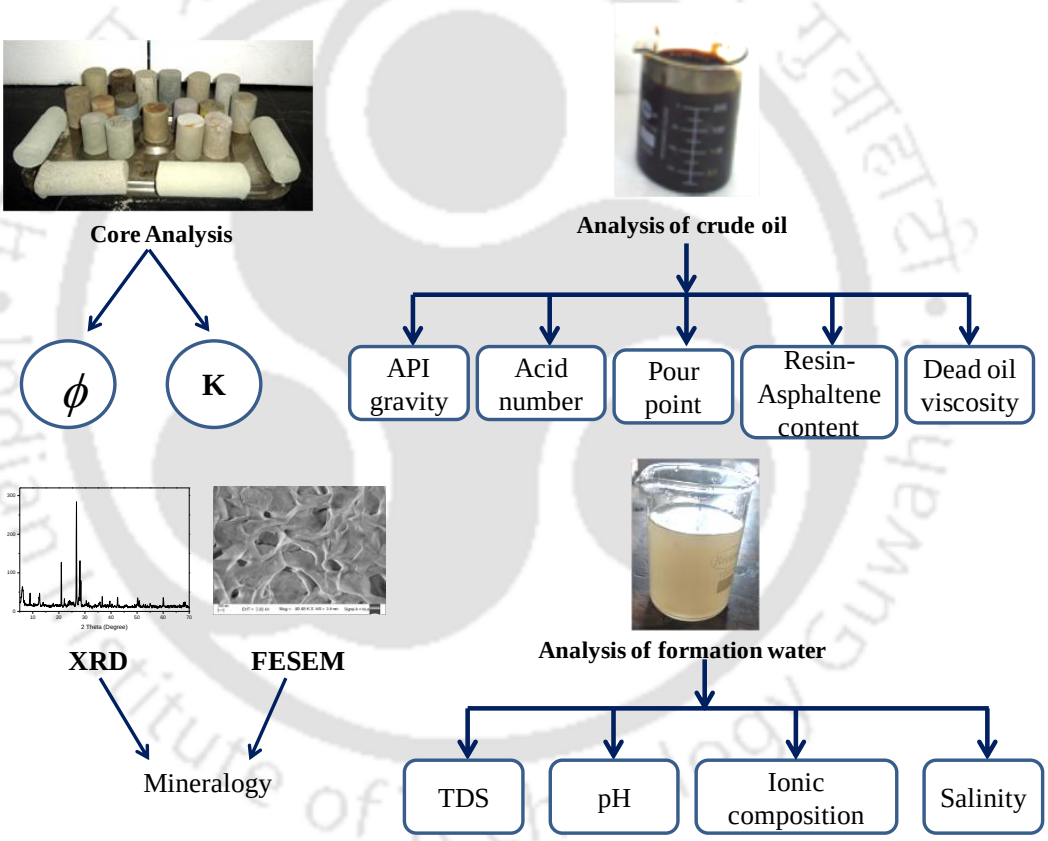

Chapter 3

Reservoir Rock and Fluid Analyses

This chapter consists of three sections. The first section describes the core analysis which includes the core plug preparation along with the determination of porosity and permeability. The reservoir rock characterization with XRD and FESEM analysis also forms part of this section. The second section presents the analysis of the physical and chemical properties of crude oil. The last section summarizes the physical and chemical analysis of the formation water.

3.1 Core Analysis

Core analysis of reservoir rocks samples provides a direct and quantitative evaluation of important reservoir properties. These properties assist in accurately describing the reservoir rocks, total fluid contents, fluid distribution, and flow behavior. The static and dynamic reservoir models can also be designed based on formation evaluation done with core analysis [161]. For core analysis, a whole core is acquired from a particular depth of the producing formation through coring operation. Coring operation involves lowering the drilling string, with the core cutting bit at the end, to the desired depth of the formation and retrieving the whole core inside the core barrel. A typical conventional core is 7 – 13 cm in diameter and 900 – 1700 cm in length. The other type of cores are the sidewall cores. They are much smaller than the conventional cores, 2.3 cm in diameter and 5 cm in length. As it is not possible to use whole/conventional cores in the laboratory for core analysis, short representative core plugs (2.54 – 3.81 cm in diameter) from the large conventional cores are selected. The core plugs are cut from the conventional cores parallel to the bedding plane, so that measurements of horizontal

permeability may be made (Fig. 3.1). The core plugs used in this work were 3.75 cm in diameter and 6 – 8 cm in length.

There are basically two main types of core analysis performed on core plugs. Conventional/routine core analysis which includes measurements of petrophysical properties of core plugs like porosity, permeability, and fluid saturation together with the evaluation of grain density, rock texture, and lithology. Special core analyses are conducted for measuring specific properties including capillary pressure, relative permeability test, wettability test, electrical properties, formation damage, and recovery factors. These special tests are also conducted to characterize reservoirs for EOR and to study the fluid-rock interactions. Both the routine and special core analyses were performed in this study. The routine core analysis for the measurement of porosity & permeability of core plugs is reported in this chapter and special core analysis (core flooding) in later chapters. Prior to core analysis, the core plugs were required to be cleaned and dried. The detailed process of cleaning and drying requires about 80 working hours as described in Section 2.2 and Subsection 2.2.1 .

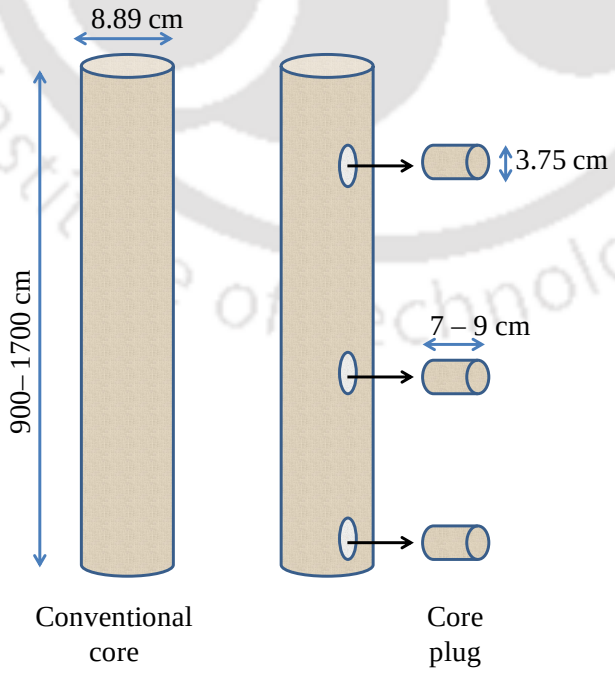

Fig. 3.1: Schematic representation of conventional cores and core plugs

3.1.1 Determination of Porosity

One of the most important reservoir rock properties is porosity, which is a measure of the space available for the storage of hydrocarbons. There are two distinct types of porosity of reservoir rock: absolute porosity, which is the ratio of the total pore space in the rock to that of the bulk volume; and effective porosity, which is the percentage of interconnected pore space with respect to the bulk volume. It is the effective porosity that is important in most reservoir engineering calculations as it represents the pore space that are interconnected and containing the recoverable crude oil.

$$\text{Porosity, } \phi = \frac{\text{Pore volume}}{\text{Bulk volume}} = \frac{\text{Bulk volume - Grain volume}}{\text{Bulk volume}} \tag{3.1}$$

The grain volume of the core plugs was measured with the Helium Porosimeter and the porosities were calculated using Eq. (3.1). The grain volume measurements were repeated and the average of three values was taken to calculate the porosity of each core plug. The results of the porosity measurements are presented in Table 3.1 and the sample calculations are summarized in Appendix A. As can be seen, the values of porosities of the core plugs vary from 25 – 28% at a shallower depth, 19 – 21% at intermediate depths, and 11 – 13% at deeper depths. Similar values of porosity of the Upper Assam oilfield core samples were reported earlier [162]. The porosity/depth data of the core plugs are summarized in Table 3.2. The low porosity values were observed with core plugs obtained from deeper depth (3940 – 3947 m), while relatively high porosity for core plugs from depths of 2480 – 2486 m. Thus, the porosities of the core plugs were found to decrease with the depth of the formation from where the conventional cores were collected. This is consistent with the known fact that porosity bears an inverse correlation with depth. The porosity-depth correlation is influenced by many factors but the most obvious reason for this inverse relation is owing to the combined effects of compaction and cementation

[163]. An increase in the depth of progressive burial increase the overburden pressure or compaction resulting in the reduction of porosity. As the effective stress and temperature increase with the burial depth, the porosity depth correlations are also dependent on effective stress. The other factors which influence porosity profiles are subsidence history, oil/gas saturation, and mineralogy. However, it is difficult to isolate the effect of any single factor or process responsible for the observed relation [164].

Table 3.1: Porosity measurement of core plugs from different depths

Core Plug ID	Depth (m)	Diameter (cm)	Length (cm)	Bulk volume (cm^3)	Weight (g)	Grain Volume (cm^3)	Porosity (%)
CP1	2480 - 2486	3.75	7.75	85.61	195.74	63.45	25.69
CP2		3.75	7.02	77.54	161.15	56.16	27.57
CP3		3.75	6.81	75.02	156.11	54.65	27.15
CP4	2925 - 2943	3.75	8.11	89.58	199.34	71.28	20.44
CP5		3.75	7.43	82.07	186.28	65.52	20.14
CP6		3.75	6.90	76.22	159.61	61.03	19.96
CP7		3.75	6.95	76.77	160.27	60.81	20.76
CP8		3.75	7.50	82.85	188.82	65.91	20.49
CP9		3.75	7.61	84.06	190.36	66.37	21.04
CP10		3.75	6.75	74.56	154.72	59.95	19.57
CP11		3.75	7.55	83.40	189.83	65.50	21.46
CP12		3.75	7.00	77.32	158.54	61.81	20.09
CP13		3.75	6.89	76.11	159.34	60.44	20.52
CP14		3.75	7.48	82.63	187.86	65.76	20.39
CP15		3.75	7.53	83.18	188.65	65.41	21.35
CP16		3.75	6.97	76.99	162.32	61.04	20.73
CP17		3.75	7.60	83.95	189.69	66.09	21.27
CP18	3940 - 3947	3.75	7.58	83.73	188.16	73.49	12.23
CP19		3.75	6.88	76.00	156.97	67.15	11.64
CP20		3.75	7.50	82.85	188.56	73.36	11.45

Table 3. 2: Porosity and permeability values of core plugs as a function of depth

Depth (m)	2480 - 2486	2925 - 2943	3940 - 3947
Porosity range (%)	25 - 28	19 - 21	11 – 13
Measured liquid permeability (mD)	27.21	6.32	3.25
Estimated liquid permeability (mD)	31 - 39	7 - 10	4 – 7

3.1.2 Determination of Permeability

The permeability of the core plugs was determined using the procedure described in Section 2.2.3. The liquid permeability experimental results of all the core plugs are summarized in Table 3.3**,** while Table 3.4 presents the gas permeability measurement results of three core plugs of different depths. The values of the liquid permeability of the core plugs ranged from 3 – 30 mD, while the gas permeability varied from 16 – 47 mD. The measured range of permeability of the core plugs classifies the Upper Assam formation as fair to moderate permeability reservoirs [165]. The permeability measured by flowing gas (N_2) was observed to be greater than the permeability value obtained by flowing liquid (formation brine). The observed difference between liquid and gas permeability values of the core plugs was due to the Klinkenberg effect (discussed earlier). The porosity and permeability of the core plugs were directly related as more porous ones were found to be more permeable and vice-versa (Table 3.2). However, the effects of a number of parameters like grain size, compaction, packing, and diagenetic processes related to development influences the porosity-permeability of a particular formation [166]. Nind [167] reported that there is no direct correlation for porosity and permeability, however, permeability generally increases with porosity for sandstones reservoirs formed under similar depositional environment.

Table 3. 3: Liquid permeability measurement of core plugs

Core plug ID	Diamter (cm)	Length (cm)	Fluid Collect (cm^3)	Time (sec)	Δp (atm)	Area (cm^2)	Q (cm^3/sec)	K (mD)	K_{avg} (mD)
CP1		7.75	10.00	204.00	1.35	11.05	0.05	25.50	
CP2	3.75	7.02	10.00	188.00	1.14	11.05	0.05	29.61	27.21
CP3		6.81	10.00	195.00	1.19	11.05	0.05	26.53	
CP4		8.11	10.00	420.00	2.47	11.05	0.02	7.09	
CP5		7.43	10.00	480.00	2.62	11.05	0.02	5.36	
CP6		6.90	10.00	489.00	1.99	11.05	0.02	6.40	
CP7		6.95	10.00	514.00	2.33	11.05	0.02	5.26	
CP8		7.50	10.00	476.00	2.01	11.05	0.02	7.11	
CP9		7.61	10.00	415.00	2.07	11.05	0.02	8.02	
CP10	3.75	6.75	10.00	585.00	2.30	11.05	0.02	4.54	6.32
CP11		7.55	10.00	482.00	2.39	11.05	0.02	5.92	
CP12		7.00	10.00	465.00	2.07	11.05	0.02	6.58	
CP13		6.89	10.00	497.00	2.27	11.05	0.02	5.52	
CP14		7.48	10.00	465.00	2.23	11.05	0.02	6.53	
CP15		7.53	10.00	480.00	2.33	11.05	0.02	6.08	
CP16		6.97	10.00	500.00	2.47	11.05	0.02	5.12	
CP17		7.60	10.00	385.00	2.00	11.05	0.03	8.93	
CP18		7.58	10.00	600.00	3.01	11.05	0.02	3.79	
CP19	3.75	6.88	10.00	650.00	3.15	11.05	0.02	3.04	3.25
CP20		7.50	10.00	689.00	3.38	11.05	0.01	2.91	

Confining pressure: 380 psi Temperature: 28 ^oC Liquid viscosity (μ):1 cP

Table 3. 4: Gas permeability measurement of core plugs

Core Plug ID	Diameter (cm)	Length (cm)	P_1 (atm)	P_2 (atm)	P_m (atm)	$1/P_m$	Gas Flow (Q) (cm^3/s)	Permeability (K) (mD)
CP1	3.75	7.75	2.02	1.00	1.51	0.66	5.01	46.32
			2.36	1.00	1.68	0.6	7.23	45.02
			2.70	1.00	1.85	0.54	9.70	43.86
			3.04	1.00	2.02	0.49	12.23	42.22
			3.38	1.00	2.19	0.46	15.33	41.83
CP6	3.75	6.90	1.34	1.00	1.17	0.85	0.98	31.30
			1.60	1.00	1.34	0.75	2.00	27.79
			2.02	1.00	1.51	0.66	3.23	26.58
			2.36	1.00	1.68	0.6	4.25	23.55
			2.70	1.00	1.85	0.54	5.72	23.01
CP19	3.75	6.88	1.34	1.00	1.17	0.88	0.68	21.82
			1.55	1.00	1.27	0.79	1.12	20.31
			1.82	1.00	1.41	0.71	1.67	18.35
			2.09	1.00	1.54	0.65	2.40	18.08
			2.36	1.00	1.68	0.6	2.88	15.92

Temperature: 28 ^oC Gas/N_2 viscosity (μ): 0.02 cP

Fig. 3.2 shows the permeability to gas (N_2) of three core plugs of different depths plotted against the inverse of the mean pressure (P_m) based on the Klinkenberg principle [144]. The gas permeability linearly increased with an increase in $1/P_m$ and extrapolating to the point where $1/P_m = 0$, the liquid permeability was estimated. From Table 3.2, it can be seen that the estimated liquid permeability and measured liquid permeability to brine are in good agreement. Although the estimated permeability was found to be slightly greater than measured liquid permeability, this difference is much smaller compared to the variation of the permeability values of the core plugs to liquid and gas.

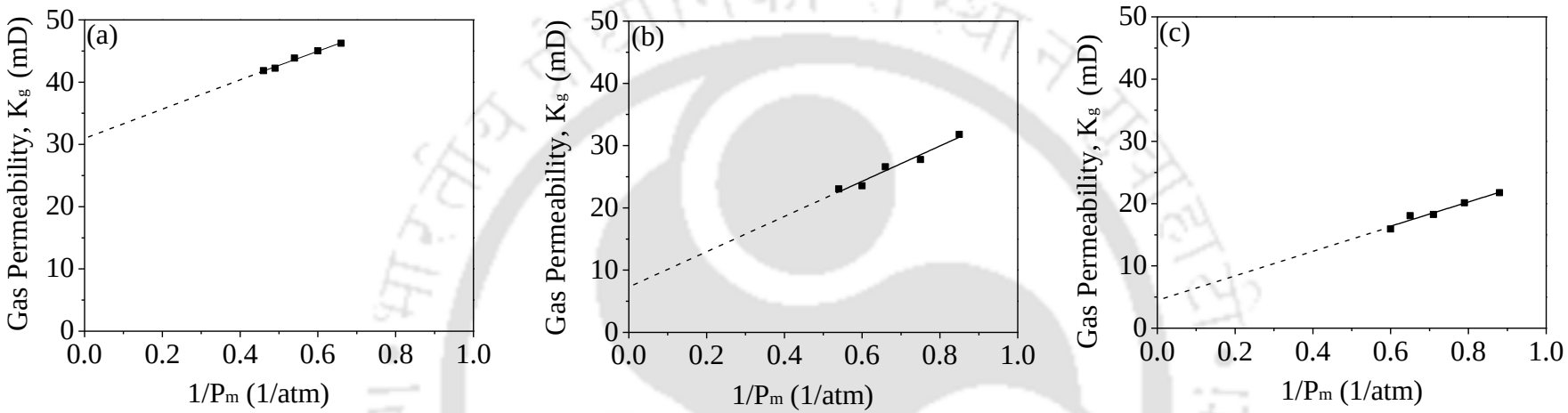

Fig. 3.2: Gas permeabilities and estimated liquid permeabilities of core plugs in the depth range: (a) 2480 – 2486 m; (b) 2925 – 2943 m; (c) 3940 – 3947 m

3.2 Characterization of Reservoir Rocks

The characterization of the reservoir rock was performed to evaluate its mineralogy and clay content using XRD and FESEM respectively. XRD is known to be an important tool to identify the mineralogical of reservoir rock [168]. Fig. 3.3(a) presents the XRD pattern of the powdered core sample with characteristics peaks at 8.96^0, 12.59^0, 20.96^0, 26.72^0, and 28.07^0. This peak information and analysis with MATCH! 3 indicated the presence of silica (quartz) as the dominant mineral. The large and abundant quartz peaks in the XRD diffractogram support the observation. The occurrence of other minerals like feldspar and clays (kaolinite and illite) is also indicated by the XRD spectra. Since silica carries a negative charge at normal formation water pH [169], the reservoir rock was found to be of anionic nature.

FESEM study of the rock samples was conducted for the identification of clay minerals. FESEM micrograph of the rock sample is shown in Fig. 3.3 (b). Based on the analysis of the image using established literature [170], the presence of smectite group of clays was indicated as a thin, webby crust in the matrix of the core sample. The minerals normally present in sandstone reservoirs are quartz, feldspar and clay minerals. The common types of clay minerals present are montmorillonite, smectite, illite, chlorite, and kaolinite, depending upon the depositional environment [171, 172]. The presence of these clay minerals makes the surfactants injected for the purpose of EOR susceptible to be adsorbed onto the reservoir rocks [173].

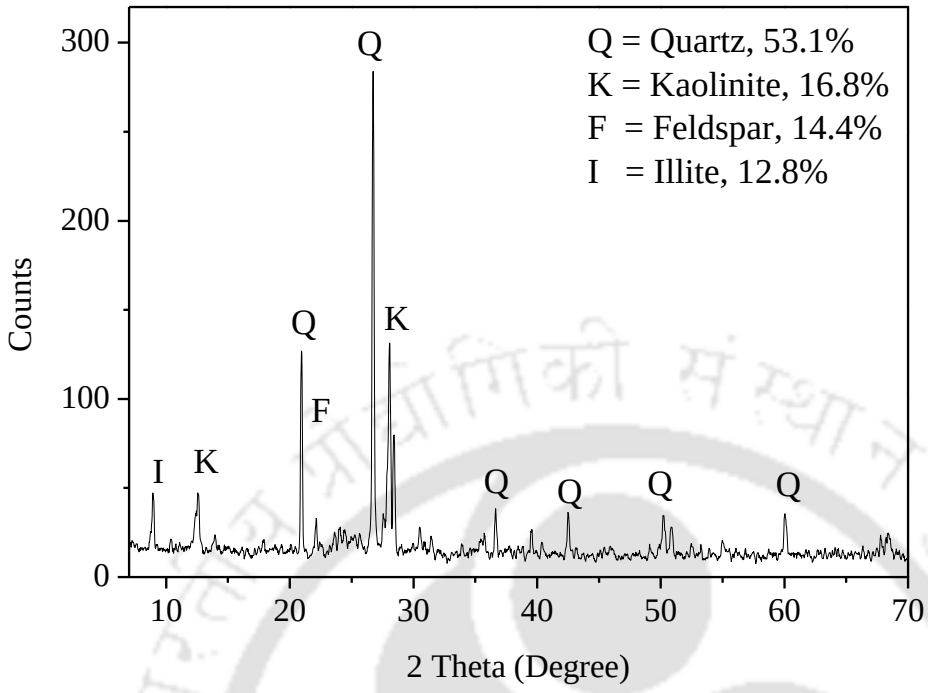

(a)

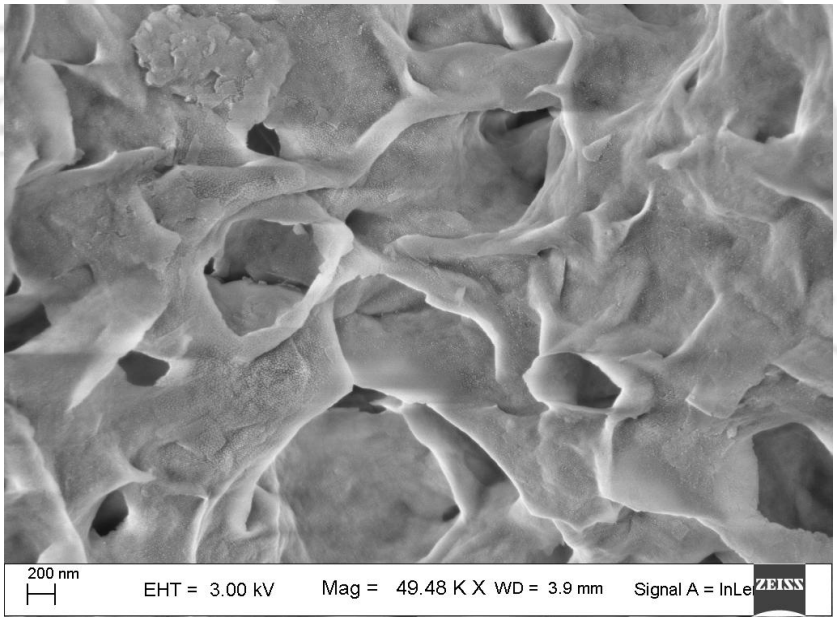

(b)

Fig. 3.3: (a) XRD patterns, and (b) FESEM micrographs of rock samples showing the presence of quartz and clay minerals

3.3 Characterization of Crude Oil

The important physicochemical properties of crude oil affecting the process of recovery include API gravity, viscosity, pour point, resin-asphaltene content, and acid number. The knowledge of these properties is essential before embarking on any EOR process and for selecting the most appropriate method based on the crude oil properties. The results of the crude oil analyses are discussed below and summarized in Table 3.5.

3.3.1 API Gravity

In the oil industry, it is customary to express the density of crude oil in ^{o}API. With water having an API gravity of 10, the liquids lighter than water have API gravity greater than 10. On this scale, gasoline has a gravity of 60 ^{o}API, while crude oils may have a typical value of around 35 ^{o}API [174]. The density of crude oil measured with hydrometers was found to be 863 ± 3 kg/m^3 at an room temperature of 28 ^{o}C. The corresponding density value at 15.56 ^{o}C or 60 ^{o}F was 871 kg/cm^3 after applying the necessary correction factor (of 0.9908) obtained from Table 53A of the Petroleum Measurements Tables [175]. The API gravity of the crude calculated using Eq. 2.5 was obtained as 31^{o}API. Crude oils are generally classified based on its measured API gravity as light, medium, or heavy [176]:

(a) Light crude oils : $\geq$ 31.1 °API

(b) Medium crude oils: 22.3 - 31.1 °API

(c) Heavy crude oils: $\leq$ 22.3 °API

As per this classification, the crude oil of the Upper Assam oilfield used in this study falls under the category of medium oil. CO_2 flooding being the leading EOR technique for light and medium oil reservoirs, this preliminary information suggested that the crude oil under study was suitable for CO_2-EOR application.

3.3.2 Dead Oil Viscosity

Viscosity is an important physical property of crude oil that controls the rate of flow and recovery of crude oil from reservoirs. Crude oil viscosity is a strong function of the temperature, pressure, oil gravity and gas solubility. An increase in temperature causes a decrease in crude oil viscosity, while an increase in pressure increases oil viscosity, provided the only effect of pressure is to compress the liquid. Additionally, a decrease in the solution gas also increases crude oil viscosity. The viscosity of crude oils based on pressure can be classified as [18]:

(a) Dead-oil viscosity, which is the viscosity of crude oil at atmospheric pressure with no gas in solution and at system temperature.

(b) Saturated-oil viscosity, which is the viscosity of the crude oil at saturation pressure and reservoir temperature.

(c) Undersaturated-oil viscosity, represents the viscosity of the crude oil at pressure more the bubble-point and reservoir temperature.

Fig. 3.4 shows the plot of the dynamic viscosity of the crude oil sample as a function of temperature. The experimental results of viscosity measurements are presented in Appendix B. As expected the dynamic viscosity decreased with the increase of temperature from a value of 10.21 ± 0.3 cP at room temperature (28 ^{o}C) to 4.46 ± 0.5 cP at reservoir temperature (70 ^{o}C). This value of the crude oil viscosity less than 100 cp classified the crude oil as light to medium [177]. Based on the screening criteria given in the literature [132, 138], the viscosity value of the crude oil indicates its suitability for alkaline-surfactant (AS) and CO_2 flooding.

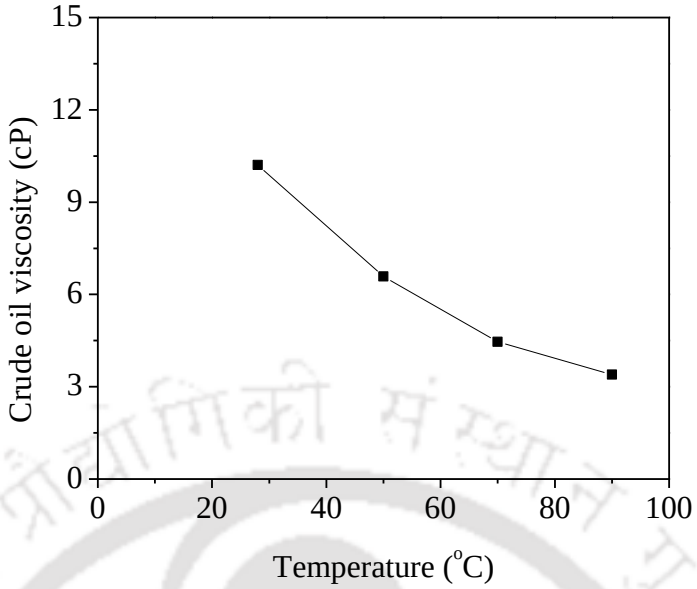

Fig. 3.4: Crude oil viscosity as a function of temperature

3.3.3 Pour Point

The pour point of crude oil is the temperature at which it becomes semi-solid and ceases to flow. For the crude oil used in the study, the pour point was found to be 24 ± 3 °C and consequently a high pour point crude. This was based on the rule of thumb that high-pour-point crude oils generally have pour points in the range of 15 to 52 °C, and may be solid at room temperature. It has been observed that high pour point is generally associated with crude oils with high paraffin content and lower pour point with crudes of more aromatic nature [178]. Assam crude oil, in general, has been reported to have higher pour points (30 °C) and higher wax content (11 wt %) [179].

3.3.4 Resin, Asphaltene, and Wax Content

The asphaltene content of the crude oil was found to be 1.4 ± 0.2 wt% and resin content 16.73 ± 0.5 wt%. The R/A ratio for the crude oil was found to be greater than 3, so based on the Leontaritis criterion [49], there are enough amounts of resins for asphaltene stabilization. So, the possibility of asphaltene precipitation from the crude oil during CO_2

flooding is less. The wax content of the crude oil was fairly high at 12.47 ± 0.70%. A similar observation on the wax content of Assam crude oil was made by Kandwal et al. [179]. The experimental results of resin, asphaltene and wax content determination are presented in Appendix B.

3.3.5 Acid Number

Acid number is a measure of the amount of acidic components present in crude oil. It is expressed as the milligrams of KOH that is required to neutralize 1 gm of oil sample. For a reservoir to be a good candidate for alkaline flooding, the acid number of crude oil should be at least 0.5 mg/g. Crude oils with an acid number greater than 0.5 mg KOH/g of crude oil are known as acidic crudes [180]. The acid number of the present crude oil was estimated as 1.2 ± 0.2 mg KOH/g of crude oil. Thus, the crude oil considered in this study is acidic and suitable for alkaline flooding.

FTIR spectra of the crude oil was recorded between 400 and 4000 cm^{-1} to study the presence of major functional groups present. The dominant spectra of crude oils normally include the absorption bands of aliphatic C-H bonds along with other additional bands of groups containing oxygen, aromatics, nitrogen, and sulfur. The FTIR spectrum of the crude oil is shown in Fig. 3.5. The peak at 2932 cm^{-1} indicated the presence of single bond alkanes, while the peaks at 1724 cm^{-1}, 1603 cm^{-1}, 1454 cm^{-1}, and 1377 cm^{-1} account for carboxylic acids, aromatics, $-CH_2$ and $-CH_3$ functional groups respectively. Other peak at 745 cm^{-1} indicates the existence of long-chain alkyl groups [181, 182]. Thus the presence of acidic groups in the crude oil was identified by the FTIR analysis and support the acid number measurement.

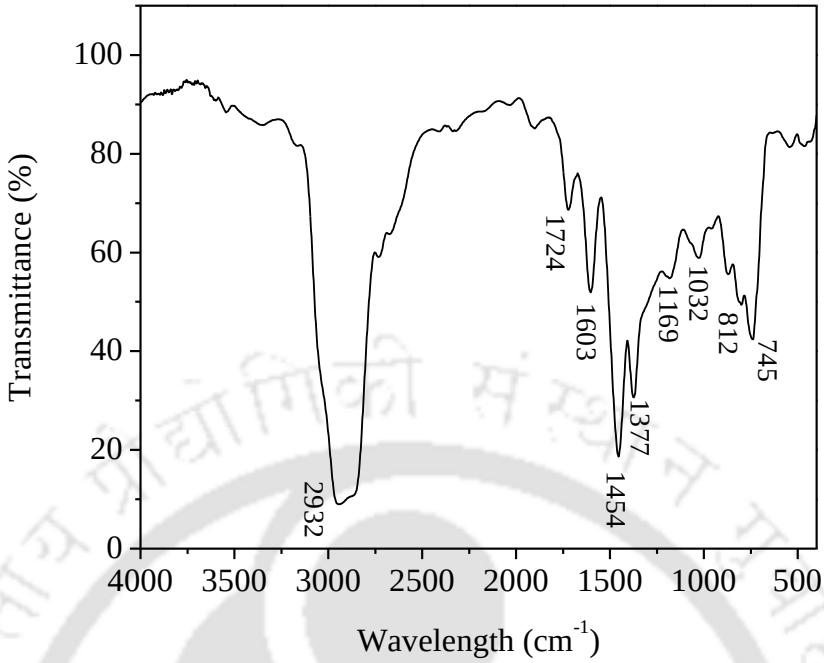

Fig. 3.5: FTIR spectra of crude oil sample

Table 3. 5: Physical and chemical properties of crude oil

Sl. No.	Properties	Value	Remarks
1	Density (kg/m^3) at 15.6 ^{o}C	871	Medium gravity oil
2	API gravity (^{o}API)	31	
3	Dynamic viscosity (cP) (at reservoir temperature, 70 ^{o}C)	4.46 ± 0.5	Decreases with temperature
4	Pour point (^{o}C)	24 ± 3	Pour point was high indicating high paraffin content
5	Asphaltene content (wt%)	1.4 ± 0.2	High R/A indicating asphaltene stabilization
6	Resin content (wt%)	16.73 ± 0.5	
7	Wax content (wt%)	12.47 ± 0.70	Waxy crude
8	Acid number (mg KOH/g of crude oil)	1.2 ± 0.2	Acidic crude

3.3 Characterization of Formation Water

The water that naturally exists along with oil and gas in the reservoir is called reservoir/formation water. The pH value of formation water is typically between 4 and 9. The pH value below and above this range is not desirable because of the tendency of corrosion and scaling respectively [183]. Formation water almost invariably contains dissolved salts and the chemical analyses have indicated a wide variation in the type and amount of the dissolved ions. The commonly present cations and anions are Na^{+}, K^{+}, Ca^{+}, Mg^{++}, Ba^{++}, Cl^{-}, SO_4^{--}, HCO_3^{-}, and CO_3^{--} [184]. The total salinity of formation water can be calculated by summing up the cationic and anionic concentrations [183]. Table 3.6 lists the physical and chemical properties of the formation water considered in the study. The sample calculations of the titration methods for Cl^{-} ion, Mg^{++} ion, and alkalinity determination of formation water are presented in Appendix C, D, and E respectively. The presence of divalent ions (Ca^{++} and Mg^{++}) in the formation water was observed although in small amounts. The total salinity of the water sample was 3458 mg/L. Synthetic formation brine (SFB) at this salinity was prepared to mimic the formation water and used for the preparation of solution. The SFB was diluted with distilled water to varying degrees to obtain SFB of different salinities for phase behavior studies and core flooding experiments.

Table 3. 6: Physical and chemical properties of formation water

Property	Measured value
Density, kg/m^3 (at 28 ^{o}C)	1012
Viscosity, cP (at 28 ^{o}C)	0.93
pH (at 28 ^{o}C)	8.23
Total dissolved solids (ppm)	3516
Major components (ppm)	
Sodium (Na^+)	1555
Calcium (Ca^{++})	82
Potassium (K^+)	12
Magnesium (Mg^{++})	17
Chloride (Cl^-)	724
Bicarbonate (HCO_3^-)	1068
Salinity (mg/L)	3458

3.4 Summary

The analyses of crude oil, core samples and formation water of the Upper Assam oilfield were presented in this chapter. The routine core analysis was done for the measurement of porosity and permeability of core samples. The porosities of the core plugs ranged from 11- 28% and were found to bear an inverse correlation with the depth of the formation. The values of the liquid and gas permeability of the core plugs ranged from 3 – 30 mD and 16 – 47 mD respectively, which classifies the oilfield formation as fair to moderate permeability reservoirs. Further, the XRD and FESEM analysis of rock samples indicated the presence of silica (quartz) as the dominanat mineral, along with the presence of clays minerals.

The experimental investigation of the crude oil confirmed that the crude oil was medium gravity (API gravity 31^{o}), with dead oil viscosity of 4.46 cP (at 70 ^{o}C). The pour point of the crude oil was high (24 ± 3 ^{o}C) which indicated the paraffinic nature of the crude oil. The wax content was also fairly high at 12.47 ± 0.70 %. The resin to asphaltene ratio of the crude oil was high enough for asphaltene stabilization. The analyses also marked the crude as acidic and suitable for alkaline flooding. The formation water analysis showed the presence of different types of dissolved cations and anions with total salinity of 3458 ppm.

CHAPTER 4

Optimum Formulation of Chemical Slug for ASAG Flooding

Foam stability

Oil-water IFT

Phase behavior study

Static and dynamic adsorption

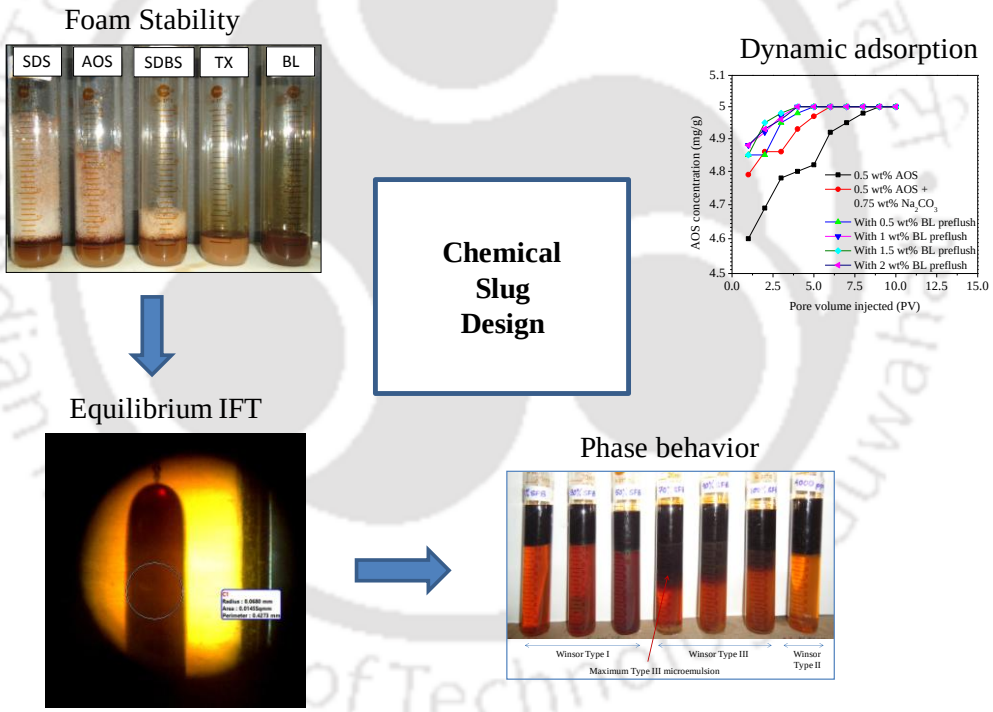

Work published as:

1. R. Phukan, S.B. Gogoi, and P. Tiwari, *Effects of CO2-foam stability, interfacial tension and surfactant adsorption on oil recovery by alkaline-surfactant-alternated-gas/CO_2 flooding*. Colloids and Surfaces A: Physicochemical and Engineering Aspects, Elsevier, 2020;597:124799.

Chapter 4

Optimum Formulation of Chemical Slug for ASAG Flooding

This chapter presents the screening of chemicals for the design of optimum chemical formulations for ASAG flooding. The first section focuses on the foam stability study conducted to screen different types and concentrations of surfactants with optimized foaming behavior. In the second section, the equilibrium IFT measurements were performed to select suitable alkalis and their optimum concentrations for preparing AS formulations are presented. The third section summarizes the results of phase behavior study of the alkaline-surfactant (AS) formulation to identify the optimal salinity region. Finally, the last section presents the adsorption studies where the roles played by alkali and black liquor(BL) (as preflushing agent) in reducing surfactant adsorption are discussed.

4.1 Chemical Slug for ASAG Flooding

The successful application of the ASAG process for improving oil recovery from an oil reservoir requires the usage of an appropriate chemical slug. Therefore, it is desirable to screen optimal chemical formulations that would fulfill the two basic requirements of a chemical slug for ASAG flooding; lowering the oil-water IFT to ultra-low value and ensuring good mobility control through proper foaming in the reservoir rock. Experiments were performed to screen chemical slugs for ASAG flooding through foam stability study, IFT measurements, phase behavior study, and adsorption study. Both anionic surfactants (AOS, SDS, and BL) and non-ionic surfactants (TX-100) were evaluated for their ability to form stable foam in the presence of crude oil. The CO_2-foam

stability of the aqueous solutions of surfactants at reservoir temperature (70 ^{o}C) in the presence of crude oil was tested to identify the optimum concentrations of surfactants. Three types of alkalis including Na_2CO_3, NaOH, and $Na_2B_4O_7.10H_2O$ were considered in this study to formulate the AS slug with surfactants in synthetic formation brine (SFB) as the aqueous phase. The equilibrium oil-water IFT measurements were performed to select suitable alkalis and their concentrations for preparing AS formulations. Phase behavior study was conducted to confirm the optimal salinity of AS formulation. Further, static and dynamic adsorption studies were performed to evaluate the adsorption behavior of the surfactants onto reservoir rocks and to select appropriate concentrations of BL, used as a secondary surfactant, for preflushing operations.

4.2. Surface Tension and Interfacial Properties of Different Surfactants

The surface tensions of the different surfactants (SDS, AOS, SDBS, and TX-100) in synthetic formation brine were measured and plotted as function of concentration as shown in Fig. 4.1(a). The surface tension decreased with increasing surfactant concentration, as the surfactant molecules gets adsorbed on the liquid-gas interface, until it reached a minimum at the CMC value [190]. The CMC is defined as the lowest concentration at which the monomers cluster to form micelles. Beyond the CMC, the surface tension values almost remain constant as further increase in the surfactant concentration only increases the micelle concentration and hardly change the monomer concentration. The lowest surface tension value was achieved by SDS (27.8 mN/m) which is sufficiently lower than the surface tension of water (~ 66 mN/m). The CMC values of surfactants were 0.15 wt%, 0.2 wt%, 0.25 wt%, and 0.03 wt% for SDBS, SDS, AOS, and TX-100 respectively. The equilibrium oil-water IFT of all the surfactants were measured at reservoir temperature (70 ^{o}C) for different surfactant concentrations and plotted as shown in the Fig. 4.1(b). The concentration of each surfactant was varied from 0.08 to 1 wt%. The

IFT measurements below 0.08 wt% could not be performed as the required oil droplet shape (L/D ratio > 4) was not formed. For all the anionic surfactants, with an initial increase in the surfactant concentration a little reduction in IFT was observed due to increase in the adsorption capacity of the surfactant molecules at the oil-water interface. However, with further increase in surfactant concentration negligible reduction in IFT values were observed due to adsorption saturation. The lowest IFT values obtained were 0.31 mN/m, 0.19 mN/m, 0.34 mN/m, and 0.14 mN/m for SDBS, SDS, AOS, and TX-100 respectively.

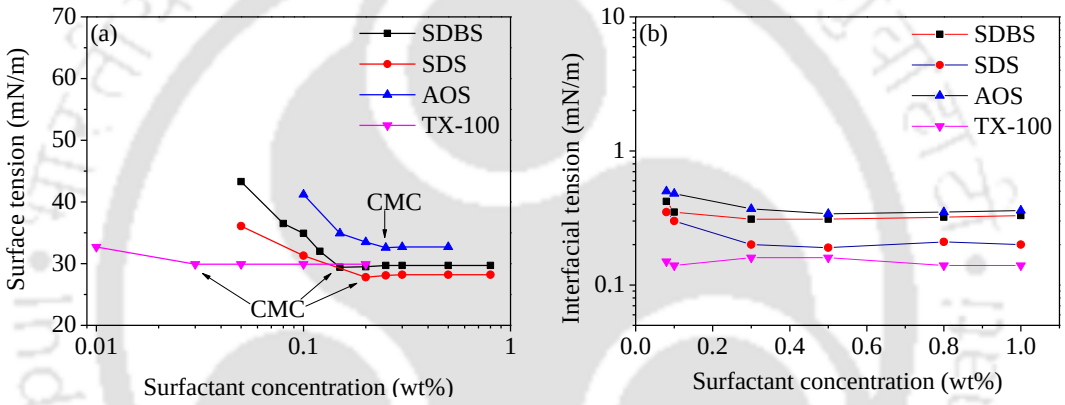

Fig. 4. 1: (a) Surface tension versus surfactant concentration; and (b) Oil-water interfacial tension versus surfactant concentration

4.3 Evaluation of Foam Stability

The effectiveness of the foam-based EOR process is greatly influenced by the ability of the foaming agents to form strong/stable foam under reservoir conditions. The selection of these foaming agents/surfactants is normally done on the basis of their foamability and foam stability [185]. Both these properties of foam are interrelated and, in most cases, greater the foamability more stable are the foam films. A method commonly used to quantify foam stability is the half-decay time [186]. Of the different factors controlling foam stability, the anti-foaming effect of oil is considered to be the most

crucial. Some literature reported that the presence of oil destabilizes the foam generated and others observed that foam stability in contact with oil can be maintained by the use of certain foaming agents [187-189]. In fact, foam stability in the presence of oil is a major challenge for the successful implementation of foam-based EOR methods.

4.3.2 Foam Stability of Different Surfactants

Initially, foamability and foam stability of the surfactants were tested using the standard shaking method as explained in Section 2.2.7. Fig. 4.2(a) and (b) show the snapshots of the foam formed, immediately following its generation, by different surfactants at 0.5 wt% concentration in the absence and presence of crude oil respectively. The foaminess was obtained by visual measurements using the volume expansion method [191]. The foaminess is defined as:

$$\text{Foaminess} = \frac{V_{foam} - V_{liquid}}{V_{foam}} \tag{4.1}$$

where V_{foam} is the volume of foam formed immediately after shaking (in ml)

V_{liquid} the volume of liquid placed in the test tube (in ml).

Fig. 4.3 shows the foaminess values of different surfactants at 0.5 wt% concentration with and without crude oil. Foaminess was found to be maximum for SDS followed by AOS, SDBS, TX-100, and BL without and with crude oil. Xu [192] observed that the foamability of non-ionic surfactants (TX-100) was much less compared to anionic surfactants (AOS, SDS) and amphoteric surfactants.

Fig. 4.4 (a) and (b) shows the changes in the foam volume as a function of time for all the surfactants considered (at 0.5 wt%), with and without crude oil. In Fig. 4.4 (c) the half-decay times ($t_{1/2}$) of the surfactants without and with crude oil are shown. Under similar experimental conditions, it was observed that anionic surfactants (except BL) have better foamability and longer $t_{1/2}$ compared to the non-ionic surfactant, TX-100. SDS

exhibited the highest foamability and also generated the most stable foam with $t_{1/2}$ of approximately 240 min, followed by AOS and SDBS. BL displayed the weakest foaming behavior amongst the surfactants considered indicating its poor foaming ability. The presence of crude oil (at 10 vol%) lowered the foamability and $t_{1/2}$ of all the surfactants indicating the destabilizing effect of oil. When oil droplets accumulate at the plateau borders and lamellas, surfactant molecules are transferred from the gas-water interface to the oil-water interface which weakens the foam film strength and decreases the Marangoni effect leading to decrease in foam performance [189, 193]. The foam stability of TX-100 totally diminished in the presence of crude oil. In fact, TX-100 foam with crude oil decayed in less than 5 min. The electrostatic double layer effect resulting from charge interactions at the film interface is suppressed in non-ionic surfactants, and for this reason, the stability of TX-100 was very low [114].

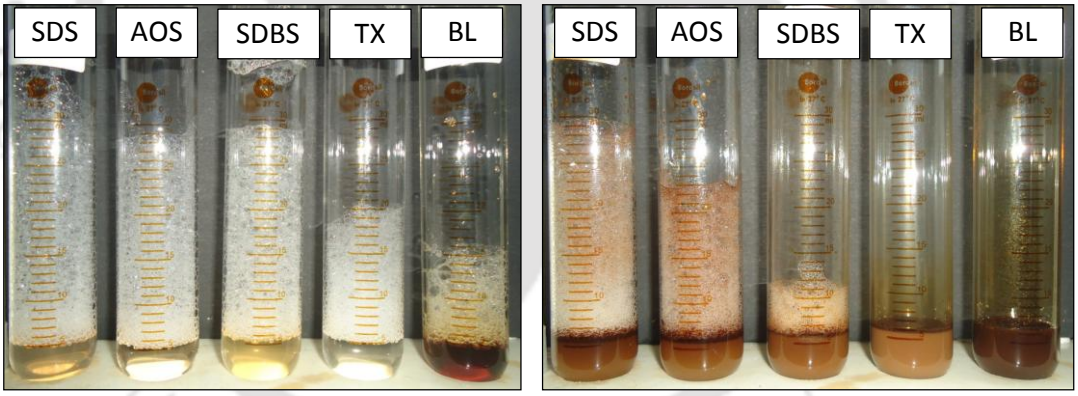

(a) (b)

Fig. 4. 2: Snapshots of foam generated with different surfactants at 0.5 wt% concentration (a) in the absence of crude oil, and (b) in the presence of crude oil (at 10 vol%)

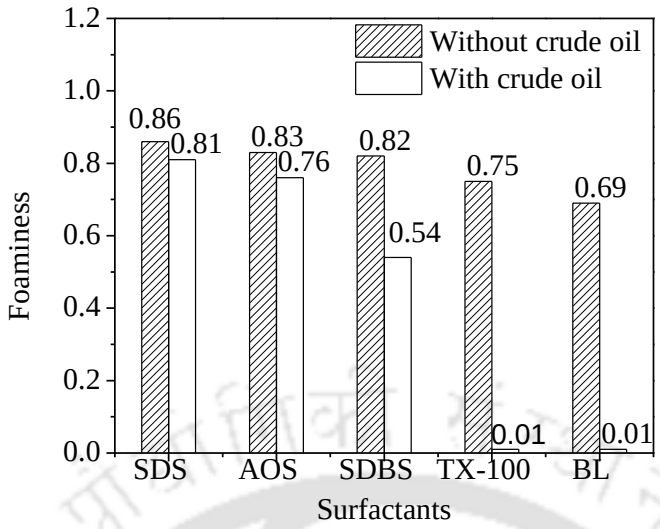

Fig. 4. 3: Gas holdup values of different surfactants at 0.5 wt% concentration with and without crude oil

[SDS: sodium dodecyl sulphate; AOS: alpha olefin sulphate; SDBS: sodium dodecyl benzene sulphonate; TX-100: triton X-100; BL: black liquor]

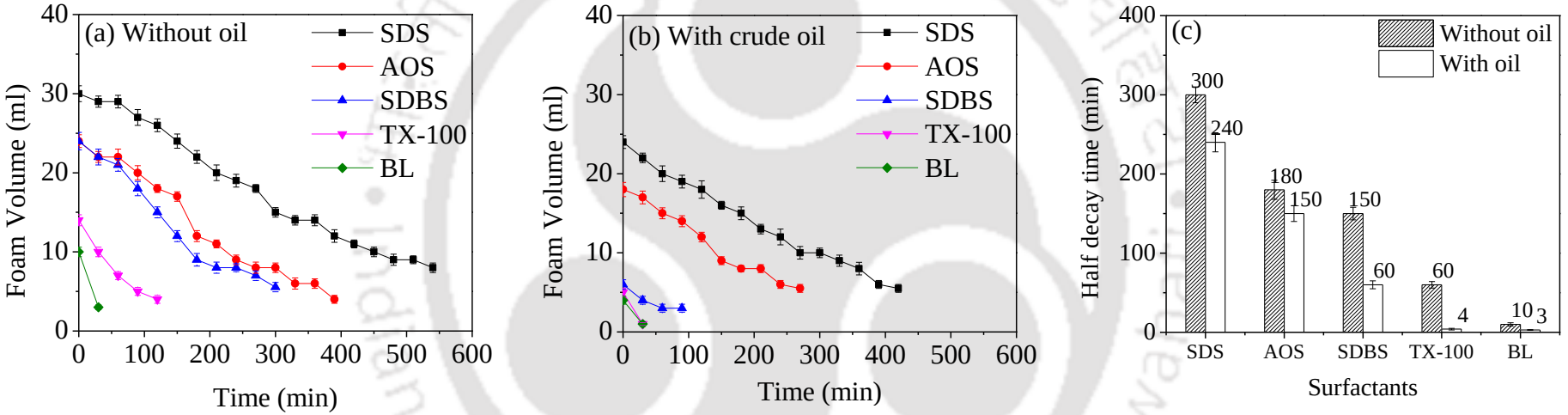

Fig. 4. 4: Foam volume as a function of time of surfactants (at 0.5 wt%) (a) without crude oil, and (b) with crude oil; (c) Half decay times of surfactants ($t_{1/2}$) without and with crude oil

Fig. 4.5 shows foamability (V_i) of the surfactants at different concentrations with crude oil. It was observed that V_i increased with increasing surfactant concentration, which is the generally accepted trend of surfactant solutions [149, 194]. The formation of foam depends on the movement of surfactant monomer to the gas-liquid interface. At low surfactant concentration, slower movement of the surfactant to the gas-liquid interface resulted in a lower value of fomability. As surfactant concentration increased adsorption of surfactant gradually increased at the gas-liquid interface resulting in higher foamability [195]. However, beyond a certain surfactant concentration, the foamability of all the surfactants almost leveled off as the interface got slowly saturated with surfactant molecules.

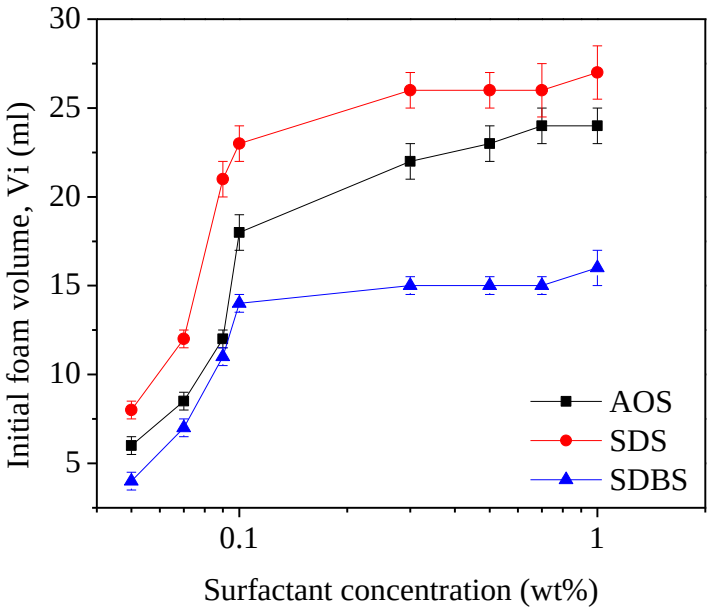

Fig. 4. 5: Foamability as a function of the concentration of surfactants in the presence of crude oil.

4.3.2 CO_2-Foam Stability of Different Surfactants

Initially, all the surfactants of the anionic and non-ionic types were studied for their CO_2-foam stability at room temperature (28 ^oC) with crude oil (at 10 vol%) [as explained

in Section 2.2.7] with the objective of selecting suitable surfactants that will generate the most stable CO_2-foam. For comparison, the concentration of the surfactants was fixed at 0.5 wt% and the volume foam generated, by passing CO_2 gas through the surfactant solution, was observed with respect to time for determining the $t_{1/2}$ value. The foam stability curves of the surfactants are shown in Fig. 4.6. The non-ionic surfactant (TX-100) displayed the lowest foam stability with $t_{1/2}$ value of 4.5 min. On the other hand, the anionic surfactants namely SDS, AOS, and SDBS generated foams having higher foam stability with $t_{1/2}$ values of 40 ± 2, 31 ± 2 and 25 min respectively at room temperature (Table 4.1).

Thus, SDS and AOS displayed comparatively better CO_2-foam stability with the crude oil under similar experimental conditions. Earlier studies have also demonstrated that foam-stability depends on the type of surfactants used for foam generation. Simjoo et al. [189] reported that AOS was the most stable surfactant compared to other anionic and amphoteric surfactants in the presence of oil while in absence of oil the amphoteric surfactant was the most stable. Similarly, Farzaneh and Sohrabi [151] observed that non-anionic surfactants have lower foam stability than the anionic surfactants under similar experimental conditions. Azdarpour et al. [196] ranked the surfactants on the basis of foam stability in presence of paraffin oil as SDS > AOS > SDBS > TX-100 with $t_{1/2}$ values of 17, 14, 13, and 12 min respectively.

4.3.3 Effect of Temperature on CO_2-Foam Stability

As the highest $t_{1/2}$ values were observed for SDS followed by AOS at ambient temperature, so CO_2-foam stability of the SDS and AOS was also studied at a temperature of 70 ^oC, which is the reservoir temperature. Foam generated in the glass column above the liquid level was regularly monitored and recorded with respect to time at reservoir

temperature. The time required for foam to reach half of its initial volume was noted with care.

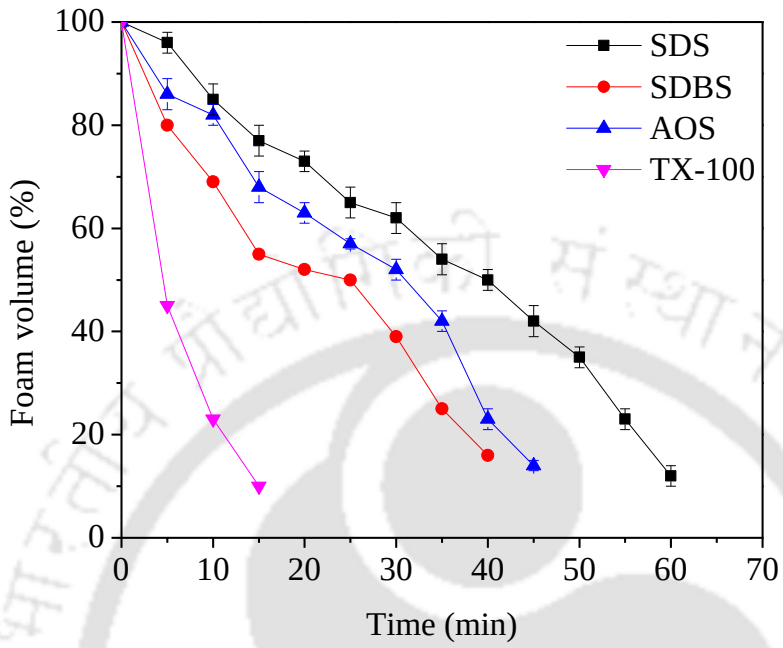

Fig. 4. 6: CO_2-foam stability curves of surfactants in the presence of crude oil at room temperature (28 ^oC). Concentration of surfactants fixed at 0.5 wt% and crude oil was 10 vol%

Fig. 4.7 shows the foam stability curves of SDS and AOS at 28^oC and 70^oC at fixed surfactant concentration (0.5 wt%). With the increase in temperature, the foam stability characterized by $t_{1/2}$ decreased to less than half for both the surfactants. For SDS, $t_{1/2}$ values decreased from 40 ± 2 min at 28 ^oC to 14 ± 1 min at 70 ^oC, and for AOS from 31 ± 2 min to 10 ± 1 min (Table 4.1). Wang et al. [197] observed that the foam stability of all surfactants tested decreased with temperature. The primary reason for the lower foam stability was related to the lower surface viscosity at a higher temperature which results in faster liquid drainage. Kamal [198] investigated the effect of temperature on the foam stability of betaine surfactant and reported a similar decrease in CO_2-foam stability from 8 min at 25 ^oC to 3 min at 80 ^oC.

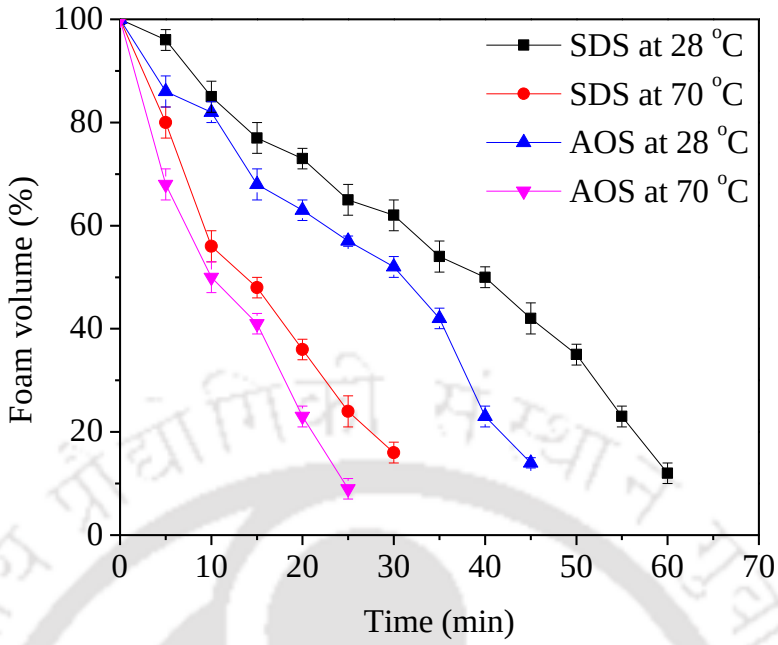

Fig. 4. 7: CO_2-foam stability curves of SDS and AOS at room (28 °C) and reservoir temperature (70 °C) in the presence of crude oil. Concentration of surfactants fixed at 0.5 wt% and crude oil was 10 vol%

4.3.4 Effect of Surfactant Concentration

To observe the effect of surfactant concentration on CO_2 foam stability and to select suitable concentrations for preparing chemical slug, similar experiments at reservoir temperature were conducted with SDS and AOS surfactants. These two surfactants were selected on the basis of their better CO_2-foam stability at room and reservoir temperature. Fig. 4.8 shows the foam stability curves of SDS and AOS as a function of their concentrations. The obtained results show that foam stability improved with increasing surfactant concentration up to a certain concentration, beyond which no further improvement was observed even if the surfactant concentrations were increased. The observed trend was due to the formation of a monolayer at the gas-liquid interface with increasing surfactant concentration which in turn caused better foam stability. However, at a certain concentration, the surface of the interface gets saturated with molecules and

further increasing the surfactant concentration had little or no effect on foam stability. Previous studies investigating the effect of surfactant concentration on foam stability have reported similar observations [149, 151, 193]. Thus, it can be concluded that maximum CO_2-foam stability (with the highest value of $t_{1/2}$) for a particular surfactant occurred at a certain specific surfactant concentration. The maximum CO_2 foam stability was obtained at 0.3 wt% SDS and 0.5 wt% AOS concentrations which were selected as the optimum values for further studies. The $t_{1/2}$ values of SDS and AOS at these optimum concentrations were found to be 16 ± 1 min and 10 ± 1 min respectively (Table 4.1).

Table 4. 1: CO_2-foam stability of different surfactants at room (28 ^oC) and reservoir temperature (70 ^oC)

Sl. No.	Surfactant			Temperature (^oC)	CO_2-foam stability ($t_{1/2}$) (min)
	Name	Type	Concentration (wt%)		
1	SDS	Anionic	0.5	28	40 ± 2
2	AOS	Anionic	0.5		31 ± 2
3	SDBS	Anionic	0.5		25
4	TX-100	Non-ionic	0.5		4.5
5	SDS	Anionic	0.05	70	4 ± 0.5
6			0.07		6 ± 0.5
7			0.1		11 ± 0.5
8			0.3		16 ± 1
9			0.5		14 ± 1
10			1		13.5 ± 1
11	AOS	Anionic	0.05	70	4 ± 0.5
12			0.07		5 ± 0.5
13			0.1		6 ± 0.5
14			0.3		8 ± 0.5
15			0.5		10 ± 1
16			1		9 ± 0.5

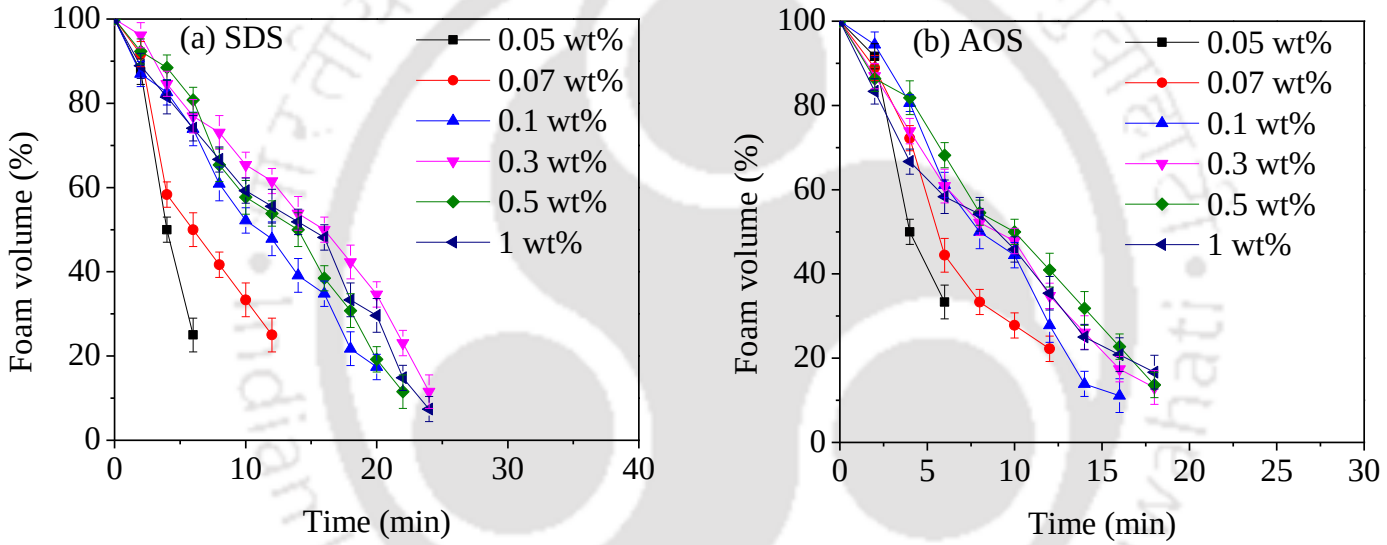

Fig. 4. 8: CO_2- foam stability curves at different concentrations of the surfactants (a) SDS and (b) AOS in the presence of crude oil at 70 ^{o}C

4.4 Equilibrium IFT Measurements

After screening the surfactants based on the CO_2-foam stability, suitable alkalis and their optimum concentrations for preparing AS formulations were identified by performing IFT measurements. Fig. 4.9 shows the variation in the equilibrium oil-water IFT values of the optimum SDS and AOS formulations at different concentrations of the alkalis namely Na_2CO_3, NaOH, and $Na_2B_4O_7.10H_2O$ at reservoir temperature (70 ^oC). The results show that for the surfactants, the equilibrium oil-water IFT value decreased with the increase in alkali concentration up to a certain concentration and then the value was either constant or slightly increased. The IFT value decreased due to the generation of in-situ surfactant caused by the interaction of alkali and acidic components of crude oil. As the concentration of alkali increased, the production of in-situ surfactant increased thus lowering the oil-water IFT further [199]. However, after reaching a minimum value at a particular alkali concentration, the IFT value no longer decreases because the amount of the acidic components in crude oil is limited. It can be observed from Fig. 4.8 that, with 0.3 wt% SDS the minimum IFT values of 0.0068 mN/m, 0.0092 mN/m, and 0.016 mN/m were obtained at 1 wt% Na_2CO_3, 0.75 wt% NaOH, and 1.25 wt% $Na_2B_4O_7.10H_2O$ respectively. Similarly, with 0.5 wt% AOS the minimum IFT values were found to be 0.0087 mN/m, 0.0098 mN/m, and 0.019 mN/m when mixed with 0.75 wt% Na_2CO_3, 0.75 wt% NaOH, and 1.25 wt% $Na_2B_4O_7.10H_2O$ respectively. Thus, both Na_2CO_3 and NaOH were found to be efficient in reducing the oil-water IFT values to the ultra-low range (< 0.01 mN/m) when combined with SDS and AOS in appropriate proportion. However, Na_2CO_3 can be the preferred selection as the IFT values were the lowest. Additionally, the use of Na_2CO_3 has certain advantages like it is cheaper, less corrosive, reduce retention, lower mineral dissolution, and lower formation damage [97, 98]. The Na_2CO_3 concentrations (1 wt% and 0.75 wt%) at which the minimum IFT values were achieved when combined with 0.3 wt%

SDS and 0.5 wt% AOS respectively, were considered as the optimum alkali concentrations. Kumar and Mandal [7] also reported ultra-low IFT value (0.0032 mN/m) for SDS (at CMC value) + 0.2 wt% Na_2CO_3 formulation with crude oil of Ankleswar oilfield, India.

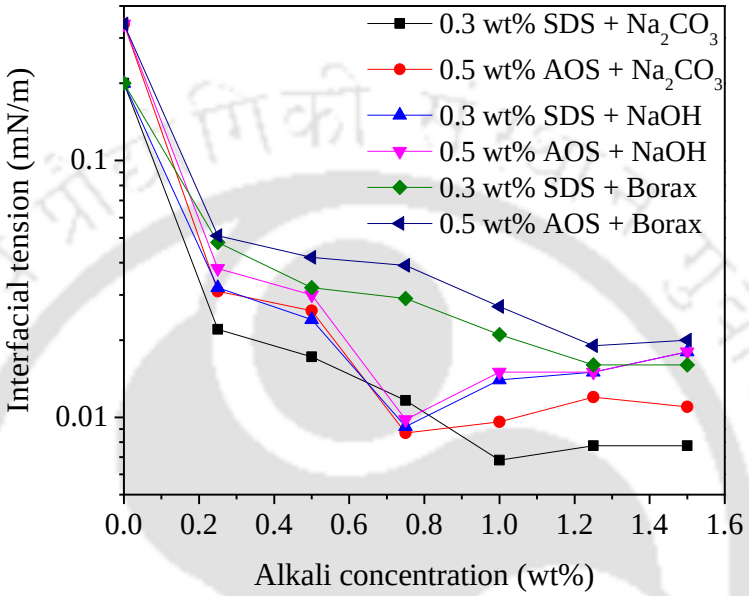

Fig. 4. 9: Equilibrium oil-water IFT of alkali-surfactant (AS) formulations

The AS formulations designed based on foam stability study and IFT measurements were used for performing the ASAG core flooding experiments as described in Chapters 5 and 6. Further, in order to investigate the effect of salinity gradient application during ASAG flooding (as described in Chapter 6), experiments were done to identify the optimal salinity of the AS formulation containing 0.5 wt% AOS + 0.75 wt% Na_2CO_3 through IFT measurements and phase behavior study. To identify the optimal salinity, the equilibrium IFT of the AS formulation at different SFB salinities ranging from 0% (0 ppm) to 100% salinity (3458 ppm) were measured. Fig. 4.10 shows the plot of the equilibrium oil-water IFT values of the formulation as a function of formation brine salinities. It was observed that as the salinity of SFB increased from 0% to 100%, the

equilibrium IFT values decreased from 0.024 mN/m to 0.0087 mN/m. With the increase of salinity, surfactant molecules adsorb more firmly at the water-oil interface which causes the IFT to decrease [200, 201]. Fig. 4.9 shows that the IFT values at first decreased with an increase in salinity reached the lowest value (at 70% of SFB salinity, 2400 ppm) and then slightly increased when the SFB salinity reached 100% (3458 ppm). The 70% SFB salinity with the lowest IFT value (0.0066 mN/m) was considered as the optimal salinity of SFB for the above formulations. Kumar and Mandal [7] reported that the decreasing trend of IFT with salinity was due to the combined effect of salt and surfactant mixtures. With increase in salinity, the surface energy of crude oil in the presence of surfactant solutions is lowered and so the IFT decreases. Similarly, Ruckenstein and Rao [202] observed that IFT decreased with increasing salinity and became reduced to zero at higher salt concentrations.

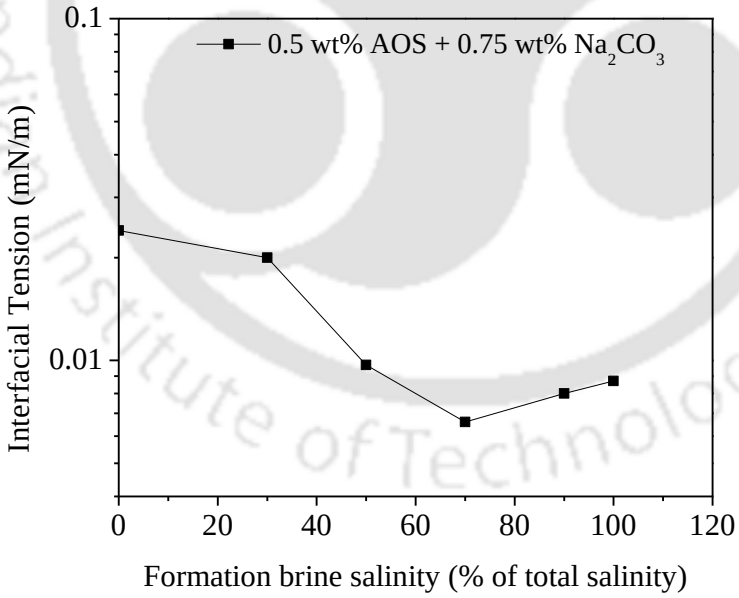

Fig. 4. 10: Effect of formation brine salinity on the equilibrium oil-water IFT of AS formulation

4.5 Phase Behavior Study

Aqueous stability tests were initially performed with the two selected AS formulations namely 0.3 wt% SDS + 1 wt% Na_2CO_3 and 0.5 wt% AOS + 0.75 wt% Na_2CO_3 in the SFB salinity ranging from 0 to 20,000 ppm. Fig. 4.11 (a) and (b) show the results of the aqueous stability tests for the AS formulations considered. No deposition, separation or cloudiness was observed for both the formulations in the selected salinity range. Thus, the AS formulations were found to be compatibility in aqueous solution within the salinity range of the SFB used in the experiments.

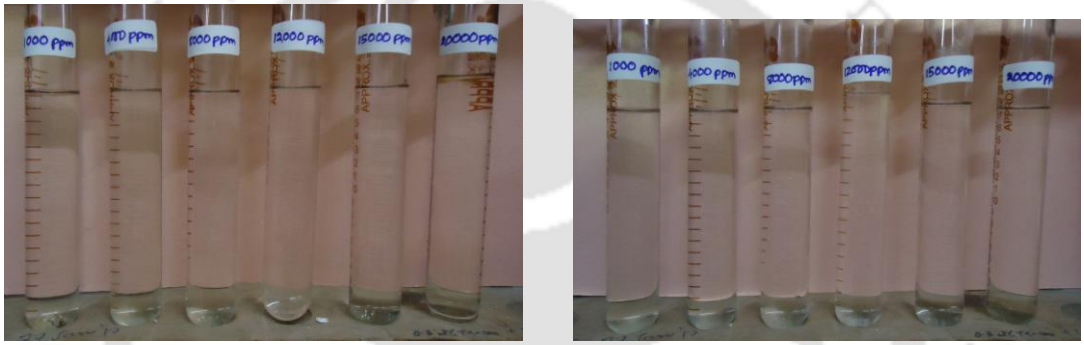

(a) (b)

Fig. 4. 11: Aqueous stability at different salinities of AS formulations: (a) 0.3 wt% SDS + 1 wt% Na_2CO_3 and (b) 0.5 wt% AOS + 0.75 wt% Na_2CO_3

The salinity scan of phase behavior study was performed to confirm the optimal salinity of the AS formulation as identified with IFT measurements. Fig. 4.12 shows the phase behavior study results performed with the AS formulation: 0.5 wt% AOS + 0.75 wt% Na_2CO_3 at various SFB salinities (ranging from 0 to 4000 ppm) with crude oil in the water/oil ratio of 2:1. Winsor type I microemulsion was observed at lower SFB salinity and Winsor type III at intermediate SFB salinities. At salinities higher than formation brine salinity (4000 ppm), Winsor type II microemulsion was observed. Microemulsion phase changes generally occur from Winsor type I (at lower salinity) to Winsor type II (at higher salinities) through Winsor type III microemulsion (at intermediate salinity). The increase in salinity causes the hydrophobicity of the anionic surfactant to increase, thus the surfactants

are driven out of the brine to form middle (Type III) or upper phase (Type II) microemulsions [203]. The maximum Type III microemulsion volume was observed at 2400 ppm (70% of SFB salinity). Sheng [10] reported that maximum type III microemulsion volume occurs at optimal salinity. It is at this optimal salinity that oil-water IFT is the lowest and consequently the point of maximum oil recovery. Thus, 70% of SFB salinity (2400 ppm) was considered as the optimum brine salinity.

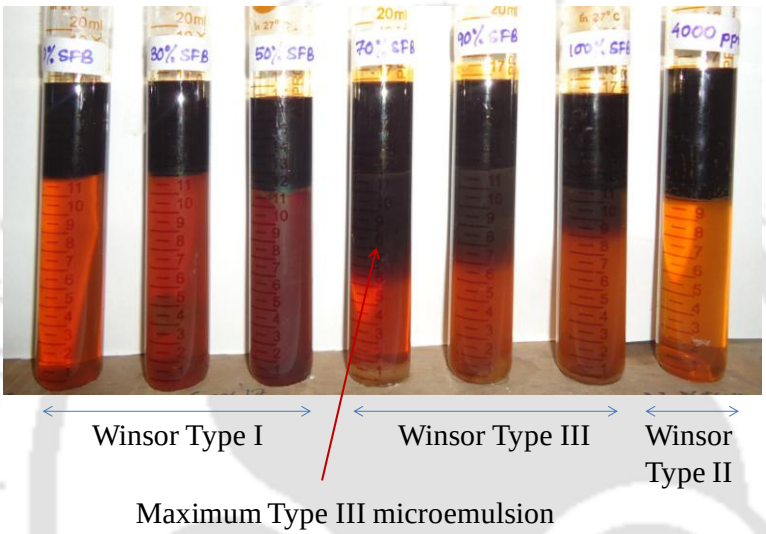

Fig. 4. 12: Snapshot of phase behavior of AS formulation (0.5 wt% AOS + 0.75 wt% Na_2CO_3) and crude oil (Salinity of formation brine ranging from 0 to 4000 ppm)

Healy and Reed [204] defined the solubilization parameters (V_o/V_s and V_w/V_s) for phase behavior test. V_o/V_s is defined as the volumetric ratio of solubilized oil to surfactant, and V_w/V_s is water to surfactant in the microemulsion phase. *Vo/Vs* increases with salinity, while V_w/V_s decreases with salinity. The amount of oil and brine solubilized in the surfactant phase are approximately equal at optimum salinity and the corresponding ratio is called the optimum solubilization ratio. Huh [156] derived a theoretical relationship between IFT and optimal solubilization ratio known as the Huh equation:

$$\lambda = \frac{C}{\left(\sigma^*\right)^2} \tag{4.2}$$

where λ is the IFT, σ* is the optimal solubilization ratio & C is around 0.3 mN/m. Estimating the IFT from the Huh's equation is much quicker than direct measurement (e.g. with spinning drop tensiometer) and sufficiently accurate. Fig. 4.13 represents the solubilization data of the phase behavior test. An optimal solubilisation ratio of 6.2 was obtained at an optimum salinity of 2300 ppm. The corresponding IFT value calculated from Hun's equation was 0.0078 mN/m. These optimum salinity and IFT values agreed well with experimental values obtained from the phase behavior test and the IFT measured with spinning drop tensiometer respectively.

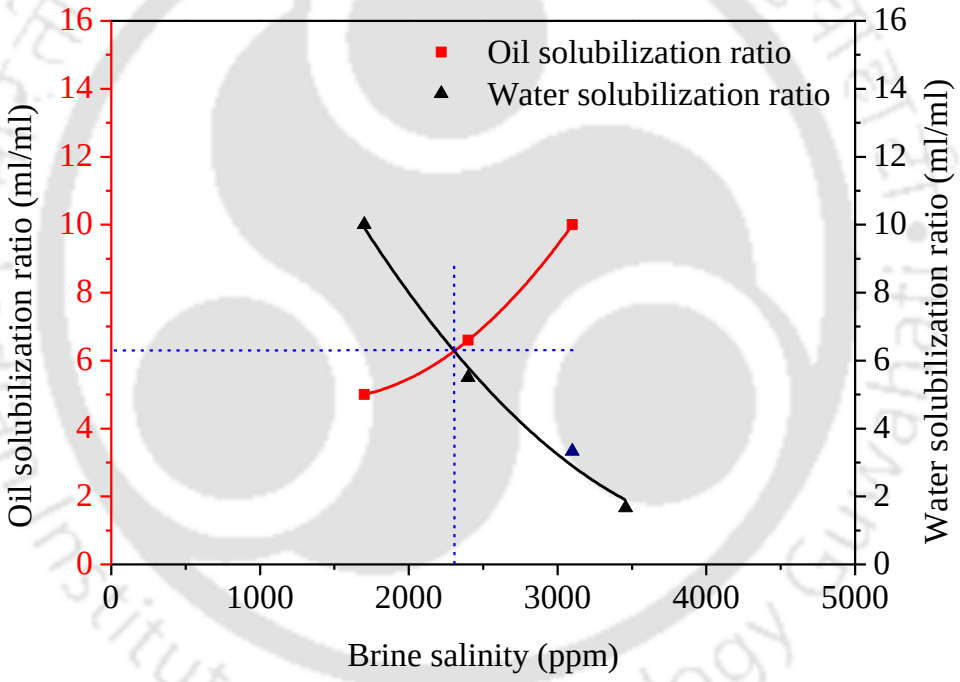

Fig. 4. 13: Solubilization data of phase behavior test of (0.5 wt% AOS + 0.75 wt% Na_2CO_3) and crude oil at 70 ^oC.

4.6 Adsorption Study

In order to investigate the effects of adding alkali (Na_2CO_3) and preflushing with BL on the adsorption behavior of the surfactants onto reservoir rocks, the static and dynamic adsorption studies were carried out. Fig. 4.14 shows the static adsorption

isotherms of SDS and AOS onto the reservoir rock grains for a range of surfactant concentrations. It can be observed that initially, the adsorption isotherm increased with the increase in surfactant concentration due to the electrostatic interaction between the charged sites on the rock grain surfaces and the head groups of the surfactant. Additionally, adsorption also occurs due to the formation of surfactant molecule aggregates on the surface of rock grains as a result of lateral interaction between hydrocarbon chains [205]. Fig. 4.14 also shows the adsorption isotherm of the two surfactants on to the reservoir rock in the presence of Na_2CO_3. The addition of Na_2CO_3 to SDS and AOS solutions considerably decreased the surfactant adsorption. This effect of alkali on surfactant adsorption has been reported earlier [206, 207]. Alkali increases the solution pH making the sand surface more negative and thus the electrostatic repulsive forces decrease the adsorption of the negatively charged surfactant [208].

The plots of fitting the adsorption equilibrium data for the two surfactants SDS and AOS into Linear, Langmuir, Freundlich, and Temkin models are shown in the Fig. 4.15 and Fig.4.16 respectively. The corresponding equations, correlations, regression coefficient (R^2) and other parameters for all the adsorption isotherms are presented in Table 4.2. For both the surfactants Langmuir model was the best fitting plot with maximum R^2 values. The nondimensional Langmuir constant (R_L) was evaluated which varied between 0.322 – 0.877 and 0.562 – 0.9551 for SDS and AOS respectively. This indicated that adsorption of the surfactants onto the reservoir rocks was favorable [157]. The results indicated monolayer adsorption on homogenous surface of finite number of identical sites with no interaction between adsorbed molecules. Ahmadi and Shadizadeh [160] also reported similar observation while investigating the adsorption of natural surfactant on shale-sandstone reservoir rocks.

The dynamic adsorption method can better simulate the adsorption of surfactant by reservoir rocks. Thus, the results are more realistic and field-like. Fig. 4.17 shows the dynamic adsorption curves of 0.5 wt% AOS solutions with and without the addition of Na_2CO_3 (at 0.75 wt%), and with BL preflush. An equilibrium state during the surfactant injection process was obtained when the surfactant concentration in the effluent was almost equal to the injected surfactant concentration. This was the condition when surfactants are no longer adsorbed by the core plug and breakthrough occurred. A longer equilibrium time implied greater adsorption of surfactants onto the core plug, while a shorter equilibrium time meant lower or reduction of adsorption [209]. From Fig. 4.17 and Table 4.2, it can be observed that the addition of alkali to the surfactant shifted the equilibrium state from 9 PV to 6 PV. The surfactant (AOS) adsorption was reduced by more than half from 1.41 mg/g to 0.52 mg/g by 0.75 wt% Na_2CO_3 addition to surfactant solution. Ahmadi and Shadizadeh [160] performed core flooding experiments (at temperature = 90 ^oC and pressure = 2500 psi) for dynamic adsorption of natural surfactant onto the surface of shale-sandstone core plugs obtained adsorption values of 3.32 mg/g and 6.89 mg/g respectively. Lv et al. [205] reported the dynamic adsorption study of alkyl benzene sulfonate and betaine solutions injected through sand pack containing kaolinite. Their results indicated reduction of alkyl benzene sulfonate and betaine adsorption from 1.676 and 3.206 mg/g to 0.355 and 0.686 mg/g respectively with the addition of Na_2CO_3 alkali.

During the preflushing with BL, the SFB used for initial injection was mixed with BL (at various concentrations) followed by the injection of AS solution. This was done to investigate the ability of BL to act as sacrificial adsorbate for reducing the loss of primary surfactant by adsorption and also to find the appropriate concentration of BL for preflushing. The results show that preflushing with BL could further reduce adsorption from 0.52 mg/g (without preflushing) to 0.37 and 0.21 mg/g by increasing the BL preflushing concentration from 0.5 to 1 wt% respectively. It has been reported that

preflushing with lignosulphonate causes the strongly-ionized sulphonate groups to pre-adsorb on the potential adsorption sites of the reservoir rock by means of electrostatic attraction or hydrogen bonding. Thus the negative charge of the reservoir rock surfaces is increased in such a way that rock grain surfaces has little or no affinity for the primary surfactant, reducing its adsorption loss [210-213]. Lignosulphonate, the main constituent of BL, was thus instrumental in reducing surfactant (AOS) adsorption when used for the preflushing prior to surfactant injection. The adsorption results indicated that increasing the BL concentration in the preflush to 1.5 and 2 wt% could not further reduce the adsorption below 0.21 mg/g. This was due to the characteristic property of surfactant adsorption onto solid surfaces of reaching a limiting adsorption value at the critical micelle concentration (CMC) value [214]. The CMC of BL in formation brine (SFB) was determined by plotting surface tension versus the surfactant concentration. The CMC concentration corresponds to the point of first lowest surface tension and after the CMC, the surface tension remains fairly constant. Fig. 4.18 shows the plot of surface tension as a function of BL concentration and the CMC value of BL as 1 wt%. Thus, based on the dynamic adsorption study it was observed that the CMC value of BL could be considered as the most suitable concentration for preflushing operation.

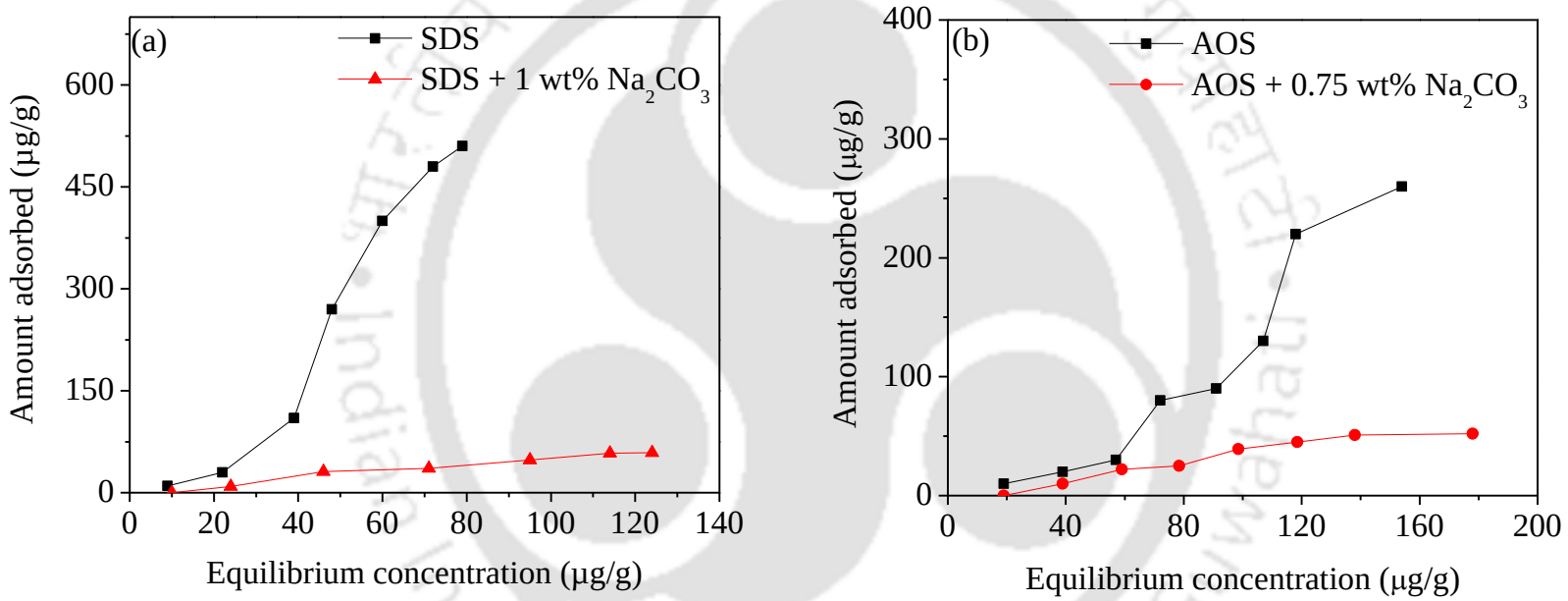

Fig. 4. 14: Static adsorption isotherms of surfactants: (a) SDS and (b) AOS onto reservoir rock at 28 ^{o}C with and without Na_2CO_3 alkali

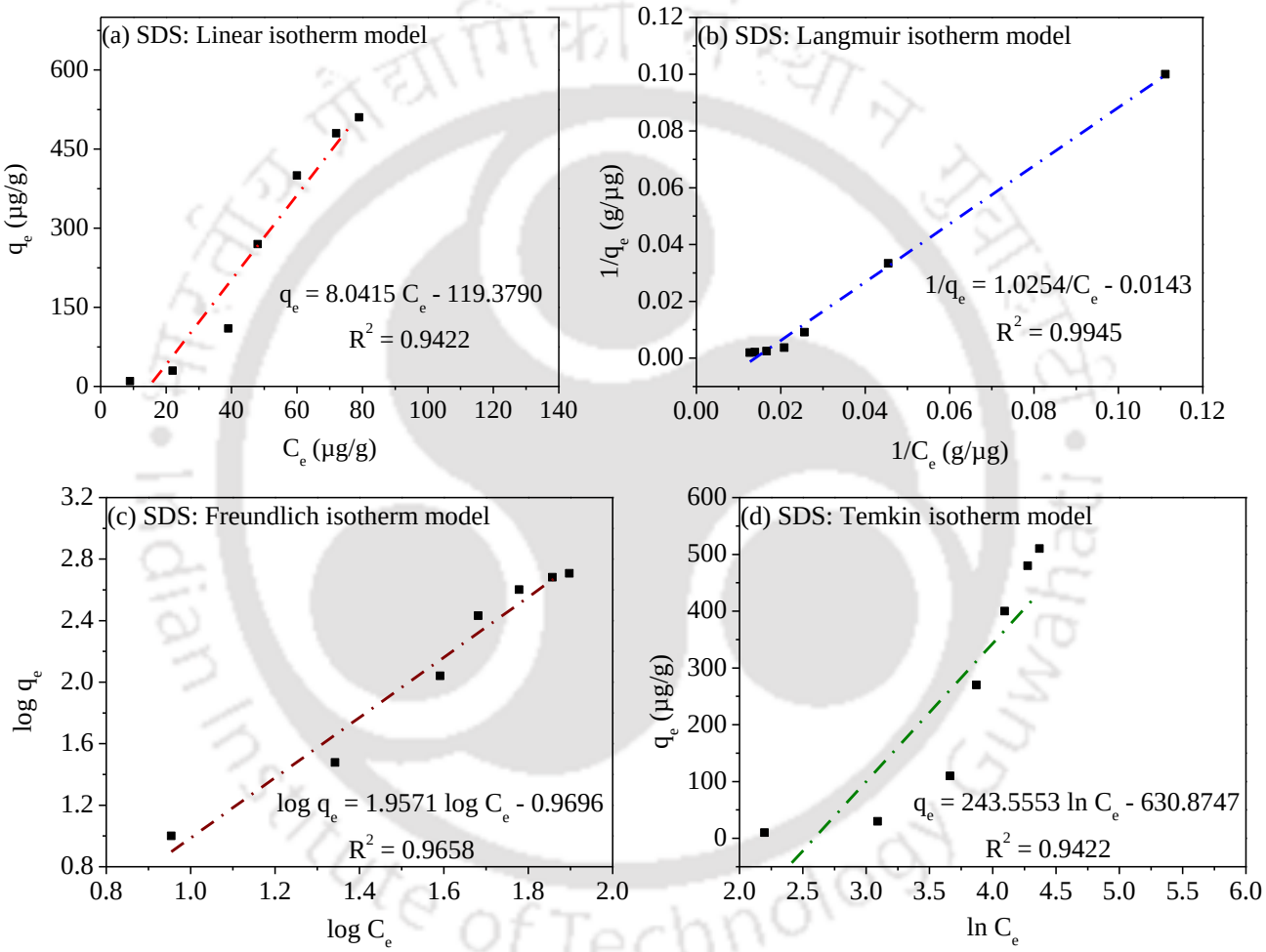

Fig. 4. 15: Adsorption Isothermal model fitting of SDS on reservoir rock samples (a) Linear isotherm model (b) Langmuir isotherm model (c) Freundlich isotherm model and (d) Temkin isotherm model.

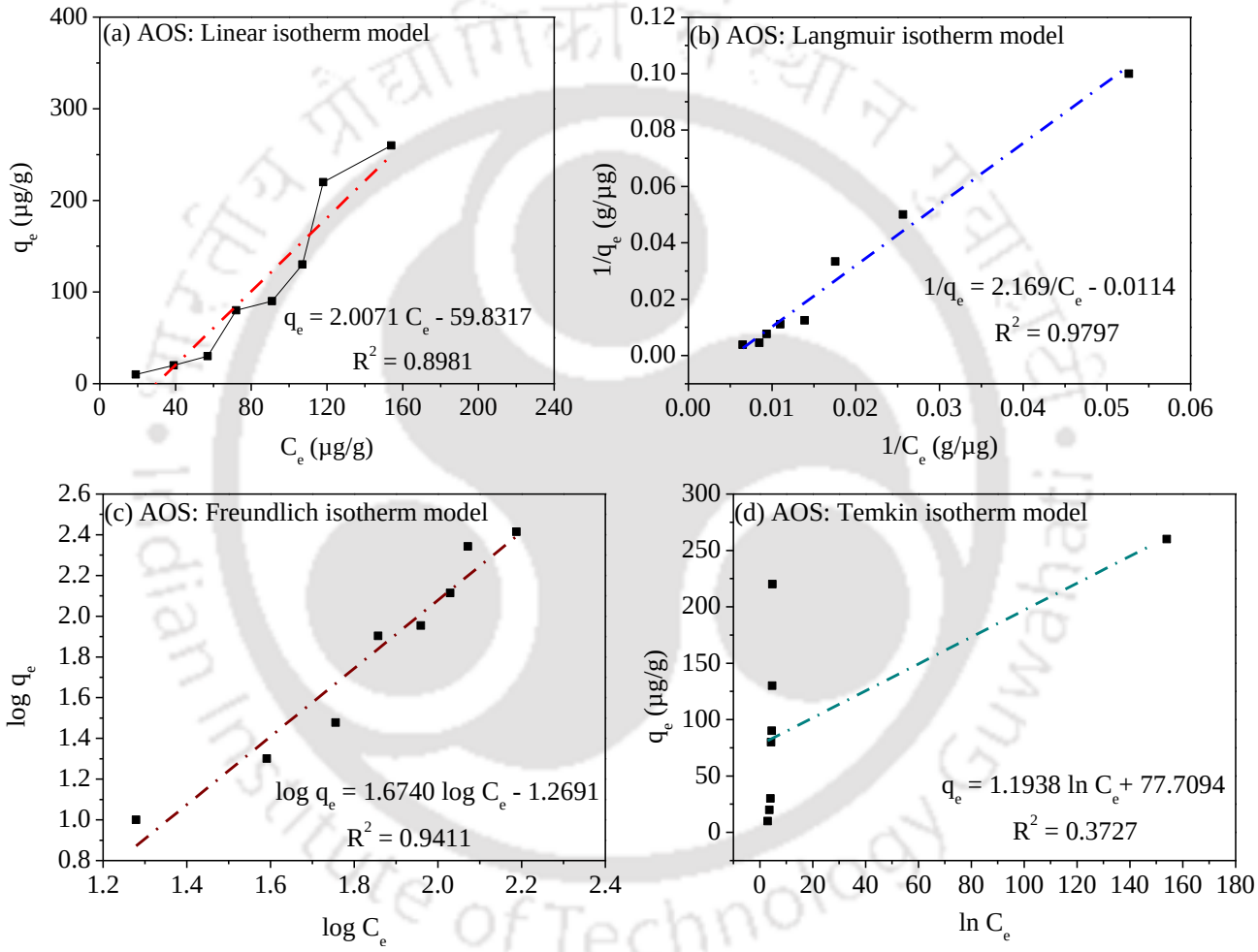

Fig. 4. 16: Adsorption isothermal model fitting of AOS on reservoir rock samples (a) Linear isotherm model (b) Langmuir isotherm model (c) Freundlich isotherm model and (d) Temkin isotherm model.

Table 4. 2 Parameters of different adsorption isotherm model fitting

Isotherm model	Equation	Surfactant	Correlations	Parameters		R^2
Linear isotherm	$q_e = K_H C_e$	SDS	$q_e = 8.0145C_e - 119.3790$	K_H=8.0145	C=-119.3790	0.9422
		AOS	$q_e = 2.0071\ C_e - 59.8317$	K_H=2.0071	C=-59.8317	0.8981
Langmuir	$q_e = \frac{q_{max} K_L C_e}{1 + K_L C_e}$	SDS	$1/q_e = 1.025/C_e - 0.0143$	q_{max}= 69.93	K_L=0.014	0.9945
		AOS	$1/q_e = 2.1690/C_e - 0.0114$	q_{max}= 87.72	K_L=0.0052	0.9797
Freundlich	$q_e = K_F C_e^{1/n}$	SDS	$\log q_e = 1.9571 \log C_e - 0.9696$	n=0.5109	K_F=0.1073	0.9658
		AOS	$\log q_e = 1.6740 \log C_e - 1.2691$	n=0.5974	K_F=0.0538	0.9411
Temkin	$q_e = B \ln K_T + B \ln C_e$	SDS	$q_e = 243.5553 \ln C_e - 630.8747$	K_T=0.075	B=243.5553	0.9422
		AOS	$q_e = 1.1938 \ln C_e + 77.7094$	K_T=1.86e[28]	B = 1.8619	0.3727

C_e = equilibrium concentration (µg/g); q_e = Adsorption at equilibrium time (µg/g); K_H = Linear isothermal model constant;
K_L = Langmuir constant; q_{max} = Langmuir adsorption capacity (µg/g); n = Freundlich constant;
B = Temkin constant. K_T = Temkin constant

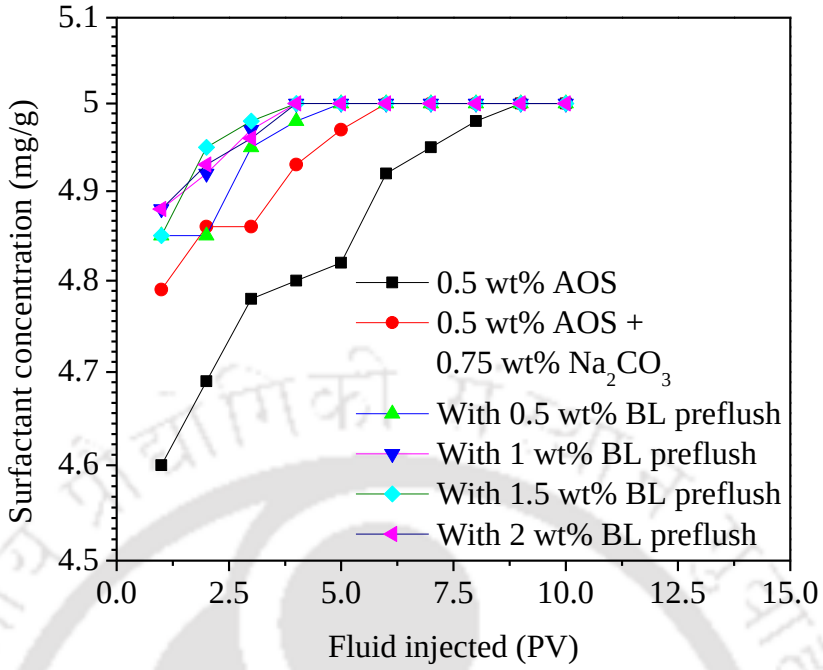

Fig. 4. 17: Surfactant concentration as a function of the pore volume of the fluid injected in dynamic adsorption experiments performed at 70 ^{o}C

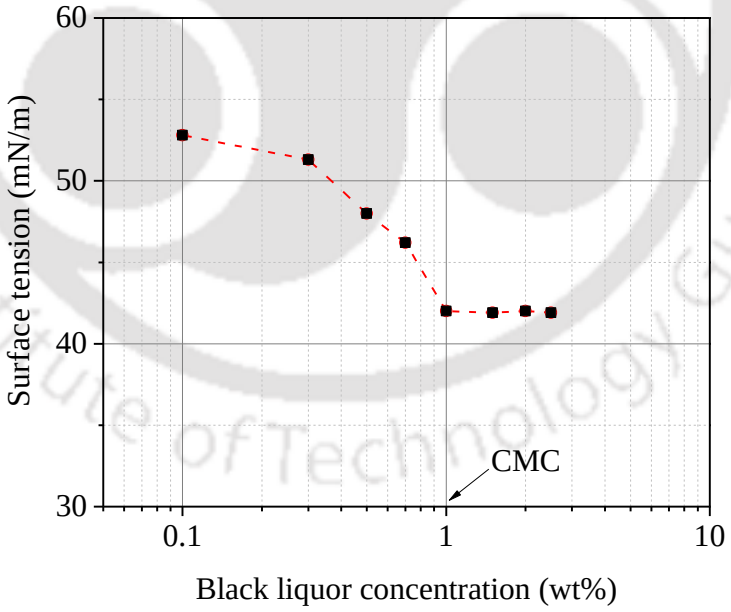

Fig. 4. 18: Surface tension versus black liquor concentration curve for determining CMC

Table 4. 3: Summary to core flood experiments performed to study the dynamic adsorption of surfactant on to core plugs

Sl. No.	PV of core plug (ml)	Dry weight of core plug (g)	Preflush by BL (wt%)	Injected chemical formulation		Equilibrium time (PV)	Adsorption (mg/g)
				AOS (wt%)	Na_2CO_3 (wt%)		
1	18.31	199.34	0	0.5	0	9	1.41
2	16.52	186.28	0	0.5	0.75	6	0.52
3	15.94	160.27	0.5	0.5	0.75	5	0.37
4	16.98	188.82	1	0.5	0.75	4	0.21
5	15.53	158.54	1.5	0.5	0.75	4	0.22
6	16.85	187.86	2	0.5	0.75	4	0.21

4.7 Summary

The optimum chemical formulations for ASAG flooding were designed to fulfill two objectives which are lowering oil-water IFT to ultra-low value and providing good mobility control. The presence of crude oil was found to have a destabilizing effect lowering both the foamability and foam stability of the foaming agents/surfactants. CO_2-foam stability of the surfactant solutions was found to be lower at reservoir temperature (70 ^oC) compared to room temperature (28 ^oC). The maximum CO_2-foam stability in the presence of crude oil at reservoir temperature occurred at 0.3 wt% SDS and 0.5 wt% AOS. The equilibrium IFT measurements showed that when combined with the optimum SDS and AOS formulations, both the alkalis Na_2CO_3 and NaOH could reduce the oil-water IFT values to the ultra-low range. However, Na_2CO_3 was chosen as the IFT values were the lowest. The phase behavior study indicated that 70% of SFB salinity (2400 ppm) corresponded to the optimal salinity where Winsor type III microemulsion volume was maximum. The IFT measurements confirmed that the oil-water IFT value at optimal salinity was the lowest. Further, the addition of alkali was found to considerably decreased the surfactant adsorption onto the reservoir rocks. Additionally, dynamic adsorption studies showed that alkali addition could reduce surfactant (AOS) adsorption by core plug by more than half from 1.41 mg/g to 0.52 mg/g. Preflushing with BL reduced the surfactant loss due to adsorption and the optimum concentration of BL for preflushing was its CMC value.

CHAPTER 5

Enhanced Oil Recovery by ASAG Flooding

Continuous gas injection

Water alternated gas flooding

Surfactant alternated gas flooding

Alkali-surfactant-alternated-gas/CO_2 flooding

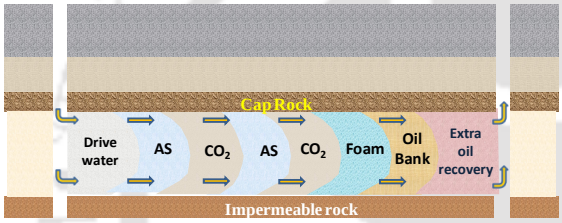

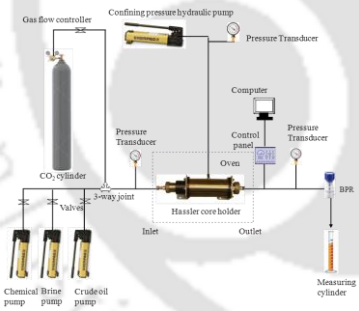

ASAG core flooding

Enhanced oil recovery

Work published as:

1. R. Phukan, S.B. Gogoi, and P. Tiwari, *Enhanced oil recovery by alkaline-surfactant-alternated-gas/CO_2 flooding.* Journal of Petroleum Exploration and Production Technology, Springer, 2019. **9**: p. 247-260.

Chapter 5

Enhanced Oil Recovery by ASAG flooding

This chapter elaborates upon the potential of ASAG flooding for EOR through lab-scale core flooding experiments. A comparative assessment of the additional oil recovering ability of the other EOR techniques like tertiary CGI, CO_2-WAG, SAG, AS, and ASAG flooding is also presented.

5.1 Core Flooding Experiments

The core flooding experiments were performed in a lab-scale core flooding apparatus on sandstone reservoir core plugs using crude oil to evaluate the oil recovery potential of the different EOR injection schemes. After the initial crude oil saturation as described in Section 2.2.11, synthetic formation brine (SFB) was injected at constant pressure with the temperature maintained at 70 ^{o}C during the secondary waterflooding process. Thereafter, fluids were injected under different injection schemes depending on the tertiary EOR process. The injection of liquid was maintained at constant pressure (around 500 psi), while the volumetric gas injection rate was fixed at 0.2 ml/min in most of the experiments. In this study, the potential of the tertiary WAG, SAG and ASAG flooding for EOR was evaluated under immiscible conditions. According to the concept of immiscible flooding, CO_2 is injection at subcritical conditions (critical pressure of CO_2 is 1071 psi) [215]. From the CO_2 phase diagram (shown in Fig. 5.1), it is observed that CO_2 will be in the gaseous state under the experimental conditions (subcritical pressure and reservoir temperature of 70^{o}C). Although the core flooding experiments were conducted under similar experimental conditions, they were not similar entirely. Some core plugs were reused after complete cleaning and drying following its previous flooding operation.

The core plugs could be reused as no appreciable alteration was observed in porosity and permeability values after the flooding process. In each experiment, connate water saturation (S_{wc}), absolute permeability to brine (K_{abs}), oil recovery by secondary water flooding, additional oil recovery, cumulative oil recovery, and pressure drop (ΔP) data were recorded. The oil recovery values obtained from secondary water flooding were found to be in good agreement and in the range of 34 – 37 %OOIP. However, in the BL preflushing experiments during secondary water flooding, the oil recovery was slightly higher in the range of 39 – 40 %OOIP.

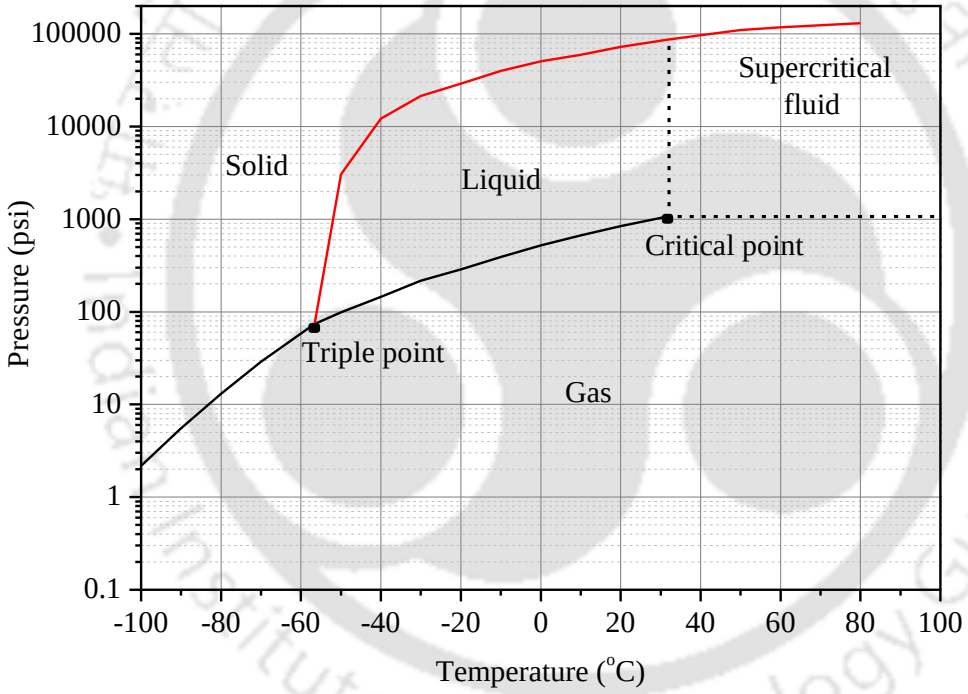

Fig. 5. 1: CO_2 phase diagram [216]

5.2 Comparison of Various EOR Injection Schemes

Eight core flooding experiments were performed to evaluate and compare the performances of tertiary continuous gas injection (CGI), CO_2-WAG, SAG, AS, and ASAG flooding. Similar core plugs with porosity and permeability values in the range 20 – 21% and 6 – 8 md respectively were used in these flooding experiments. In order to ascertain

whether foam was formed in the core plugs during SAG and ASAG flooding, the ΔP data were used to calculate the mobility reduction factor (MRF). MRF is a factor used to characterize the strength of foam generated and is defined as the pressure drop across the core with and without foam [217, 218].

$$MRF = \frac{\Delta P_{foam}}{\Delta P_{no\ foam}} \quad (5.1)$$

where ΔP_{foam} = average pressure drop across the core plug in the presence of foam.

$\Delta P_{no\ foam}$ = average pressure drop across the core plug in the absence of foam.

An MRF value > 1 is an indication of foam formation, and an increase in the value of MRF takes place when stronger foam is formed [217]. The experimental details and results of the eight core flooding experiments are summarized in Table 5.1. The oil recoveries by secondary water flooding were identical, implying that the residual oil saturation in the core plugs was similar prior to the injection of tertiary injection schemes.

5.2.1 Tertiary Continuous Gas Injection (CGI)

In tertiary CGI, gas/CO_2 was continuously injected into the core plug at the constant volume injection rate of 0.2 ml/min under immiscible conditions after secondary water flooding at reservoir temperature (70 ^oC). CO_2 injection was terminated after 3 PV was injected and when no more oil was produced. Fig. 5.2 shows the cumulative oil recovery and ΔP versus the PV of fluid injected. The secondary water flooding resulted in an oil recovery of 36.88 %OOIP. The oil recovery by tertiary CGI was 3.46 %OOIP. The residual oil was produced from the core plug due to the CO_2 invasion into pores which were inaccessible by water flooding [12]. Upon its dissolution with the residual oil, the CO_2 become instrumental in reducing oil viscosity and causing oil swelling in the pores spaces which contribute towards improving the oil recovery from the core plug. However, the recovery was low probably due to the water shielding effect caused by brine injected

during secondary waterflooding, and early injection gas breakthrough. Due to the initial high water saturation after water flooding, the injected gas/CO_2 could not contact a large part of the residual oil in the core plug and had to first displace the water to reach the oil. Additionally, high gas mobility also resulted in poor volumetric sweep efficiency (E_{vo}). The ΔP during CGI was initially around 50 psi but dropped rapidly indicating injection gas breakthrough. Kulkarni and Rao [60] studying the tertiary immiscible CGI with n-decane and Berea core had also reported recovering 4 - 22 %OOIP in their core flooding experiments.

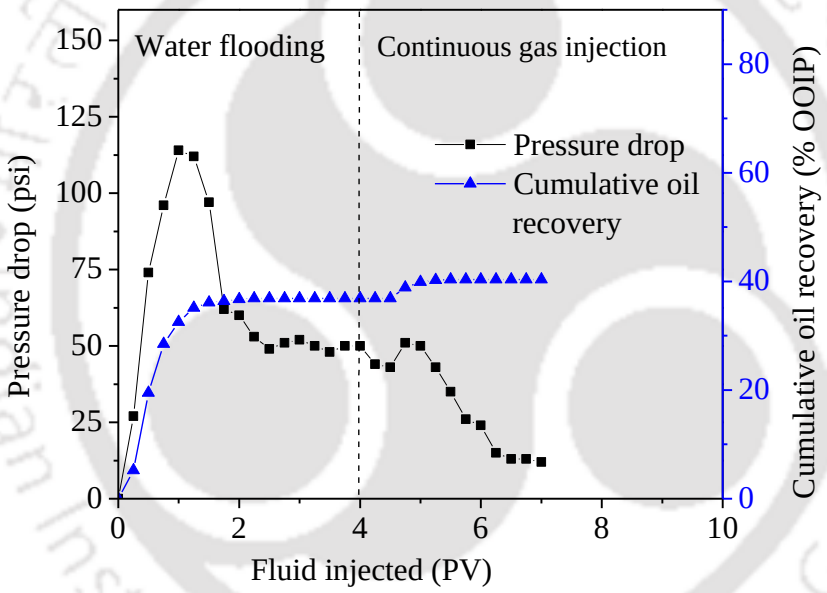

Fig. 5.2: Cumulative oil recovery and pressure drop versus pore volume of fluid injected in tertiary CGI

5.2.2 CO_2-Water Alternating Gas (CO_2-WAG) Flooding

In this experiment, the oil-saturated core plug was subjected to secondary water flooding until no more oil was produced. The oil recovery after injection of 4 PV of SFB was 36.17 %OOIP. The core plug with residual oil was then subjected to immiscible CO_2-WAG flooding during which four cycles of WAG were injected with each cycle consisting of 0.25 PV of CO_2 and 0.25 PV of SFB. Thus the total volume of fluid injected during the

CO_2-WAG process was 2 PV. WAG injection was followed by the drive in the form of 4 PV of extended water flooding (EWF). Fig. 5.3 shows the cumulative recovery and ΔP versus PV of fluid injected in CO_2-WAG flooding. The oil recovery post water flooding increased to 7.96 %OOIP. This amounted to a cumulative oil recovery of 44.13 % OOIP. The improvement in oil recovery by CO_2-WAG was 4.5 %OOIP over tertiary CGI. The combination of CO_2 and water in the WAG process reduced gas/CO_2 mobility due to the increased water saturation in core plugs [82]. The result was an improved frontal displacement of the residual oil and consequently higher oil recovery. As CO_2 and water were injected in short alternate slugs, the early breakthrough of the gas/CO_2 was prevented that improved the sweep efficiency. Thus, additional oil was mobilized by the injected gas/CO_2 and consequently higher oil recovery resulted. The drastic decline in the ΔP was not observed in WAG flooding unlike the CGI process. This clearly indicated that the gas mobility was effectively controlled. A cyclic trend of ΔP was observed throughout the WAG cycle as the injected fluid switched between CO_2 and brine. After oil bank breakthrough and production of residual oil, the ΔP across the core plug stabilized during the EWF period. The average ΔP during the WAG process was 51.63 psi. The oil recovery by CO_2-WAG injection was in good agreement with data reported in the literature. Kulkarni and Rao [60] while conducting immiscible CO_2-WAG core flooding on Berea cores with n-decane as the oil phase obtained oil recovery of 8.3 %OOIP, which was much lower than miscible WAG recovery (35 %OOIP). The field incremental oil recovery by CO_2-WAG is also reported to be low and in the range of 5 to 10 %OOIP [59, 61, 219].

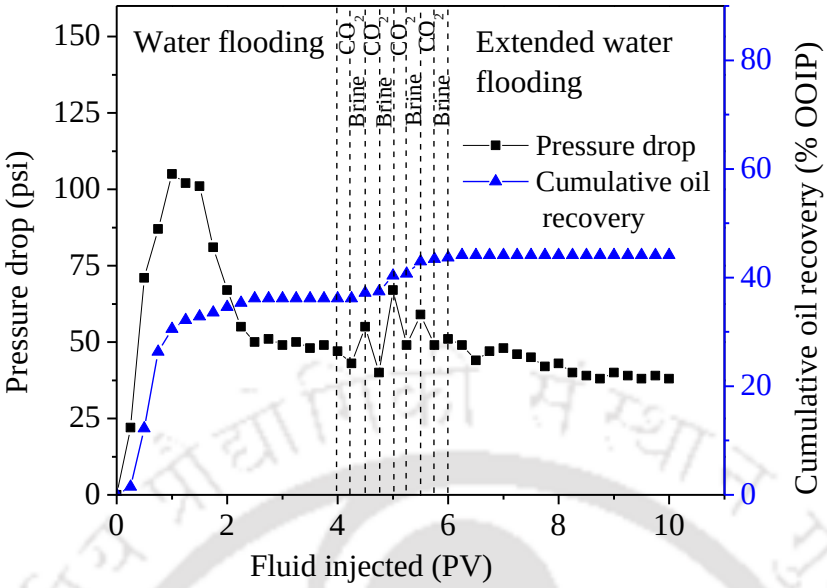

Fig. 5.3: Cumulative oil recovery and pressure drop versus pore volume of fluid injected in CO_2 - WAG flooding

5.2.3 Surfactant Alternating Gas (SAG) Flooding

The surfactant formulations which displayed the best CO_2-foam stability at reservoir temperature in presence of crude oil (0.3 wt% SDS and 0.5 wt% AOS) were chosen as the chemical slugs for the SAG core flooding experiments. The core plug was initially subjected to water flooding which resulted in oil recoveries in the range of 35 – 37 %OOIP after 4 PV of brine (SFB) injection. This was followed by SAG flooding which included four cycles of alternated 0.25 PV gas/CO_2 and 0.25 PV of surfactant solution injection. Finally, the core plugs were flooded with 4 PV of SFB during EWF. The additional oil recoveries obtained were 18.89 %OOIP and 17.23 %OOIP for the two core flooding experiments. This amounted to an improvement of more than twice the oil recovery by the CO_2-WAG process. As the test conditions were maintained the same as in CO_2-WAG, the additional recovery highlights the beneficial effect of surfactant addition to brine on the oil recovery during the WAG process. Fig. 5.4 (a) - (b) shows the cumulative

oil recovery and the ΔP as a function of the PV of fluid injected in the two SAG processes. The average ΔP increased to 60.00 psi and 61.13 psi during the two SAG injection experiments, and the corresponding MRF values were 1.16 and 1.18. These MRF values > 1 were indicative of in-situ foam formation in the core plug due to the alternate cycles of surfactant solution and gas/CO_2 injection during SAG flooding [76, 186]. Foam generation in the core plug had increased the apparent viscosity of CO_2 gas, thus making the mobility ratio favorable. Consequently, better gas mobility control and improvement in E_{vo} resulted in higher oil recovery. The increased recovery during the SAG process could also be attributed to the decrease in the oil-water IFT caused by the addition of surfactant to brine. The results of IFT measurements indicated that the addition of surfactants (SDS and AOS) could lower the oil-water IFT values to as low as 0.2 – 0.3 mN/m. These IFT values were much lower than the typical crude oil-brine IFT values of 18 – 32 mN/m [220]. With the decrease in the IFT, the capillary number (N_{cap}) increased which helped in mobilizing the trapped oil in the core plug leading to higher oil recovery. In addition, injecting the surfactant solutions is also known to alter wettability of the reservoir rock to more water-wet condition which helps in improving the oil recovery [221]. Further, a correctly designed surfactant solution can combine with brine and crude oil to form microemulsion at oil-water interface further reducing the IFT to the lowest value for improved oil recovery [222]. Moayedi et al. [223] reported incremental oil recovery of 12 %OOIP, which was 9% higher than WAG flooding, from tertiary SAG core flooding experiments performed using Berea sandstone cores with Hibernia crude oil.

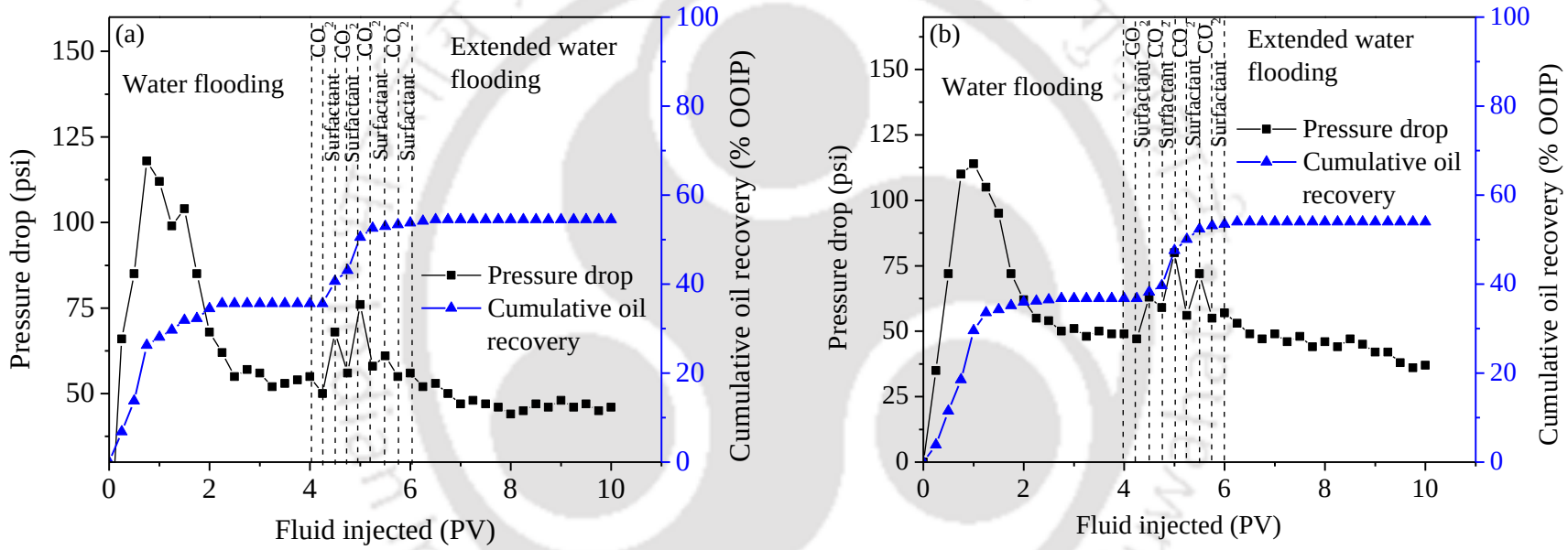

Fig. 5.4: Cumulative oil recovery and pressure drop versus pore volume of fluid injected in immiscible SAG flooding with chemical slug: (a) 0.3 wt% SDS, and (b) 0.5 wt% AOS

5.2.4 Alkaline-Surfactant (AS) Flooding

Two additional core flooding experiments were performed with only the AS formulation without gas to compare the effect of chemical flooding with combined gas-chemical flooding. The chemical slug used in the two AS flooding experiments were 0.3wt% SDS + 1 wt% Na_2CO_3 and 0.5wt% AOS + 0.75 wt% Na_2CO_3 respectively. Following secondary water flooding, the core plug was subjected to 1 PV of chemical slug injection at a constant rate followed by 5 PV of SFB injection. Fig. 5.5 (a) – (b) shows the cumulative oil recovery and ΔP data of the two tertiary AS flooding experiments. The residual oils recovered were 16.34 %OOIP and 15.20 %OOIP respectively - higher than CGI and WAG flooding. Kumar et al. [224] reported incremental oil recovery of 20 – 40 %OOIP from AS flooding in sand packs with heavy oils of Alaska. Several mechanisms are responsible for oil recovery by AS flooding including a decrease in oil-water IFT, the formation of in-situ surfactants by the reaction between alkali and acidic components of crude oil, wettability alteration, and emulsification of oil in water [138]. Adding alkali and surfactants at optimum concentrations decreased the oil-water IFT values of the alkali-surfactant (AS) formulations to ultra-low values (0.0068 mN/m and 0.0087 mN/m). Thus the capillary held residual oil in the core plug could be mobilized and extra oil recovery was obtained. In addition, it was observed from the phase behaviour study that alkali-surfactant solutions at optimum salinity formed Winsor type III microemulsion This type of microemulsion plays a very crucial role in enhanced oil recovery operations because of its ultra-low IFT environment and ability to produce maximum oil [155]. It can be observed from the figures that a rise in ΔP occurred during the AS injection as the oil bank was formed due to the mobilization of the residual oil by the chemical slug. But after the oil bank and injection fluid breakthrough, the ΔP decreased continuously before stabilizing at around 40 psi during the EWF. The average pressure drop during AS injection period were 62.50 psi and 59.75 psi respectively for the two experiments.

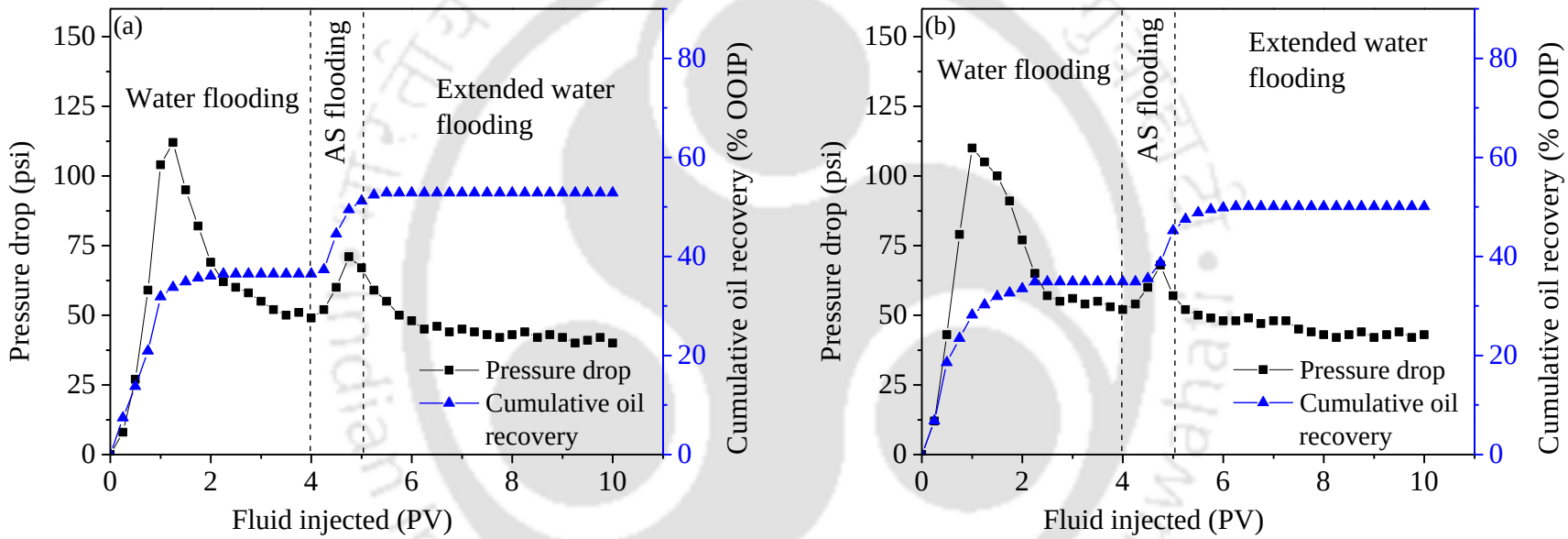

Fig. 5.5: Cumulative oil recovery and pressure drop versus pore volume of fluid injected in tertiary AS flooding performed with chemical slugs: (a) 0.3 wt% SDS + 1 wt% Na_2CO_3, and (b) 0.5 wt% AOS + 0.75 wt% Na_2CO_3

5.2.5 Alkaline-Surfactant-Alternated-Gas (ASAG) Flooding

The performance of tertiary ASAG flooding was studied by performing two core flooding experiments for the two selected AS chemical slug. SFB was first injected into the oil-saturated core plug during the secondary water flooding. The experiment was then switched to ASAG flooding in which 4 cycles of alternated 0.25 PV gas/CO_2 and 0.25 PV AS slug were injected. Fig. 5.6 (a) – (b) shows the cumulative oil recovery and ΔP versus PV of fluid injected during the ASAG flooding experiments. With core plugs of identical properties, the oil recoveries of equivalent magnitude were obtained by secondary water flooding (35 – 37 %OOIP) under similar experimental conditions. The immiscible tertiary ASAG flooding resulted in additional oil recoveries of 23.85 %OOIP and 21.87 %OOIP respectively, which were 7.51 %OOIP and 6.67 %OOIP higher than the respective AS flooding experiments. The higher oil recovery by ASAG flooding compared to AS flooding highlighted the synergic effect of AS and gas/CO_2 alternate injection. The early breakthrough of the injected chemical slug resulted in reduced E_{vo} and consequently lower oil recovery during AS flooding. However, during ASAG flooding the early injection fluid breakthrough was prevented due to the injection of both AS and gas/CO_2 in short alternate slug. The presence of both injected fluids reduced the mobility of each other. Moreover, high gas mobility was controlled due to in-situ foam generation during ASAG flooding. Foam does not make the CO_2 gas less mobile, but increases the apparent viscosity of the gas and decreases the relative permeability of the liquid thus making the mobility ratio favorable [57]. Further, the injection of the AS formulations lowered the oil-water IFT to the lowest values to produce the adherent oil from the core plug. The CO_2 injected also resulted in oil-swelling and viscosity reduction, thereby improving oil recovery. Thus, combination of all the above mechanisms accounted for the highest oil recovery obtained by ASAG flooding. Luo et al. [124] reported better oil recovery during ASP/CO_2 flooding (27.43 %OOIP) for Saskatchewan heavy oils, compared to CO_2-WAG flooding (9.43

%OOIP) in core flooding experiments performed on sand packs prepared with Ottawa sands. Srivastava et al. [78] had reported incremental oil recovery of 29% OOIP from immiscible ASG (AS alternated CO_2) flooding with Berea sandstone cores and Limbodara crude oil.

As shown in Figure 5.6, the ΔP continuously fluctuated as the chemical slug and the gas/CO_2 were alternately injected during the ASAG cycle. At the beginning of water flooding, the ΔP across the core plug build up and then sharply decreased after reaching a peak following water breakthrough. ΔP was further observed to stabilize to a steady-state value towards the end of the waterflood. During the ASAG flooding, when the first slug of gas/CO_2 was injected, the ΔP decreased slightly due to the low viscosity of CO_2 gas. The injected CO_2 gas mobilized some of the residual oil due to dissolution forming an oil bank, so a slightly increasing trend of ΔP was observed towards the end [61]. Thereafter, the increasing trend of ΔP continues during the first alternating chemical slug injection because of the change in viscosity of the injected fluid (from gas to liquid) and as oil bank grew while moving through the core plug. The injection of chemical slug mobilized residual oil increasing the oil bank size. The increase in the oil bank size and foam generation also raised the ΔP. During the second slug of CO_2 injection, a decreasing trend of ΔP was again observed like in the first cycle. However, ΔP increased during the second alternating chemical slug injection reaching the peak ΔP value just ahead of the oil bank breakthrough. The formation of a second ΔP peak was related to the generation of a second oil bank. The highest ΔP peak value occurred in the second cycle because of the flow resistance offered by the propagating oil banks and foam generated. As a major part of the residual oil was produced during the first two cycles, the sizes of oil banks formed in the later cycles decreased gradually resulting in a lowering of ΔP peak values. The average ΔPs recorded during the two ASAG flooding were 65.75 psi and 66.13 psi respectively (Table 3.1). A comparison of these values with the data of AS flooding experiments indicated that the higher average ΔP in ASAG flooding was because of in-situ foam

generation and not due to the displacement of microemulsion formed during the process. Similar difference in the average ΔP during ASG flooding (with gas) and AS flooding (without gas) was reported by Cottin et al. [79].

The MRF values were calculated using Eq. (5.1), and found to 1.27 and 1.28 respectively. The values were greater than 1which suggested the generation of foam during these processes. Further, the higher MRF values of ASAG flooding compared to SAG implied stronger in-situ foam formation in the core plug. With stronger foam formed, gas mobility control had improved and a more efficient displacement front was formed leading to an increase in E_{vo}. Alkali is known to react with the naphthenic acids present in crude oils to produce in situ surfactants. The presence of both the injected and in-situ surfactants helped to lower the oil-water IFT to ultra-low value. This ultra-low IFT was instrumental in mobilizing the capillary held residual oil, thereby increasing the oil recovery. Additionally, the presence of alkali also reduced the adsorption of surfactant by the core plug. With less adsorption, more surfactants were available for foam formation and its propagation through the core plug resulting in the better displacement of the residual oil. Combinations of all these factors were responsible for the observed increase in the oil recovery during ASAG flooding.

To study the water production behavior during ASAG flooding, the water-cut data along with the cumulative oil recovery plot for the first ASAG flooding experiment were plotted and is shown in Fig. 5.7. During the oil saturation phase, crude oil was injected into the core plug at a constant rate until the water cut in the effluent reached 0%. During the water flooding operation, 4 PV of SFB was injected again at a constant rate to establish residual oil saturation indicated by 99% water cut. At the start of waterflooding, only crude oil was produced (water cut ≈ 0 %) until water breakthrough occurred at 0.75 PV. From there onwards the water cut gradually increased until it reached 99% at about 2.75 PV and continuing to the end of water flood.

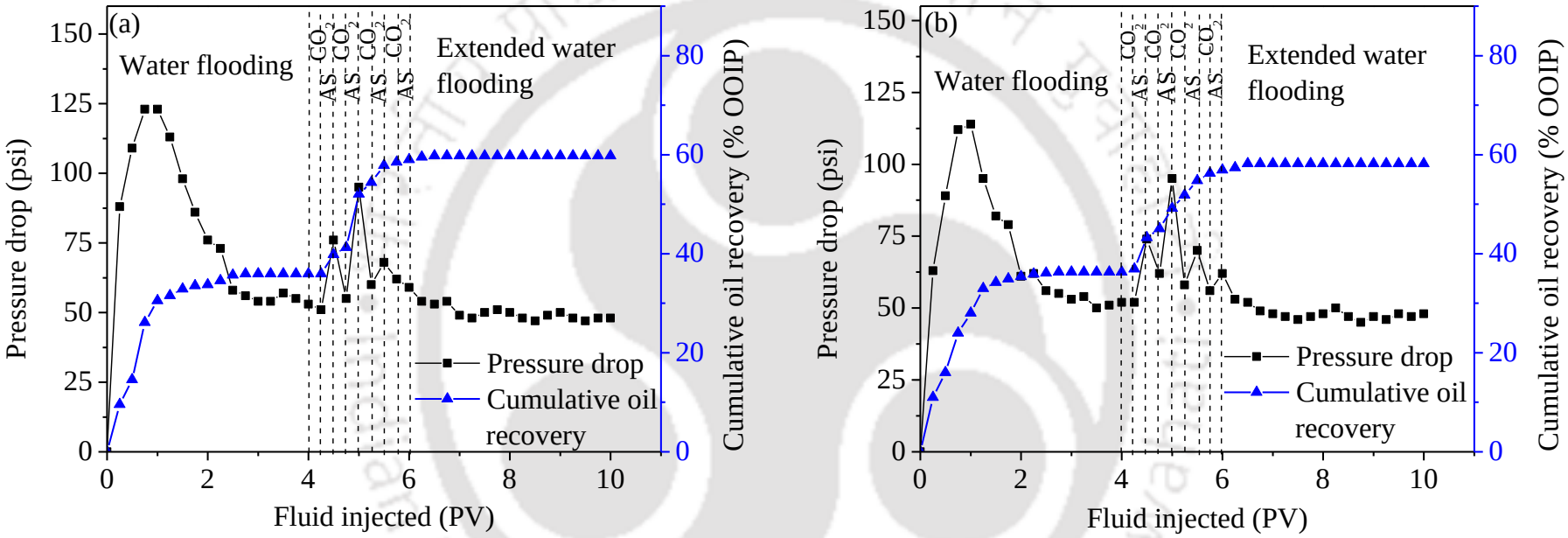

Fig. 5.6: Cumulative oil recovery and pressure drop versus pore volume of fluid injected in immiscible ASAG flooding performed with chemical slugs: (a) 0.3 wt% SDS + 1 wt% Na_2CO_3, and (b) 0.5 wt% AOS + 0.75 wt% Na_2CO_3

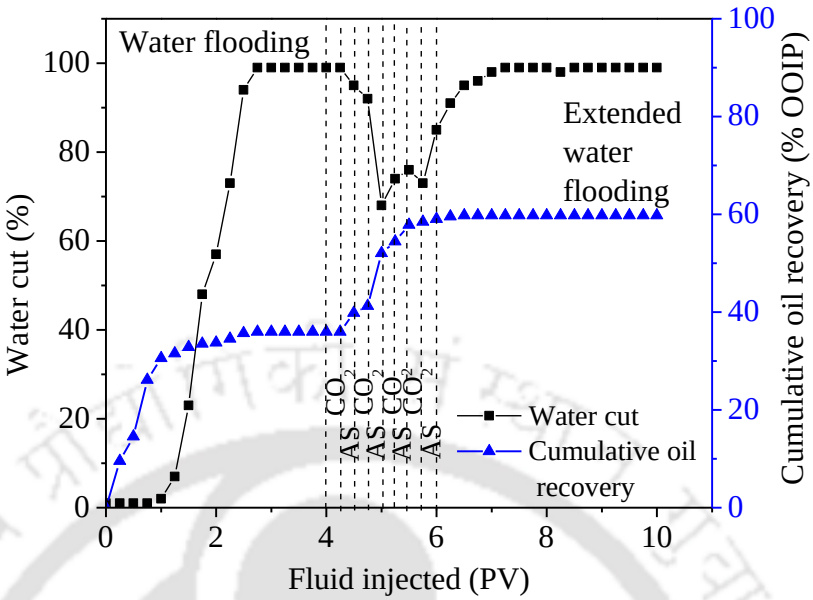

Fig. 5.7: Water-cut and cumulative oil recovery versus pore volume of fluid injected in ASAG flooding performed with the chemical slug: 0.3 wt% SDS + 1 wt% Na_2CO_3

As the four-cycle ASAG flooding mobilized and recovered residual oil, the water cut in the effluent was also observed to change. In the first cycle, a little oil was produced so the water cut was around 94%. However, during the second cycle maximum oil production was observed so that the effluent water cut reached the lowest value of 68% at 5 PV. In the subsequent third and fourth cycles, an increasing trend of water cut was observed as the amount of oil produced in the effluent decreased gradually. Finally, the water cut reached 99% during the EWF period when very little oil was produced.

Table 5. 1: Summary of core flooding experiments performed with various EOR injection schemes

Sl. No.	Description	ϕ (%)	K (mD)	Saturation (%)		Fluid Injected (PV)			Avg. ΔP	MRF	Recovery (% OOIP)		
			K_{abs}	S_{oi}	S_{wc}	WF	EOR	EWF	(psi)		WF	EOR	Total
1	Tertiary CGI	20.49	6.58	73.52	26.48	4.00	3.00		30.75	-	36.88	3.46	40.34
2	WAG	20.76	7.11	74.82	25.18	4.00	2.00	4.00	51.63	-	36.17	7.96	44.13
3	SAG (with SDS)	20.73	6.87	73.31	26.69	4.00	2.00	4.00	60.00	1.16	35.62	18.89	54.51
4	SAG (with AOS)	20.52	7.42	72.65	27.35	4.00	2.00	4.00	61.13	1.18	36.74	17.23	53.97
5	AS flooding (with SDS)	20.69	6.98	74.14	25.86	4.00	1.00	5.00	62.50		36.48	16.34	52.82
6	AS flooding (with AOS)	20.14	6.50	73.16	26.86	4.00	1.00	5.00	59.75		34.87	15.20	50.07
7	**ASAG I** (with SDS)	20.27	6.87	74.21	25.79	4.00	2.00	4.00	65.75	1.27	35.94	23.85	59.79
8	**ASAG II** (with AOS)	20.49	6.10	73.35	26.65	4.00	2.00	4.00	66.13	1.28	36.31	21.87	58.18

5.3 Summary

This chapter highlighted the successful application of combined alkali, surfactant, and gas/CO_2 injection for improving oil recovery of medium gravity crudes through core flooding experiments performed with sandstone core plugs. The oil recovery by tertiary CGI was low (3.46 %OOIP) due to the early injection gas breakthrough. Unlike CGI, the drastic decline in ΔP was not observed in CO_2-WAG flooding due to gas mobility control which resulted in the incremental oil recovery of 7.96 %OOIP. The oil recovery by SAG flooding increased by more than double (~ 18 %OOIP) compared to CO_2-WAG when the best performing surfactant formulations were injected alternately with gas/CO_2. Higher oil recovery was possible primarily due to the lowering of oil-water IFT due to surfactant addition and gas mobility control caused by in-situ foam formation (MRF values > 1).

Further, the effect of adding the optimum AS formulations to brine in the WAG process was evaluated through ASAG flooding. The highest oil recovery (~ 23 %OOIP) amongst all the EOR processes was achievable by the tertiary immiscible ASAG flooding. The attributes that made ASAG flooding the favorable option include attainment of ultra-low IFT, reduction of fluid mobility, stronger foam generation, and reduction of surfactant adsorption. A fluctuation of ΔP was observed as the chemical slug and the gas were alternately injected during the ASAG cycle. The mobilization of residual oil by the injected fluids resulted in the formation of the oil banks which were indicated by the development of ΔP peaks during ASAG flooding. Moreover, ΔP behavior of AS flooding and ASAG flooding revealed that higher average ΔP during ASAG flooding was due to in-situ foam generation and not due to displacement of microemulsion formed during the process.

CHAPTER 6

Key Parameters Influencing ASAG Flooding

Key operational parameters

Slug size

Slug ratio

Tapering

Application of salinity gradient

Black liquor preflushing

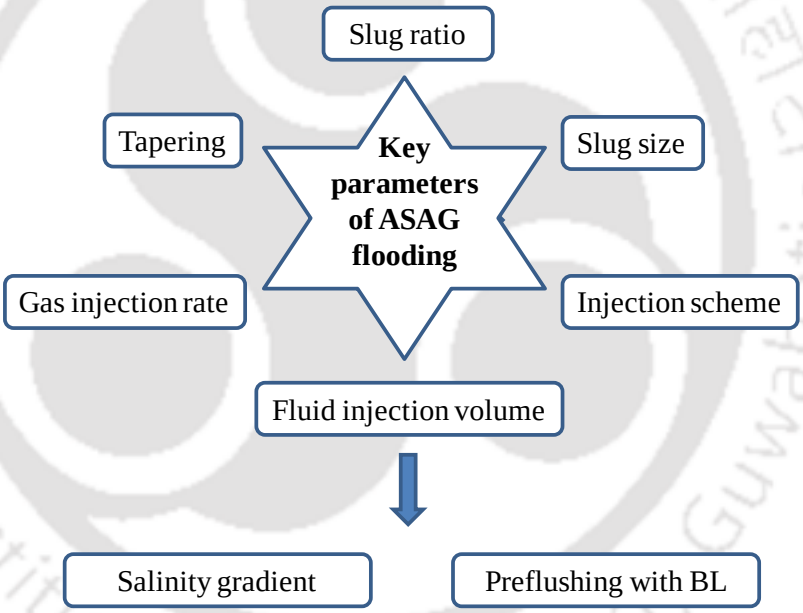

Work published as:

1. R. Phukan, S.B. Gogoi, and P. Tiwari, *Alkaline-surfactant-alternated-gas/CO_2 flooding: Effects of key parameters.* Journal of Petroleum Science and Engineering, Elsevier, 2019. 173: p. 547-557.
2. R. Phukan, S.B. Gogoi, P. Tiwari, and R.S.Vadhan, *Optimization of immiscible alkaline-surfactant-alternated-gas/CO_2 flooding in an Upper Assam oilfield*, in *SPE Western Regional Meeting* 2019, Society of Petroleum Engineers: San Jose, California, USA. p. 23, SPE-196262-MS.

Chapter 6

Key Parameters Influencing ASAG Flooding

This chapter addresses the effects of key operational parameters on the performance of ASAG flooding. The optimum conditions for the best oil recovery by ASAG flooding evaluated based on the core flooding experiments is presented. For the purpose of improving process efficiency, this chapter also highlights the applications of salinity gradient and preflushing during ASAG flooding.

6.1 Introduction

Chapter 5 highlighted the potential of ASAG flooding for EOR and showed that its overall displacement efficiency was better compared to SAG and WAG flooding. The alternate injection of gas/CO_2 and AS slug resulted in in-situ foam generation during the ASAG flooding as indicated (MRF value > 1). Foam was instrumental in providing mobility control and increasing the volumetric sweep efficiency (E_{vo}). However, in order to establish ASAG flooding as a viable EOR method, the effects of key parameters on the performance of ASAG flooding require further investigation. These operating parameters are to be adjusted and optimized before ASAG flooding can be successfully applied in a particular oil reservoir. A number of ASAG core flooding experiments were performed to ascertain the performance of ASAG flooding under different injection schemes and to find the optimum operating conditions. ASAG I and ASAG II described in section 5.2.5 represented the ASAG flooding experiments performed with the most suitable operating parameters using the two optimum chemical formulations 0.3 wt% SDS + 1 wt% Na_2CO_3 and 0.5 wt% AOS + 0.75 wt% Na_2CO_3 respectively. The results of the other core flooding

experiments are presented along with these two ASAG flooding experiments to examine the influence of various parameters on the performance of the immiscible ASAG flooding.

6.2 Effect of ASAG Slug Ratio

ASAG slug ratio means the ratio of the PV of chemical solution to the PV of CO_2 gas injected in each ASAG cycle. In order to study the effect of different ASAG slug ratio on the oil recovery efficiency, two core flooding experiments were performed with the slug ratios of 2:1 and 1:2. The ASAG I experiment was carried out using the first chemical formulation (0.3wt% SDS + 1wt% Na_2CO_3) with the slug ratio of 1:1. For the 2:1 slug ratio experiment, 0.167 PV gas/CO_2 and 0.333 PV AS slug were alternately injected per cycle during ASAG flooding keeping other operating conditions the same as in ASAG I. Thus liquid volume was increased per cycle and its effect on the oil recovery was studied. Fig. 6.1 (a) shows the cumulative oil recovery and ΔP across the core plug versus the PV of fluid injected with 2:1 slug ratio. The oil recovery achieved was 20.05 %OOIP, which is lower than ASAG I (23.85 %OOIP). The average ΔP also dropped to 59 psi and the corresponding MRF value decreased to 1.14. This implied that less strong foam was formed compared to ASAG I performed with a slug ratio of 1:1. Thus increasing the volume of chemical solution per cycle could not improve the oil recovery factor. The higher volume of chemical solution results in the early breakthrough of the chemical solution leading to a decrease in the E_{vo} and consequently low oil recovery. Moreover, with the increase in the volume of chemical solution the fraction of gas in the injected fluid was reduced which dispersed the gas in the aqueous phase. As the gas was held in the aqueous phase, the injected gas was unable to contact the residual oil in the pores of the core plug, reducing the microscopic displacement efficiency (E_{do}) [66].

The effect of gas volume increase per cycle during the ASAG process was observed by changing the slug ratio to 1:2. This was accomplished by injecting 0.333 PV

gas/CO_2 and 0.167 PV of AS slug alternately in each ASAG cycle. Fig. 6.1(b) shows the cumulative oil recovery and ΔP across the core plug versus the PV of fluid injected with 1:2 slug ratio. The oil recovery obtained was 21.11% OOIP, which is less than the recovery with the slug ratio of 1:1 but more than with the slug ratio of 2:1. The average ΔP during the process was 61.50 psi, and the corresponding MRF value was 1.19 Table 6.1). This implied that stronger foam was generated when the gas volume was increased during the cycle and hence the comparatively higher oil recovery. However, by increasing the gas volume the amount of chemical solution available to mobilize residual oil decreased resulting in reduced E_{do}. Furthermore, an increase of injected gas caused early gas breakthrough reducing the E_{vo}. Because of these reasons, lower oil recovery was obtained compared to the slug ratio of 1:1. Thus, among the three ASAG slug ratios, the most suitable injection scheme for ASAG flooding was 1:1 as the highest oil recovery and strongest foam were generated with this slug ratio. Salehi et al. [66] reported the achievement of maximum oil recovery efficiency with SAG ratio of 1:1 at which both the E_{do} and E_{vo} were high. Han and Gu [225] on the basis of their study on miscible WAG concluded that WAG slug ratio of 1:1 was especially suitable due to high oil recovery and production rate combined with moderate CO_2 consumption. Other researchers also observed that 1:1 slug ratio was optimum for WAG process [226-228]. However, Rahimi et al. [53] have reported that 2:1 WAG ratio was best suitable for their study on miscible CO_2-WAG which resulted in the highest oil recovery, high oil production rate, and low CO_2 consumption.

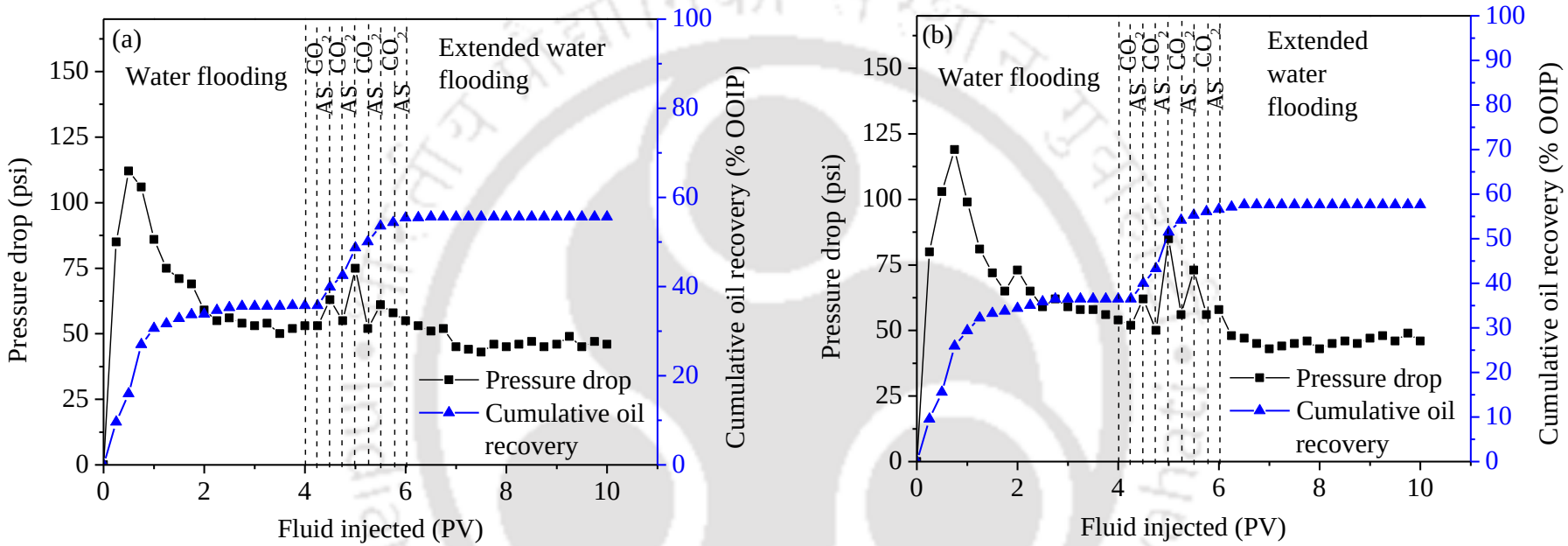

Fig. 6.1: Cumulative oil recovery and pressure drop versus pore volume of fluid injected in ASAG flooding with slug ratio: (a) 2:1, and (b) 1:2

Table 6. 1: Summary of core flooding experiments evaluating the effects of ASAG slug ratio, slug size, and injection scheme

Sl. No.	Description	ϕ (%)	K (mD)	Saturation (%)		Fluid Injected (PV)			Avg. ΔP	MRF	Recovery (% OOIP)		
			K_{abs}	S_{oi}	S_{wc}	WF	EOR	EWF	(psi)		WF	EOR	Total
1	**ASAG I** • Slug ratio (1:1) • Slug size (0.25) • GAC	20.27	6.87	74.21	25.79	4.00	2.00	4.00	65.75	1.27	35.94	23.85	59.79
2	Slug ratio (2:1)	20.73	5.72	73.17	26.83	4.00	2.00	4.00	59.00	1.14	35.56	20.05	55.61
3	Slug ratio (1:2)	20.49	6.10	72.14	27.86	4.00	2.00	4.00	61.50	1.19	36.48	21.11	57.59
4	Slug size (0.33)	20.51	5.97	73.8	26.2	4.00	1.98	4.00	59.50	1.16	36.65	19.74	56.39
5	Slug size (0.50)	20.62	5.25	75.13	24.87	4.00	2.00	4.00	55.13	1.07	35.03	17.59	52.62
6	Slug size (1.00)	20.73	6.10	76.91	23.09	4.00	2.00	4.00	53.38	1.04	34.39	12.64	50.66
7	CAG	20.37	6.35	77.15	22.85	4.00	2.00	4.00	60.24	1.17	35.42	19.78	55.20

6.3 Effect of ASAG Slug Size

Three core flooding experiments performed under similar experimental conditions with different ASAG slug size or cycle frequency were compared with the performance of ASAG I. The aim was done to study the effect of various slug sizes on the performance of ASAG flooding. These experiments were conducted with the same slug ratio of 1:1 and total fluid injection of 2 PV, but with different slug sizes of 0.33, 0.5, and 1 PV. Slug size means the PV of the fluid (AS formulation or gas/CO_2) injected per cycle. For optimal oil recovery with the best utilization of injected fluids, injection of the chemical or the gas slug in the correct volume during the ASAG process is desirable. The cumulative oil recovery and the ΔP data of the three experiments are shown in Figure 6.2 and Table 6.1. The additional oil recoveries of 19.74%, 17.59%, and 13.27% OOIP were achieved with slug sizes of 0.33 PV, 0.5 PV, and 1 PV respectively. These oil recoveries were lower than ASAG I (23.85 %OOIP) performed with the slug size of 0.25 PV. Thus, slug size affected the oil recovery by ASAG flooding. More specifically, higher oil recovery by ASAG flooding was achieved with a smaller slug size. This was probably due to the fact that with smaller slug size (consequently, more cycles) better contacts between the chemical solution and CO_2 gas were possible which improved foam generation. Increasing the slug size, on the other hand, decreases the E_{vo} due to earlier fluid breakthrough. However, too small a slug size raises the operating cost as the higher cycle frequency will require the fluids to be alternately injected more frequently [225]. Fig. 6.2 also shows that the experiment with the largest ASAG slug size of 1 PV developed the lowest ΔP peak compared with smaller slug sizes. The average ΔPs recorded were 65.75 psi, 59.91 psi, 55.00 psi, and 43.52 psi respectively for slug sizes of 0.25 PV, 0.33 PV, 0.5 PV, and 1 PV respectively. The corresponding MRF values were 1.27, 1.16, 1.07, and 1.04 respectively. Thus, using smaller slug size resulted in better foaming behavior during ASAG flooding

and hence improved mobility control. The results indicated that slug size of 0.25 PV was more appropriate for ASAG flooding of this study. Majidaie et al. [61] observed that the optimum slug size for chemically enhanced water alternating gas (CWAG) injection was around 0.25 PV which leads to maximum oil recovery. Chen and Reynolds [229] made a similar observation in the case of WAG flooding technique that shorter cycle time, i.e. more cycles, reduces the segregation of injected water and gas. Gravity segregation was detrimental to the performance of WAG flooding processes as it yields poorer E_{vo} and E_{do}. Hussain et al. [230] found that the application of multiple-cycles SAG floods instead of single-cycle SAG results in a more stable foam front, leading to a more efficient oil displacement. Han and Gu [225] also reported that with a smaller slug size, higher oil recovery factor for miscible CO_2-WAG flooding was achievable.

6.4 Effect of Injection Scheme

Core flooding experiments were performed to compare the effect of different ASAG injection scheme on the oil recovery. Injection scheme of the ASAG process refers to the order of AS and gas/CO_2 slug injection immediately following secondary water flooding – gas alternated chemical (GAC) or chemical alternated gas (CAG). While ASAG I was conducted in the GAC injection scheme, the other ASAG flooding experiment was performed in the CAG injection mode. Along with other experimental conditions, in both the experiments the slug ratio (1:1) and slug size (0.25 PV) were maintained the same. Fig. 6.3 shows the cumulative oil recovery and ΔP data of the ASAG flooding experiment in CAG injection mode. The oil recovery by GAC injection scheme (23.85 %OOIP) was found to be higher than the CAG injection (19.78 %OOIP). The higher oil recovery of GAC injection scheme can be attributed to the hysteresis effect of drainage and imbibition processes. As the waterflooding is primarily an imbibition process, the residual oil left behind are trapped in the larger pore spaces of the core plug [231].

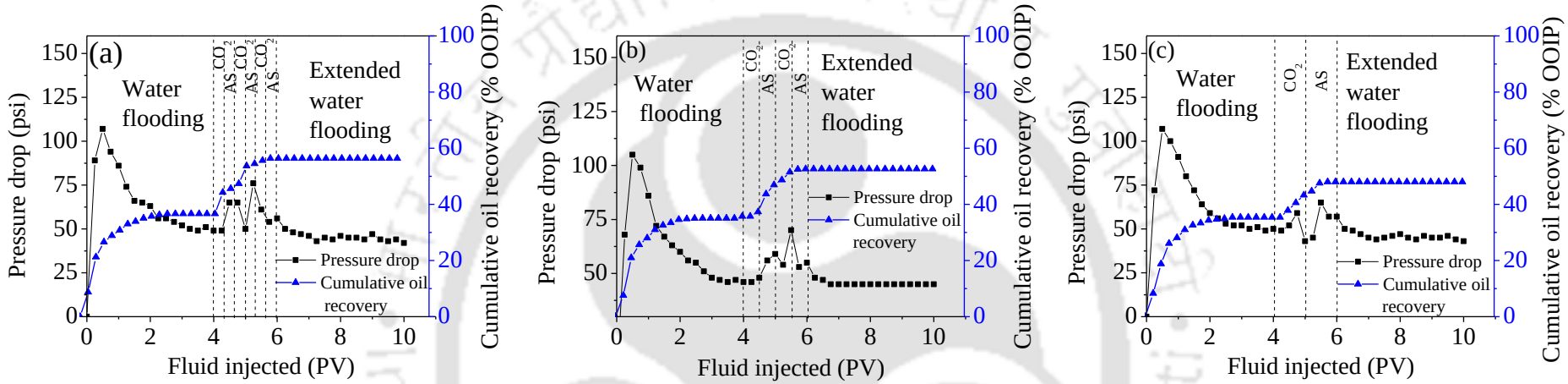

Fig. 6.2: Cumulative oil recovery and pressure drop versus pore volume of fluid injected in ASAG flooding with slug size of (a) 0.33 PV; (b) 0.5 PV; and (c) 1 PV

When gas injection immediately followed waterflooding, the drainage process of gas injection was able to drive the residual oil from the larger pore spaces more efficiently leading to higher oil recovery [223]. The average ΔP during the CAG injection mode was also observed to be lower (60.24 psi) with MRF value of 1.17 indicating comparatively less strong foam formation. Hence, it was observed that GAC injection scheme is more favorable for ASAG flooding. Moayedi et al. [223] also reported higher oil recovery by starting with gas injection during the tertiary SAG flooding compared to starting with liquid injection after secondary water flooding. Han and Gu [225], however, obtained higher ultimate oil recovery with water-alternating-gas (WAG) injection sequence compared to gas-alternating-water (GAW) injection during secondary miscible WAG process. The reason for the higher oil recovery by WAG injection sequence was attributed to higher E_{vo} with initial water injection due to favorable mobility ratio compared to initial CO_2 injection. Moreover, in miscible CO_2-GAW injection mode, severe viscous fingering occurred lowering the E_{vo}.

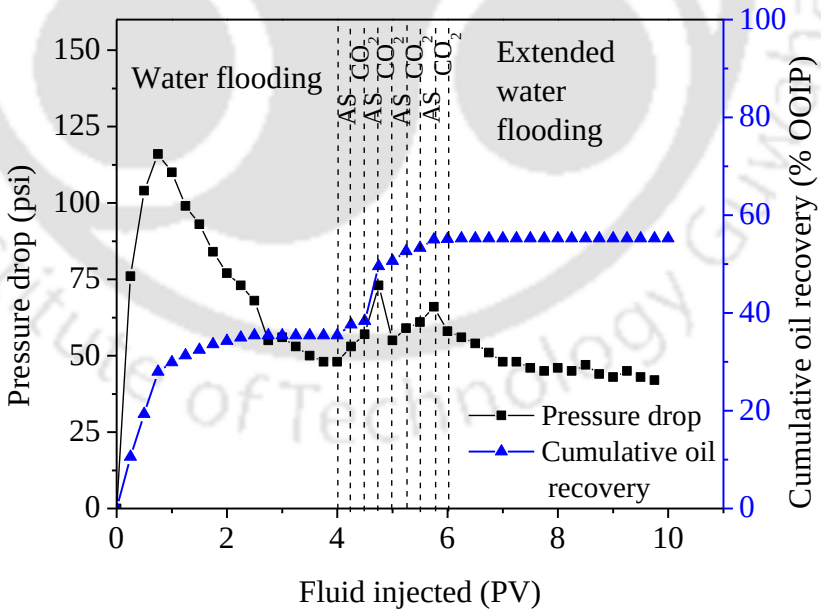

Fig. 6.3: Cumulative oil recovery and pressure drop versus pore volume of fluid injected in chemical alternated gas (CAG) ASAG injection scheme

6.5 Effect of Gas Injection Rate

ASAG core flooding experiments were carried out to investigate the effect of different gas/CO_2 injection rates on the oil recovery. The experiments were conducted with the same ASAG slug ratio of 1:1 and slug size of 0.25 PV, while keeping the total fluid volume injected constant at 2 PV. The experiments were performed at gas/CO_2 injection rates of 0.2 ml/min, 0.5 ml/min, 1 ml/min and 2 ml/min. The liquid was injected at a constant pressure during these tests. The cumulative oil recoveries of the experiments are shown in Table 6.2 and Fig. 6.4. It was observed CO_2 injection rate influenced the oil recovery by ASAG flooding. The oil recovery decreased slightly (from 23.85% to 22.38% OOIP) as the gas injection rate was increased from 0.2 ml/min to 0.5 ml/min. However, increasing the injection rate to 1 ml/min and 2 ml/min significantly decreased the oil recovery to 15.86% and 15.31% OOIP respectively. At higher gas injection rate, early gas breakthrough occurs due to viscous fingering effect and the consequently low E_{vo}. Moreover, a higher injection rate lowers the possibility of proper contact between the surfactant solution and the CO_2 gas in the core plug. As a result, a reduction in foam generation during the ASAG process probably took place. To study the foaming behavior at lower and higher gas flow rates, the ΔP profiles of 0.2 ml/min and 2 ml/min injection rates were studied and presented in Fig. 6.5. Higher average ΔP of 65.75 psi (MRF = 1.27) for the 0.2 ml/min injection rate experiment was recorded compared to 57.75 psi (MRF = 1.12) for the 2 ml/min injection rate. This was an indication of improper foam generation and propagation in the latter. Thus, residual oil recovery by ASAG flooding was dependent on the gas injection rate and there was an optimum rate of gas/CO_2 injection, which in this case was 0.2 ml/min. Injecting the gas below this optimum rate is also likely to decrease the oil recovery because lower injection rates induce lower ΔPs so the generated foam would not be able to totally sweep the residual oil in place. Further, if injection rates are too low gravity overriding effect becomes significant which would decrease the volume of the residual oil contacted by the injected CO_2 gas [232]. Safarzadeh et al. [233] reported that oil recovery efficiency of SAG flooding performed in sand packs was a function of the

injection rate. An early breakthrough was observed at a higher injection rate (0.25 ml/min) and the highest oil recovery of 87% was obtained at the optimal injection rate of 0.2 ml/min.

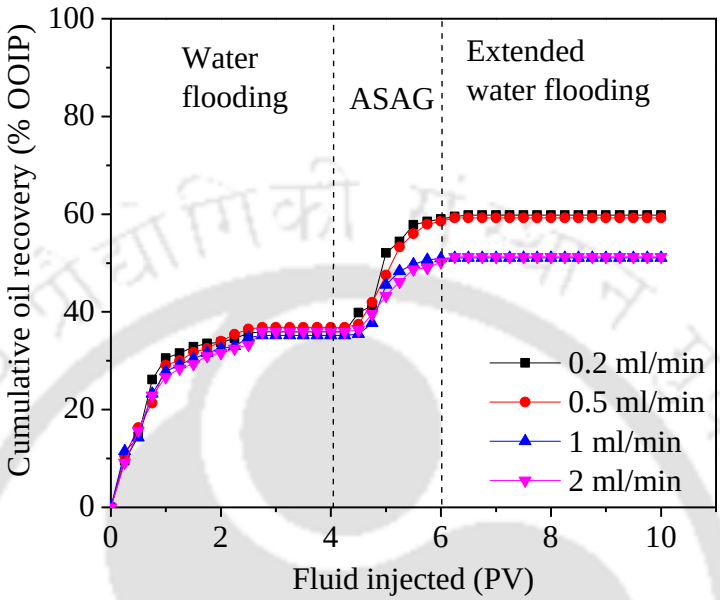

Fig. 6.4: Cumulative oil recovery versus pore volume of fluid injected in ASAG flooding with different gas injection rates

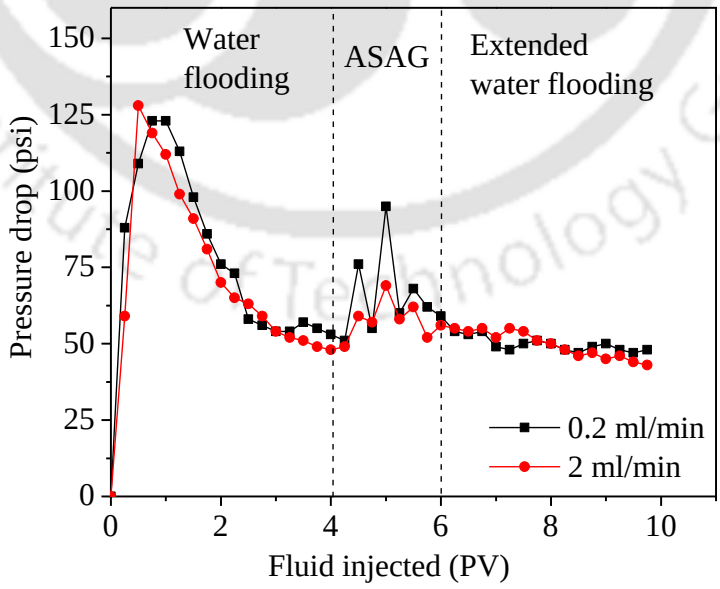

Fig. 6.5: Pressure drop versus pore volume of fluid injected in ASAG flooding with low and high gas injection rates

6.6 Effect of Total Fluid Volume Injected

To evaluate the effect of total fluid volume injected during ASAG flooding on the oil recovery by ASAG flooding, ASAG I experimental results were compared with four core flooding experiments performed with total injected fluid volumes of 0.5, 1, 1.5 and 2.5 PV. In these tests, all other operating parameters were maintained the same except for the total fluid volume injected. The injected fluid volume means the total PV of AS slug and gas injected during the complete ASAG injection cycle. The core flooding experimental results are shown in Table 6.2 and Fig. 6.6 for comparison. The oil recovery by 2.5 PV of fluid injection was the highest (24.59 %OOIP), followed by the ASAG I (23.85 %OOIP) with 2 PV. The experiments with injection fluid volume of 1 PV and 0.5 PV resulted in still lower additional oil recoveries of 9.29% and 2.76% OOIP respectively. Apparently, the residual oil recovery increased with the total volume of fluid injected during ASAG injection cycle. The availability of more chemicals and gas with an increase in injection fluid volume helped to mobilize more residual oil leading to enhancement in oil recovery. However, injecting fluids beyond a certain volume was not beneficial because most of the residual oils were produced after 2 PV fluid injection. The oil recovery curve of 2.5 PV experiment in Fig. 6.6, shows that most of the residual oils were produced during the first 4 cycles of ASAG injection and then was almost constant for fluid volumes injected beyond 2 PV. Table 6.2 also shows that only marginal incremental oil recovery (from 23.85 to 24.59 %OOIP) was obtained by increasing the injected fluid volume from 2 PV to 2.5 PV. Over injecting the fluids only leads to additional costs associated with the injection of more chemicals and gas/CO_2 but no appreciable extra oil recovery. Thus, 2 PV of total fluid injection was found suitable for the immiscible ASAG flooding and was taken as the optimum. Perera et al. [41] observed that a considerable increase in oil production for continuous CO_2 flooding with the increase of the total volume of CO_2 injected. However, beyond a certain volume, no further increase in oil production was reported

because most of the oils were recovered before the full volume of CO_2 was injected. Azzolina et al. [234] from their study of 31 numbers of CO_2-EOR projects reported that oil recovery increased as injection volume (PV) of CO_2 and water were increased.

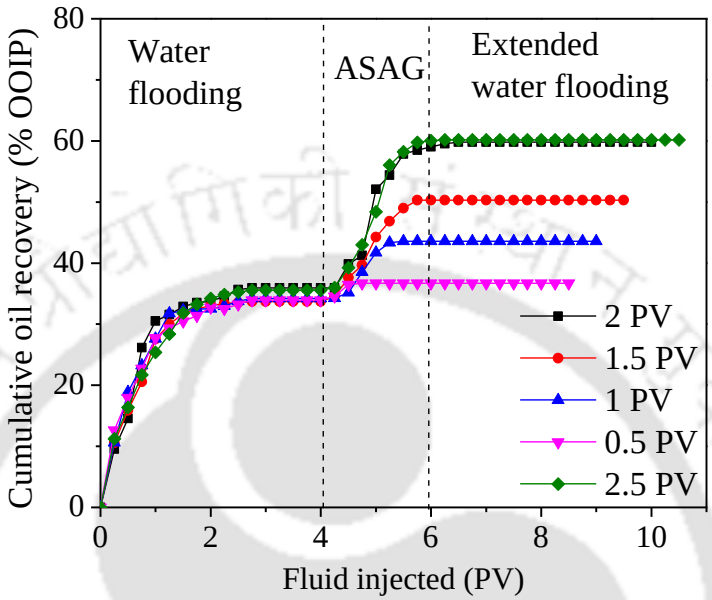

Fig. 6.6: Effect of total injected fluid volume on cumulative oil recovery in ASAG flooding

6.7 Effect of Tapering

In a typical ASAG injection process, each cycle consists of gas/CO_2 and AS slug injection of fixed PV/duration. In tapered ASAG process, size/duration of the chemical and/or gas injection varies in each progressive cycle. It is termed tapering down when the duration of fluid injection is longer initially and decreased in progressive cycles. The reverse is the case with tapering up where the duration of fluid injection is shorter initially and increased in the progressive cycles. Liquid, gas and combined liquid-gas tapering ASAG flooding experiments were performed and compared to examine their effect on oil recovery efficiency. The other operating conditions in these experiments were maintained the same as in the uniform flooding.

Table 6.2: Summary of core flooding experiments evaluating the effects of gas injection rate and total injection volume

Sl. No.	Description of ASAG process	Porosity (%)	K (mD)	Saturation (%)		Fluid Injected (PV)			Recovery (% OOIP)		
			K_{abs}	S_{oi}	S_{wc}	WF	EOR	EWF	WF	ASAG	Total
1	**ASAG I** • Gas rate (0.2 ml/min) • Injection volume (2 PV)	20.27	6.87	74.21	25.79	4.00	2.00	4.00	35.94	23.85	59.79
2	Gas rate (0.5 ml/min)	20.14	5.85	76.34	23.66	4.00	2.00	4.00	36.86	22.38	59.24
3	Gas rate (1 ml/min)	20.16	6.53	76.53	23.47	4.00	2.00	4.00	35.18	15.86	51.04
4	Gas rate(2 ml/min)	20.21	6.06	75.78	24.22	4.00	2.00	4.00	35.95	15.31	51.26
5	Injection volume (0.5 PV)	20.49	6.10	77.35	22.65	4.00	0.5	4.00	33.95	2.76	36.71
6	Injection volume (1 PV)	20.27	5.99	76.02	23.98	4.00	1.00	4.00	34.28	9.29	43.57
7	Injection volume (1.5 PV)	20.09	6.31	75.23	24.77	4.00	1.50	4.00	33.71	16.61	50.32
8	Injection volume (2.5 PV)	20.52	6.06	75.87	24.13	4.00	2.50	4.00	35.57	24.59	60.16

In order to examine the effect of liquid tapering on residual oil recovery, two tapered ASAG flooding experiments were performed and their results were compared with the uniform flooding experiment. The total volume of gas/CO_2 and AS formulation alternately injected was fixed at 2 PV. In uniform ASAG flooding as in ASAG I, each cycle of ASAG injection consisted of fixed volume (0.25 PV) of AS slug and CO_2 gas injection, whereas, in liquid tapering, the volume of liquid injection was varied in each progressive cycle keeping the gas volume constant. In tapering down, the volume of liquid injection was larger at first and decreased in subsequent cycles. In this injection mode, during the ASAG injection, the gas/CO_2 slug size/volume was kept constant at 0.25 PV whereas the AS slug volume was decreased in each progressive cycle in the sequence 0.4, 0.3, 0.2 and 0.1 PV. In the tapering up mode, the liquid volume increased in each progressive cycle in the sequence of 0.1, 0.2, 0.3 and 0.4 PV. Fig. 6.7 shows the cumulative oil recoveries and the ΔP versus the PV of fluid injected during the liquid tapering ASAG flooding experiments. The liquid tapering up ASAG flooding resulted in better incremental oil recovery (27.48 %OOIP) compared to liquid tapering down injection (25.72 %OOIP). However, the additional oil produced by both these tapered injection schemes were higher than the uniform ASAG flooding (23.85 %OOIP). Thus, liquid tapering had a positive effect on the oil recovery by ASAG flooding. In liquid tapering up method, the slug ratio was low in the first cycle which means that the volume of the injected chemical solution was lower while gas/CO_2 volume was higher. With higher initial gas saturation, the CO_2 injected into the core plug could cause maximum dissolution with crude oil. This resulted in an increase in the relative permeability of residual oil in the core plug probably due to the oil swelling and viscosity reduction caused by the dissolution of injected CO_2 gas. When the chemical slug was alternately injected, the displacement efficiency was further enhanced because of IFT reduction and foam formation. As the

liquid volume increased towards the end of the ASAG injection during liquid tapering up, the increase in liquid volume helped to control the early gas/CO_2 breakthrough by reducing the relative permeability to gas.

To study the effect of gas tapering on ASAG performance, ASAG flooding experiments were performed in gas tapering down and gas tapering up modes. In the gas tapering down ASAG injection, the core plug with residual oil was subjected to 4 cycles of CO_2 and AS slug alternate injection. The size of chemical slug injected was kept constant at 0.25 PV in each cycle, while gas slug size was decreased progressively in the sequence 0.4, 0.3, 0.2 and 0.1 PV. In the other experiment, the gas tapering up ASAG injection was applied where the gas slug size was increased progressively in sequence 0.1, 0.2, 0.3 and 0.4 PV. The total PV of fluid injected during the ASAG cycles was kept constant at 2 PV. The cumulative oil recovery and ΔP as a function of the PV of fluid injected during the gas tapering down and gas tapering up ASAG flooding processes are shown in Fig. 6.8 (a) - (b). The additional oil recoveries of 26.98 % and 24.75 % OOIP were obtained during the gas tapering down and tapering up ASAG injection respectively. These recoveries were better than the recovery by the uniform ASAG injection (ASAG I, 23.85 %OOIP). In comparison, the gas tapering down ASAG injection was found to be superior in terms of oil recovery. By injecting more gas in the first cycle maximum dissolution of CO_2 gas with crude oil and efficient use of gas most likely take place leading to the betterment of E_{vo} [235]. The trapping of the gas/CO_2 also resulted in improved oil recovery due to more stable foam formed during the next cycle of AS slug and gas injection [236]. More stable foam formation was evident from the increase in the average ΔP to 68.38 psi (MRF = 1.33) during gas tapering down injection scheme. The average ΔP during the tapering up scheme was 67.25 psi (MRF = 1.30) – higher than the uniform ASAG injection (MRF = 1.27). As the water-to-gas injection volume ratio increases towards the end of the gas tapering down ASAG process, this also helps to control the mobility of the gas [62].

The combined effect of applying the gas tapering down and the liquid tapering up injection in a single ASAG flooding process was also examined to observe the enhancement in oil recovery. Following secondary water flooding, the ASAG injection was performed in such a manner that the gas slug size decreased progressively in the sequence of 0.4, 0.3, 0.2 and 0.1 PV, while the liquid volume increased as 0.1, 0.2, 0.3 and 0.4 PV. The cumulative oil recovery and ΔP data are shown in Fig. 6.9 and Table 6.3. The additional oil produced was 29.35 %OOIP, which was an improvement of 5.50 %OOIP over the uniform flooding. Thus, the synergic combination of gas and liquid tapering can be successfully applied to optimize the ASAG flooding through efficient use of the injected fluids. The MRF value also increased in favor of combined tapering ASAG flooding from 1.27 to 1.40 compared to uniform fluid injection. This was an indication of improvement in mobility control which in turn caused better displacement of the residual oil. Srivastava and Mahli [237] showed that the displacement efficiency in both tapering up (20.73%) and tapering down (23.84%) WAG injection process was higher than the normal (19.3%) WAG process. The better recovery was due to improved E_{vo}, better mobility control, and increased oil relative permeability in the pores of the core sample. Khan et al. [235] in an effort to optimize the miscible WAG process observed the application of tapered injection was more favorable than uniform WAG due to efficient gas utilization, faster recovery rate, and reduction of response time. According to Tovar [238] the application of tapered WAG could reduce the residual oil saturation from 34.88% to 10.92%. Similarly, Verma [28] reported that tapered WAG is a widely used technique that improves process efficiency, prevents an early gas breakthrough, and improves CO_2 utilization.

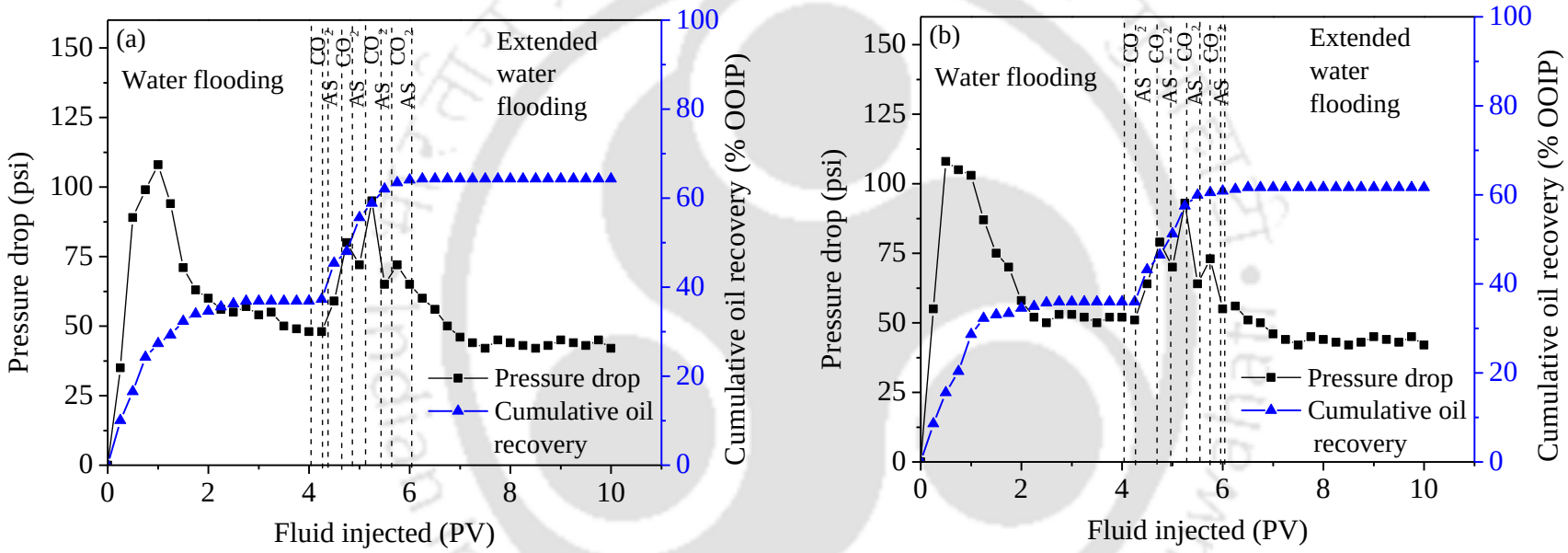

Fig. 6.7: Cumulative oil recovery and pressure drop versus pore volume of fluid injected in ASAG flooding with (a) Liquid tapering up, and (b) Liquid tapering down

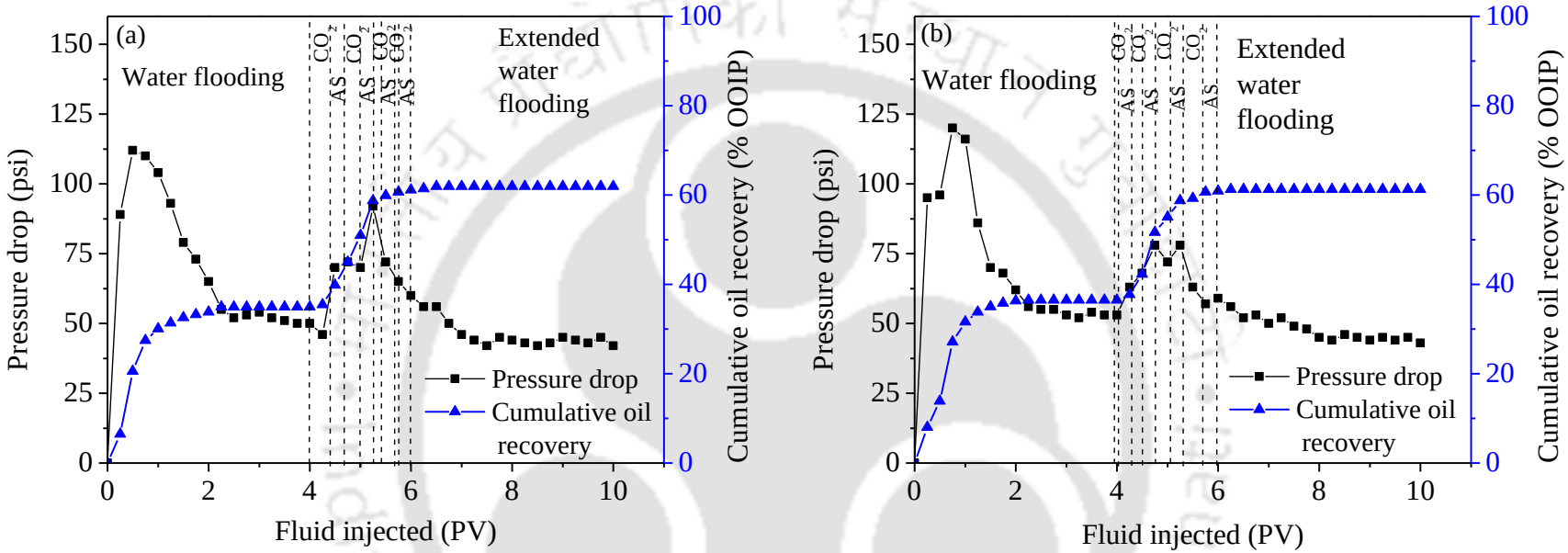

Fig. 6.8: Cumulative oil recovery and pressure drop versus pore volume of fluid injected in ASAG flooding with (a) Gas tapering down, and (b) Gas tapering up

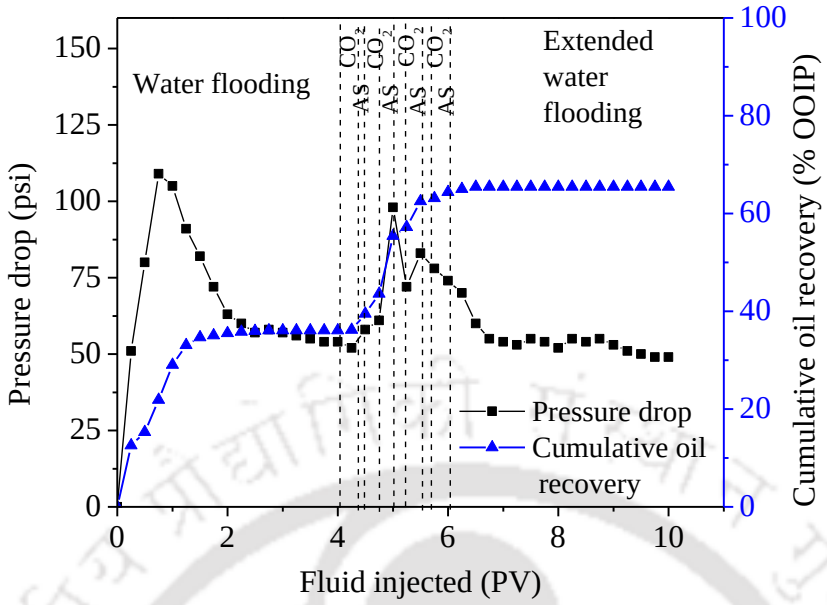

Fig. 6.9: Cumulative oil recovery and pressure drop versus pore volume of fluid injected in ASAG flooding with combined liquid tapering up and gas tapering down

6.8 Effect of Porosity/Permeability of Core Plug

When foam flow through reservoir rock, it develops a unique property called the selective mobility reduction (SMR), which causes it to reduce the mobility of gas by a greater fraction in high permeability regions of the reservoir compared to in the low permeability regions. This happens due to the formation of stronger foam in the high permeability zones where it appears to be more viscous than in low permeability zones. The stronger foam in the high permeability zones is instrumental in the diversion of fluid to the low permeability zones resulting in the smoothening of reservoir heterogeneities [57, 239, 240]. If the foam generated during ASAG flooding exhibits such a property then the process can be successfully applied in oil reservoirs which in most cases are heterogeneous.

Table 6.3: Summary of core flooding experiments evaluating the effect of tapering during ASAG flooding

Sl. No.	Description	ϕ (%)	K (mD)	Saturation (%)		Fluid Injected (PV)			Avg. ΔP	MRF	Recovery (% OOIP)		
			K_{abs}	S_{oi}	S_{wc}	WF	EOR	EWF	(psi)		WF	EOR	Total
	ASAG I												
1	Uniform injection	20.27	5.87	74.21	25.79	4.00	2.00	4.00	65.75	1.27	35.94	23.85	59.79
2	Liquid tapering down	20.68	5.99	74.01	25.99	4.00	2.00	4.00	68.63	1.33	35.95	25.72	58.98
3	Liquid tapering up	20.21	6.35	72.64	27.34	4.00	2.00	4.00	69.50	1.35	36.86	27.48	64.34
4	Gas tapering down	20.56	6.49	72.86	27.14	4.00	2.00	4.00	68.38	1.33	35.95	26.98	61.70
5	Gas tapering up	20.47	6.96	73.55	26.45	4.00	2.00	4.00	67.25	1.30	36.86	24.75	61.24
6	Combined gas-liquid tapering	20.38	6.75	73.13	26.87	4.00	2.00	4.00	72.00	1.40	36.10	29.35	62.45

In order to study the effect of rock porosity/permeability on ASAG flooding performance, two core flooding experiments were performed with core plugs of different porosity/permeability values. The first experiment was performed on a core plug of lower porosity/permeability (12.23% and 2.25 mD) and the second on a core plug of higher porosity/permeability (27.42% and 30.37 mD). All other experimental conditions in these ASAG flooding experiments were maintained the same as ASAG I except the core plugs of different porosity /permeability values were used. Fig. 6.10 (a) - (b) shows the cumulative oil recovery and ΔP as a function of the PV of injected fluid. The oil recoveries by secondary water flooding were 38.83 %OOIP and 30.41 %OOIP respectively for the lower and higher porosity/permeability core plugs. The water flooding oil recovery data for lower and higher porosity cores were found to be inversely proportional to their porosities. This agrees well with the observations reported by other workers [241]. The performance of the tertiary ASAG injection was better with oil recovery of 27.54% OOIP for the core plug with higher porosity/permeability compared to 18.03% OOIP for the lower porosity/permeability core plug (Table 6.4). Although the final cumulative oil recoveries for both the core plugs were comparable, ASAG flooding in the higher porosity/permeability core plug exhibited a higher average ΔP of 72.00 psi (MRF = 1.39) compared to 59.25 psi (MRF = 1.18) in case of lower porosity/permeability core plug. The higher MRF value was indicative of stronger foam formation in the more permeable core plugs and the lower MRF value implied comparatively weaker foam in less permeable core plugs. The stronger foam formed in the high permeability core plug provided better mobility control and hence higher oil recovery was obtained. Thus, it can be concluded that the SMR property was exhibited by in-situ foam generated during immiscible ASAG flooding. So, it is expected that ASAG flooding can reduce the detrimental effects of field-scale reservoir heterogeneity through the formation of in-situ foam having the property of SMR.

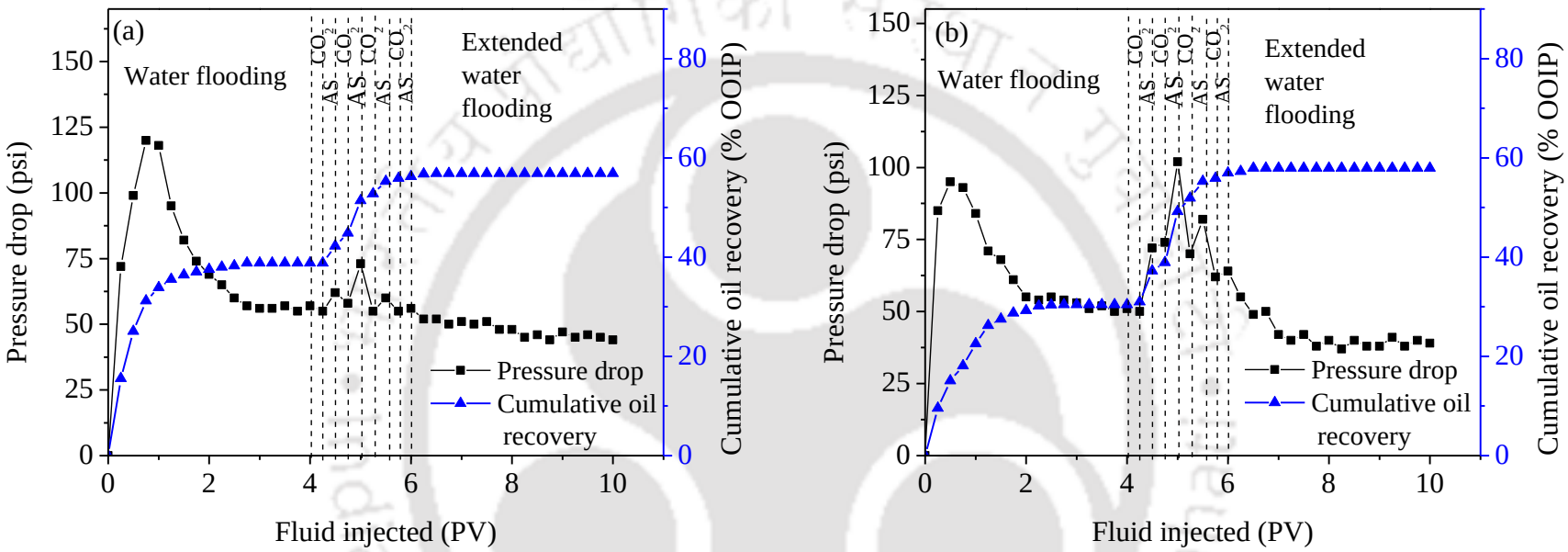

Fig. 6.10: Cumulative oil recovery and pressure drop versus pore volume of fluid injected in ASAG flooding with (a) Low porosity/permeability core plug; (b) High porosity/permeability core plug

Table 6.4: Summary of core flooding experiments evaluating the effect of rock porosity/permeability on ASAG flooding

Sl. No.	Description	ϕ (%)	K (mD) K_{abs}	Saturation (%) S_{oi}	S_{wc}	Fluid Injected (PV) WF	EOR	EWF	Avg. ΔP (psi)	MRF	Recovery (% OOIP) WF	EOR	Total
1	Lower Porosity/permeability core plug	12.23	2.25	70.02	29.98	4.00	2.00	4.00	59.25	1.18	38.83	18.03	56.86
2	Higher porosity/permeability core plug	27.42	30.37	78.23	21.77	4.00	2.00	4.00	72.00	1.39	30.41	27.54	57.95

6.9 Effect of Salinity Gradient during ASAG Flooding

Additional core flooding experiment was performed to investigate the effect of salinity gradient or brine salinity change on the oil recovery performance of ASAG flooding. Brine salinity change implies secondary water flooding at higher brine salinity is followed by the chemical slug (injected during the ASAG cycle) at optimal brine salinity and finally chased by a drive at a lower brine salinity. Thus salinity variation from higher salinity to intermediate salinity and then to lower salinity occurs in the core plug during the flooding process. As a result, the benefits of high, moderate and low salinities can be exploited during the flooding process. In the experiment, the oil-saturated core plug was waterflooded with SFB of 3458 ppm salinity which resulted in oil recovery of 37.83 %OOIP. The chemical slug (containing 0.5 wt% AOS + 0.75 wt% Na_2CO_3) was injected at optimal salinity (at 70% SFB salinity, 2400 ppm) during the ASAG injection, while the salinity of the drive (EWF) was maintained at 30% SFB salinity (1000 ppm). Fig. 6.11 shows the cumulative oil recovery and ΔP data obtained during the flooding process when salinity gradient was applied. Table 6.5 shows that the additional oil recovered by changing brine salinity during flooding increased to 25.74 %OOIP – an increment of 3.87 %OOIP over straight salinity (ASAG II). Injection of the AS slug at optimal SFB salinity helped achieve the lowest oil-water IFT which in turn mobilized capillary held residual oil. An increase in the MRF value from 1.28 to 1.36 indicated stronger foam formation during the ASAG cycle. Injecting the AS slug at a lower optimal SFB salinity has the additional benefit of decrease surfactant retention which resulted in the availability of more surfactant for residual oil recovery [242, 243]. Additionally, injecting the brine at lower salinity during EWF helps to remobilize the retained surfactant in the aqueous phase [244]. Srivastava et al. [83] reported that the application of salinity change/gradient improves the alkali-surfactant-gas (ASG) flooding by providing better foam stability through the

mobilization of trapped surfactants. The stronger foam was instrumental in providing better displacement efficiency in their ASG core flooding experiment.

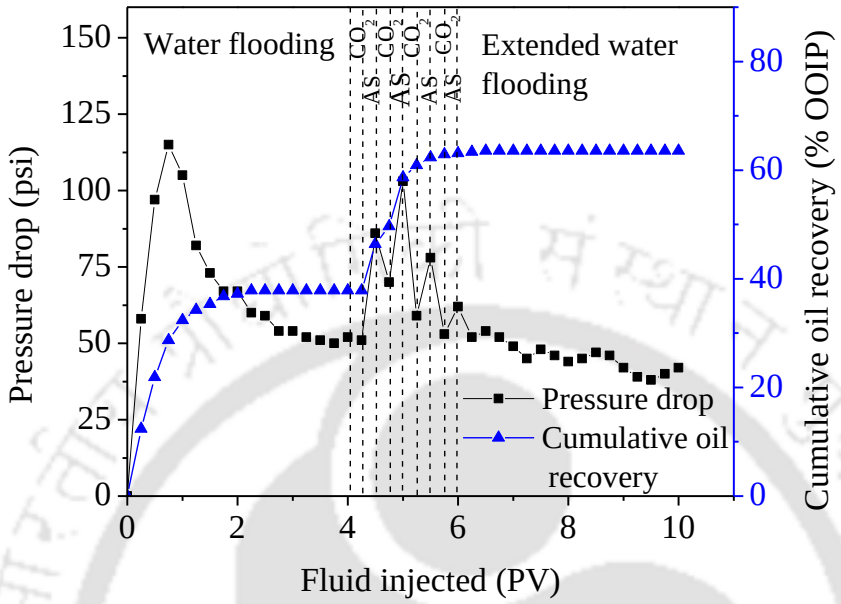

Fig. 6.11: Cumulative oil recovery and pressure drop versus pore volume of fluid injected during ASAG flooding with the application of salinity gradient

Table 6.5: Summary of core flooding experiments evaluating the effects of salinity gradient, preflushing, and combined effect

Sl. No.	Description	ϕ (%)	K (mD) K_{abs}	Saturation (%) S_{oi}	S_{wc}	Fluid Injected (PV) WF	EOR	EWF	Avg. ΔP (psi)	MRF	Recovery (% OOIP) WF	EOR	Total
	ASAG II												
1	• Straight salinity • No BL preflush	20.49	6.10	73.35	26.65	4.00	2.00	4.00	66.13	1.28	36.31	21.87	58.18
2	Salinity gradient	20.67	7.38	72.02	27.98	4.00	2.00	4.00	70.25	1.36	37.83	25.74	63.57
3	BL preflush	20.82	6.98	74.23	25.77	4.00	2.00	4.00	71.38	1.38	39.26	24.48	63.74
4	Combined effect	20.50	7.83	73.66	26.34	4.00	2.00	4.00	74.63	1.45	38.85	30.69	69.54

6.10 Use of Preflush in ASAG Flooding

In foam-based EOR application, preflushing with a less costly surfactant to precondition the reservoir is commonly practiced for improving the process economics and efficiency [213]. Along with improving the foam generation, this method reduces the adsorption of primary surfactant onto the reservoir rock thus maintaining better foam propagation [245, 246]. In order to evaluate the performance of ASAG flooding with preflushing, ASAG core flooding experiment similar to ASAG II was performed but with 1 wt% BL added to the SFB used for secondary water flooding. Fig. 6.12 and Table 6.5 show the cumulative oil recovery and the ΔP data obtained during the core flooding experiment performed with preflushing. The results show that higher residual oil recovery (24.48 %OOIP) as well as higher cumulative oil recovery (63.74 %OOIP) was obtained by ASAG flooding with BL preflushing. The higher oil recoveries were possible due to a combination of the following favorable attributes. Firstly, BL has been reported to possess the ability to reduce oil-water IFT and thus produce extra oil [142]. Adding BL to SFB thus resulted in higher oil recovery by secondary water flooding (39.26 %OOIP). Secondly, preflushing the core plug with BL reduced the adsorption of surfactant onto the reservoir rock resulting in the availability of more primary surfactant (AOS) to mobilize the residual oil trapped by capillary forces. The dynamic adsorption experiments have shown that preflushing with 1wt% BL could reduce the adsorption of surfactant by more than half. Thirdly, improved foam performance was possible during ASAG injection by preflushing with BL. The preconditioning caused the reduction of foaming agent adsorption onto reservoir rock, which in turn lead to better foam generation and propagation during the ASAG flooding. An increase in the MRF value to 1.38 indicated better foam stability during ASAG flooding with BL preflushing. Thus, preflushing prior to ASAG flooding can be applied to optimize the process by increasing the effectiveness of the foam in improving the oil recovery. Tsau et al. [247] reported that lignosulphonate

could reduce the adsorption of primary foaming agent in CO_2 flooding by 24 – 60 % in Berea sandstone. They observed that preflushing the core was more effective in reducing the surfactant adsorption than co-injecting the lignosulphonate and the foaming agent.

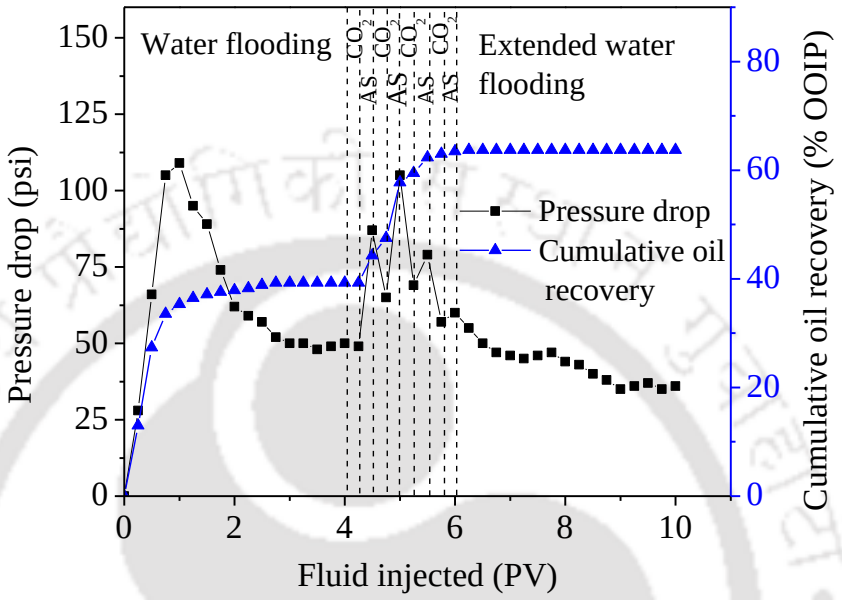

Fig. 6.12: Cumulative oil recovery and pressure drop versus pore volume of fluid injected in ASAG flooding with black liquor preflushing

6.11 Combined ASAG Flooding

Finally, one additional core flooding experiment was performed with the second chemical slug (0.5 wt% AOS + 0.75 wt% Na_2CO_3) incorporating all the favorable operating conditions of ASAG flooding including the application of combined gas-liquid tapering, salinity gradient and preflushing with BL. During secondary water flooding, 4 PV of SFB containing 1 wt% BL was injected into the oil-saturated core plug which resulted in an oil recovery of 38.85 %OOIP. This was followed by 2 PV of alternated gas/CO_2 and AS slug (at optimal salinity) injection in the combined gas tapering down and liquid tapering-up mode. Fig. 6.13 shows the cumulative oil recovery and ΔP as a function of the PV of fluid injected during the experiment. The oil recovery through the 4 cycle ASAG injection was

30.69 %OOIP. The ASAG injection was followed by the EWF during which 4 PV of SFB at 1000 ppm salinity was injected. The total oil recovery including water flooding, ASAG injection and the final EWF was 69.54 %OOIP. Compared to the ASAG II experiment, injecting the fluids in the manner described in the combined ASAG flooding could increase the cumulative oil recovery by an encouraging 11.36 %OOIP. The experimental results are shown in Table 6.5 also indicated better foam stability during the combined ASAG flooding as depicted by the higher MRF values (1.45). The best result obtained from the combined ASAG flooding indicated that utilizing the most favorable operating conditions, the ASAG flooding can considerably enhance oil recovery. Both E_{do} and E_{vo} were improved through better mobility control of fluids by alternating injecting the chemical slug with gas/CO_2 in the correct sequence, using the optimal AS slug for lowering of oil-water IFT to the lowest value and reducing surfactant loss by BL preflushing.

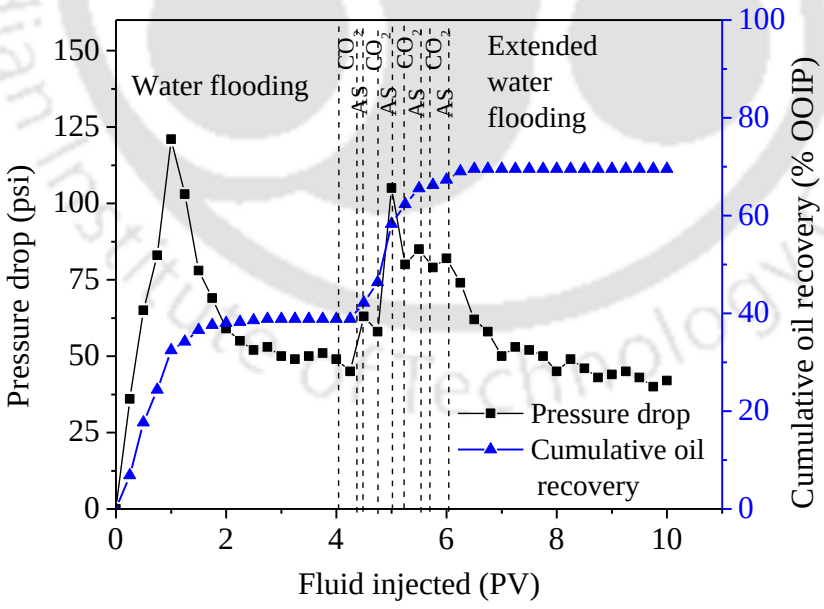

Fig. 6. 13: Cumulative oil recovery and pressure drop versus pore volume of fluid injected in the combined ASAG flooding

The formation of in-situ foam in the core plug during the different ASAG injection schemes/processes was evaluated based on the average ΔP and the MRF values. The higher average ΔP value in ASAG flooding compared to the ΔP value of AS flooding indicated that the higher value was due to the formation of in-situ foam. Among the different slug ratios of ASAG flooding, the highest ΔP (65.75 psi) was obtained when the slug ratio was 1:1. This was an affirmation that 1:1 slug ratio was a better injection scheme due to stronger foam formation and hence higher oil recovery. Among the different slug sizes of ASAG flooding, the highest ΔP was obtained with the smallest slug size of 0.25. Hence, this slug size was chosen as the optimum for this study. The order of AS and CO_2 gas slug injection during ASAG flooding also effect the average ΔP value, with GAC injection scheme proving to be a better option due to the higher value of average ΔP. A higher pressure drop of 72.00 psi was observed during the combined gas-liquid tapering process which indicated that the process is more efficient in terms of mobility control by foam generation and consequently higher oil recovery. However, the highest oil recovery (69.54 %OOIP) was obtained when all the favorable injection schemes were included during the combined ASAG flooding. The average ΔP value rose to 74.63 psi, thus indicating that stronger foam generation is possible for better fluid mobility control and maximum oil recovery.

6.11 Summary

The EOR by ASAG flooding was found to be influenced by various key operational parameters that are required to be studied and optimized before the process could be successfully applied in an oil reservoir. The most appropriate slug ratio was 1:1, as neither increasing the volume of the liquid nor the gas could improve the additional oil produced. The slug size or cycle frequency strongly influenced the effectiveness of ASAG flooding in enhancing oil recovery. It was observed that smaller the slug size better the

foaming and hence improved mobility control. The optimal slug size for ASAG flooding was found to be 0.25 PV. The GAW injection scheme proved to be more favorable for ASAG flooding compared to CAG injection. The core flooding results indicated that injecting gas immediately after secondary water flooding leads to higher oil recovery (23.85 %OOIP) compared to injecting liquid after water flooding (19.78 %OOIP). The experiments performed at different gas injection rates showed that an optimum rate of gas injection rate (0.2 ml/min) existed at which the efficiency of ASAG flooding was the maximum. Moreover, the oil recovery by ASAG flooding was determined by the total volume of fluid (gas and liquid) injected during one complete ASAG cycle and the optimum volume of fluid injected was found to be 2 PV.

Tapering, normally applied in CO_2-WAG, could be successfully applied in ASAG flooding and found to increase the oil recovery compared to uniform fluid injection due to the efficient use of the fluids. More specifically, liquid tapering up and gas tapering down approaches provided better oil recovery. The combination of these two approaches in ASAG injection could enhance the residual oil recovery to 29.35 %OOIP – an improvement of 5.50 %OOIP over uniform fluid injection. The selective mobility reduction property was found to be exhibited by foam generated in the core plug by ASAG injection. An increase in MRF value (from 1.18 to 1.39) indicated stronger foam formation in the more porous/permeable cores.

The application of salinity gradient, commonly practiced in chemical flooding, was also found to be encouraging for ASAG flooding. An increment oil recovery of 3.87 %OOIP was achieved by changing the brine salinity during flooding over straight salinity. The higher oil recovery was primarily attributed to the attainment of the lowest oil-water IFT and stronger foam formation. It was also observed that preflushing with a less expensive surfactant (black liquor, BL), added to brine used for secondary water flooding,

improved both the additional as well as cumulative oil recovery obtainable by ASAG flooding. Lower primary surfactant adsorption, reduction of oil-water IFT, and better foaming achieved by preflushing improved the performance of the ASAG process. It was observed that combining the most favorable operating conditions, ASAG flooding can significantly enhance the oil recovery due to the improvement of both E_{do} and E_{vo}. As a whole, the experimental findings in this chapter provided sufficient amount of data for optimizing the ASAG flooding through the use of the most suitable operating conditions.

CHAPTER 7

Overall Conclusions and Future Work

Summary of the work

Future scope

Chapter 7

Overall Conclusions and Future Work

This chapter summarizes the conclusions drawn from the results of the present work. The possible scope for future research has also been presented.

7.1 Conclusions

In this research work, the enhanced oil recovery by the immiscible alkaline-surfactant-alternated-gas/CO_2 (ASAG) flooding was studied in detail. Based on the analysis of reservoir rock, crude oil, and formation water, the optimum chemical formulations for ASAG flooding were designed. The key parameters influencing the oil recovery performance of ASAG flooding have also been studied. The most important findings and conclusions of this work are summarized below:

- The crude oil was found to be medium gravity and high pour point was the result of its high wax content. The asphaltene content of the crude was evaluated to be in the stable state as there were enough amounts of resins for asphaltene stabilization. The acidic nature of the crude is supported by acid number and FTIR study. Therefore, it is expected that crude oil will respond favorably to alkaline injection for the formation of in-situ surfactants. The total salinity of the formation water was found to be low (3458 ppm) and marked by the presence of several types of dissolved ions including the divalent ones like Ca^{++} and Mg^{++}.
- The porosities of the core plugs were observed to vary with the depth of the formation from where the cores were obtained. The core plug from shallower depths was found to be more porous and vice-versa. The porosities and permeabilities of the core plugs were directly related as the more porous core plugs were found to be more permeable.

From the liquid and gas permeability values, it was found that the formation could be classified as fair to moderate permeability reservoirs.

- The reservoir rock was evaluated to be of anionic type due to the presence of silica (quartz) as the dominant mineral. The existence of clays minerals in the rock matrix was also identified through XRD and FESEM studies.
- To determine the CO_2-foam stability of different surfactants, the half-decay times ($t_{1/2}$) were calculated from the changes in foam volume recorded with respect to time. SDS and AOS surfactants displayed comparatively better CO_2-foam stability with the crude oil under similar experimental conditions, with SDS having higher $t_{1/2}$ values. CO_2-foam stability was found to be decreased by more than half as the temperature increased from room to reservoir temperature. Additionally, optimum concentrations of surfactants were found to exist that correspond to the point of maximum foam stability.
- Among the alkalis considered in the study, both Na_2CO_3 and NaOH were able to reduce oil-water IFT values to the ultra-low range when combined with the optimum concentrations of SDS and AOS. But, Na_2CO_3 was chosen as the preferred alkali as the equilibrium IFT values obtained were the minimum with both the surfactants.
- The maximum Winsor type III microemulsion volume was observed at 70% of formation brine salinity (2400 ppm) during salinity scan of the phase behavior study. This SFB salinity was considered as the optimal salinity, at which the lowest oil-water IFT value was also obtained.
- Under dynamic conditions, alkali addition was found to reduce the adsorption of surfactants by reservoir rocks by more than half from 1.41 mg/g to 0.52 mg/g. Additionally, the optimum concentration of BL for preflushing was found at its CMC

value as no further reduction in surfactant adsorption was observed beyond the CMC value.

- The synergic effect of AS formulation and CO_2 gas injected during ASAG flooding resulted in higher oil recovery compared to tertiary CGI, CO_2-WAG, SAG, and AS flooding. The primary reason for the increase in oil recovery can be attributed to fluid mobility control, achievement of ultra-low oil-water IFT, and in-situ foam generation.
- The performance of ASAG flooding was found to be influenced by certain operational parameters. The optimum conditions for the best oil recovery by ASAG flooding were obtained with 1:1 slug ratio, 0.25 PV slug size, gas-alternated-chemical (GAC) injection scheme, 0.2 ml/min CO_2 gas injection rate, and 2 PV of total fluid injection.
- Application of both liquid and gas tapering schemes during ASAG flooding indicated to have a favorable effect on the oil recovery due to the efficient use of injected fluids and better fluid mobility control. More specifically, liquid tapering up and gas tapering down approaches provided better oil recovery. By combining these two approaches in a single ASAG flooding, the oil recovery could be improved by 5.50 %OOIP over uniform fluid injection.
- The application of salinity gradient during ASAG flooding helped achieve better incremental oil recovery due to the attainment of the lowest oil-water IFT and generation of the most stable foam.
- By preflushing the core plug with a less costly natural surfactant (BL), which was added to brine during secondary waterflooding, both the additional and cumulative oil recoveries can be improved during ASAG flooding. The improved performance can be attributed to the lower primary surfactant adsorption and better foam stability with preflushing.

7.2 Future Work

In this study, the potential of ASAG flooding for EOR under immiscible conditions using reservoir rock and fluids of an Upper Assam oilfield was investigated on a laboratory scale. However, taking into consideration the vastness of the subject the following future studies can be undertaken:

- This work can be extended to experimentally study the effectiveness of ASAG flooding for the present reservoir fluids under miscible conditions. As miscible CO_2 flooding is known to be more efficient for EOR, the miscible ASAG flooding is also required to be investigated.
- In ASAG flooding, the AS formulation and the gas/CO_2 slug were alternately injected in small slugs to form foam in the reservoir rock. Foam can also be formed by the coinjection of the two fluids. The coinjection of gas/CO_2 and AS slug for EOR can be studied as larger mobility reduction is obtainable through this technique. Moreover, foam quality which influences the mobility reduction characteristics can be controlled in the coinjection method.
- The effectiveness of ASAG flooding in carbonate reservoirs can be studied. These reservoirs on an average have lower porosity and permeability than sandstones, which poses various challenges for EOR by foam application as the effectiveness of foam in controlling gas mobility is lower in low-permeability rocks.
- The effects of bubble size on the injection rate and differential pressure (pressure drop) on the performance of ASAG flooding can be investigated.
- Development of EOR models and simulation studies would be useful to validate the experimental data and to further predict the performance of ASAG flooding under different reservoir and operating conditions.
- Techno-economic analysis of the ASAG flooding needs to be carried out for a successful pilot and field-scale implementation.

Appendix

Appendix

Appendix A: Sample Calculations of Porosity Measurement by TPI-219 Helium Porosimeter

Table A. 1: Helium porosimeter calibration data

Full cup pressure		**Removed billet data**	
Zero Pressure	0.04 psi	ID	C, D & E
$P_{reffull}$	92.50 psi	$V_{billet\ removed}$	93.69 cm^3
$P_{cupfull}$	39.59 psi	P_{refrem}	92.36 psi
V_{ref}	4.18	P_{cuprem}	3.73 psi

The system reference volume is calculated as:

$$V_{ref} = \frac{V_{billetremoved}}{\left(\frac{P_{refrem}}{P_{cuprem}}\right) - \left(\frac{P_{reffull}}{P_{cupfull}}\right)} \quad \text{(A.1)}$$

where, V_{ref} = System reference volume, cm^3

$V_{billetremoved}$ = Volume of billets removed, cm^3

$P_{reffull}$ = Reference pressure for full cup measurement, psi

$P_{cupfull}$ = Cup pressure with all billets in cup, cm^3

P_{refrem} = Reference pressure for measurement with billets removed, psi

P_{cuprem} = Cup pressure with billet removed, psi

Table A. 2: Core plug dimensions

Diameter (cm)	**Length (cm)**	**Volume (cm^3)**
3.75	7.75	85.38

The grain volume is calculated by the following equation:

$$V_{grain} = V_{billetsremoved} + \left[\left(\frac{P_{reffull}}{P_{cupfull}} \right) - \left(\frac{P_{refsample}}{P_{cupsample}} \right) \right] V_{ref} \quad \text{(A.2)}$$

Where, V_{grain} = Grain volume, cm^3

$V_{billetremoved}$ = Volume of removed billets, cm^3

$P_{refsample}$ = Reference system pressure with core plug, psi

$P_{cupsample}$ = Cup pressure with core plug, psi

Table A. 3: Core plug porosity measurement

Core plug ID	**Zero pressure (psi)**	**System reference pressure (psi)**	**Sample pressure (psi)**	**Sample bulk volume (cm^3)**	**Sample weight (gm)**	**Sample grain volume (cm^3)**	**Sample porosity (%)**
CP1	0.04	92.40	9.65	85.38	195.74	63.45	25.69

Appendix B

B.1. Viscosity Measurements of Crude Oil

Table B. 1: Kinematic and dynamic viscosity measurements of crude oil

Sl. No.	Temperature (^{o}C)	Density of crude oil (g/cm^{3})	Calibration constant of viscometer	Flow time (sec)		Kinematic viscosity (cSt)	Dynamic viscosity (cP)
				Test readings	Average		
1	28	0.865	0.01	1156 1212 1172	1180	11.80	10.20
2	50	0.847	0.01	796 789 746	777	7.77	6.58
3	70	0.832	0.01	509 569 530	536	5.36	4.46
4	90	0.820	0.01	428 403 408	413	4.13	3.39

B.2. Asphaltene, Resin and Wax Content Determination of Crude Oil

Table B. 2: Asphaltene content determination of crude oil

Sl. No.	Wt. of oil sample (g)	Wt. of filter paper with asphaltene (g)	Wt. of filter paper without asphaltene (g)	Wt. of asphaltene (g)	Asphaltene content = Wt. of asphaltene / Wt. of oil sample (%)
1	5.00	1.15	1.07	0.08	1.60
2	5.00	1.12	1.05	0.07	1.40
3	5.00	1.16	1.10	0.06	1.20

Table B. 3: Resin content determination of crude oil

Sl. No.	Wt. of oil sample (g)	Wt. of petri dish (g)	Wt. of petri dish with resin (g)	Wt. of resin (g)	Resin content = Wt. of resin / Wt. of oil sample (%)
1	5.00	44.06	44.92	0.86	17.20
2	5.00	44.06	44.86	0.80	16.60
3	5.00	44.06	44.89	0.83	16.39

Table B. 4: Wax content determination of crude oil

Sl. No.	Wt. of oil sample (g)	Wt. of dish (g)	Wt. of dish with wax (g)	Wt. of wax (g)	Resin content = Wt. of wax / Wt. of oil sample (%)
1	5.00	198.84	199.46	0.62	12.40
2	5.00	198.84	199.50	0.66	13.20
3	5.00	198.84	199.43	0.59	11.80

Appendix C: Determining Cl^- ion concentration of formation water by titration (Mohr's Method)

The Mohr's method was used to determine the chloride ion (Cl^-) concentration of formation water (FW) by titration with silver nitrate solution. When silver nitrate solution is added to FW, a white precipitate of silver chloride forms.

$$Ag^+(aq) + Cl^-(aq) \rightarrow AgCl(s) \qquad (C.1)$$

Potassium chromate indicator was added to visualize the endpoint, when all the chloride ions present in the FW sample were precipitated. This endpoint also demonstrates the presence of excess silver ions. The additional silver ions then react with the chromate ions of potassium chromate to form a reddish-brown precipitate of silver chromate. The formation of the precipitate indicates that all chloride ions of FW have been consumed and only extra silver ions have reacted with chromate ions.

$$2\ Ag^+(aq) + CrO_4^{2-}(aq) \rightarrow Ag_2CrO_4(s) \qquad (C.2)$$

The experimental procedure adopted was as follows: 1.25 ml of FW sample was taken in a conical flask to which 1.0 ml indicator solution (0.25 N) was added. The mixture was titrated with 0.1 N silver nitrate solution. The endpoint is identified as the first appearance of a red-brown color. Calculating chloride ion concentration as:

$$\text{Chloride ion concentration} = \frac{(A \times N \times 35.45) \times 1000}{V_{sample}} \qquad (C.3)$$

where A is volume of silver nitrate solution used (ml)

N the normality of silver nitrate solution

V_{sample} the volume of sample used (ml)

Table C. 1: Cl^- ion concentration in formation water

Sl. No.	V_{sample} (ml)	N (N)	A (ml)	Cl^- concentration (ppm)
1	25	0.1	5.1	723.18
2	25	0.1	5.05	716.09
3	25	0.1	5.15	730.27
		Average		723.18

A = volume of silver nitrate solution used (ml)

N = normality of silver nitrate solution

V_{sample} = volume of sample used (ml)

Appendix D: Determine Mg^{++} ion concentration of formation water by titration with EDTA

The titration method with EDTA (ethylenediaminetetraacetic acid) was used to find the total calcium and magnesium content of water sample. In this method, EDTA forms a complex with calcium and magnesium ions. The indicator used was a blue dye called Eriochrome Black T (ErioT). This dye too forms a complex with the calcium and magnesium ions which changes the color from blue to pink. In the titration process, the FW sample was reacted with excess of EDTA. The indicator was then added which changes the color of the solution to blue because the calcium and magnesium ions were present as complex of EDTA. Then a back titration was done with magnesium chloride solution. All the excess EDTA form a complex with magnesium ions when the end-point was reached. The remaining magnesium ions of the magnesium chloride solution then form complex with ErioT indicator which changes the color from blue to pink.

The main reaction:

$$Ca^{2+} + EDTA^{4-} \rightarrow [Ca\text{-}EDTA]^{2-} \quad (D.1)$$

Back titration:

$$EDTA^{4-} + Mg^{2+} \rightarrow [Mg\text{-}EDTA]^{2-} \quad (D.2)$$

$$ErioT + Mg^{2+} \rightarrow ErioT\text{-}Mg \quad (D.3)$$

The experimental procedure adopted was as follows: Mixing 100 ml of FW and 50 ml of 0.005 mol/L EDTA solution in a conical flask. To the mixture was added 10 ml of ammonia buffer. The buffer was prepared by dissolving 7.0 g of ammonium chloride in 57 ml ammonia solution and further diluting to 100 ml with distilled water in a volumetric flask. The pH should be 10.5. Next, 1 ml of ErioT indicator solution was added. The ErioT indicator solution was prepared by dissolving 0.2 g of ErioT indicator in 15 ml of ammonia

solution and 5 ml ethanol. The FW sample was titrated with 0.0025 mol/L $MgCl_2$ solution until pink color appears. The titrations were repeated until similar results were obtained.

Total number of moles of EDTA in the sample $= \frac{0.005}{1000} \times 50 = 0.00025$

Moles of $MgCl_2$ used in the back titration $= \frac{0.0025}{1000} \times 1 = 0.0000025$

Moles of $MgCl_2$ used in the back titration = Moles of excess EDTA

Moles of Ca^{++} and Mg^{++} in the sample

= Total moles of EDTA – Moles of excess EDTA

= 0.00025-0.0000025

= 0.0002475 moles/100 ml

= 0.002475 moles/L

$$= 0.002475 \frac{\text{mol}}{\text{L}} \times 40.078 \frac{\text{gm}}{\text{mol}} \times 1000 \frac{\text{mg}}{\text{gm}}$$

= 99 mg/L

= 99 ppm

[In a typical water sample, more calcium salts are present than magnesium salts so 40.078 gm was taken which is the molecular weight of calcium even though both Mg and Ca are present in the sample]

Concentration of Ca^{++} from flame photometer test was obtained at 82 ppm.

Therefore, the concentration of Mg^{++} = 99 – 82 = 17 ppm

Appendix E: Determination of alkalinity of formation water by titration with HCl.

The alkalinity of formation water may be due to the presence of OH-, CO_3^{2-} and HCO_3^- ions. The alkalinity can be determined separately by titration against standard acid solution, using phenolphthalein and methyl orange indicators. The reactions are as follows:

$$OH^- + H^+ \rightarrow H_2O \quad \text{(E.1)}$$

$$CO_3^{2-} + H^+ \rightarrow HCO_3^- \quad \text{(E.2)}$$

$$HCO_3^- + H^+ \rightarrow H_2O + CO_2 \quad \text{(E.3)}$$

The general procedure for the determination of alkalinity is as follows: For the estimation of CO_3^{2-}, and OH^- ions, 20 ml of FW is taken in a conical flask and 2 drops of phenolphthalein are added. If the contents of the conical flask turn pink, titration is done with standard 0.1 N HCl till the color is faint pink or just colorless. If no pink color appears, the same volume of FW sample is taken in another conical flask and 2 drops of methyl orange indicator are added. The color of the solution becomes yellow and then titration is done with 0.1 N HCl solution until the color changes to red. No pink color was obtained when phenolphthalein was added to the FW sample, indicating the alkalinity of FW was due to HCO_3^- only and the titration was done using methyl orange indicator. Table E.1 shows the results of the titration test.

Table E. 1: Analysis of formation water using methyl orange indicator

Sl. No.	Volume of Water Sample (mL)	Volume of HCl required (mL)	Mean volume of HCl (mL)
1	20	4.3	
2	20	4.3	4.27
3	20	4.2	

$$V_1 \times S_1 = V_2 \times S_2$$

where V_1 = volume of FW sample

S_1 = methyl orange alkalinity in water sample

V_2= volume of HCl

S_2= strength of HCl

$20 \times S_1 = 4.27 \times 0.1$

So, $S_1 = 0.02135$ N

Strength in terms of $CaCO_3$ equivalent = S_1 x Eq. wt. of $CaCO_3$

= 0.02135 x 50 g/L

= 1.0675 g/L

Methyl orange alkalinity = 1.0675 x 1000 mg/L

Or, HCO_3^{2-} alkalinity = 1068 mg/L or 1068 ppm

List of Publications

List of Publications

Journal Publications:

1. R. Phukan, S.B. Gogoi, and P. Tiwari, *Effects of CO2-foam stability, interfacial tension and surfactant adsorption on oil recovery by alkaline-surfactant-alternated-gas/CO2 flooding*. Colloids and Surfaces A: Physicochemical and Engineering Aspects, Elsevier, 2020;597:124799.
2. R. Phukan, S.B. Gogoi, and P. Tiwari, *Alkaline-surfactant-alternated-gas/CO_2 flooding: Effects of key parameters.* Journal of Petroleum Science and Engineering, Elsevier, 2019. **173**: p. 547-557.
3. R. Phukan, S.B. Gogoi, and P. Tiwari, *Enhanced oil recovery by alkaline-surfactant-alternated-gas/CO_2 flooding.* Journal of Petroleum Exploration and Production Technology, Springer, 2019. **9**: p. 247-260.

Publication in Refereed Conference:

1. R. Phukan, S.B. Gogoi, P. Tiwari, and R.S.Vadhan, *Optimization of immiscible alkaline-surfactant-alternated-gas/CO_2 flooding in an Upper Assam oilfield*, in *SPE Western Regional Meeting* 2019, Society of Petroleum Engineers: San Jose, California, USA. p. 23, SPE-196262-MS.

Manuscript communicated:

1. R. Phukan, S.B. Gogoi, and P. Tiwari, *Characterization of reservoir rock and fluids for CO_2 foam enhanced oil recovery application* (To be published as a book chapter of Jenny Stanford Publishing, Singapore) (in Press)

Conference Presentations (National/International):

1. R. Phukan, P. Tiwari, and S. B. Gogoi, *Characterization of reservoir rock and fluids for CO_2 foam enhanced oil recovery application*. Reflux 2019, Indian Institue of Technology, Guwahati, India.
2. R. Phukan, P. Tiwari, S. B. Gogoi, and A. Goswami, *Black liquor as a sacrificial adsorbate for EOR*. Oil & Gas Workshop 2019, Dibrugarh University, India.
3. R. Phukan, S.B. Gogoi, P. Tiwari, and R.S.Vadhan, *Optimization of immiscible alkaline-surfactant-alternated-gas/CO_2 flooding in an Upper Assam Oilfield*. SPE Western Regional Meeting 2019, Society of Petroleum Engineers: San Jose, California, USA.
4. R. Phukan, S. B. Gogoi, and P. Tiwari, *Enhanced oil recovery by combined chemical/gas flooding*. Research Conclave 2018, Indian Institue of Technology, Guwahati, India.
5. R. Phukan, S. B. Gogoi, and P. Tiwari, *Static and dynamic adsorption of surfactants by reservoir rocks*. Reflux 2017, Indian Institue of Technology, Guwahati, India.
6. R. Phukan, C. Dutta, S. B. Gogoi, and P. Tiwari, *A comparative study of adsorption of anionic, non-ionic and a natural surfactant by reservoir rocks of Upper Assam Basin*. International Conference on Advances in Petroleum, Chemical & Energy Challenges 2016, RGIPT, Amethi, India.
7. R. Phukan, S. B. Gogoi, P. Tiwari, and D. Das, *Screening of chemical formulations for alkali-surfactant-gas enhanced oil recovery process*. Chemcon 2016, Anna University and Indian Institue of Technology, Madras, India.
8. R. Phukan, P. Tiwari, and S. B. Gogoi, *Enhanced oil recovery by alkaline-surfactant-alternated-CO_2 flooding.* Chemcon 2015, Indian Institue of Technology, Guwahati, India.

References

References

[1] Outlook for Energy: A Perspective to 2040. A report by ExxonMobil; 2019.

[2] Mehta VS. Why is Today's Oil Market, a 'No Mans' Land? *Financial Express.* May 2017.

[3] Cunningham N. BP Sees Peak Oil Demand In 2030s. A report published on Oilprice.com; 2018.

[4] Alvarado V, Manrique E. Enhanced Oil Recovery: An Update Review. Energies 2010;3:1529-75.

[5] Khan MY, Samanta A, Ojha K, Mandal A. Design of Alkaline/Surfactant/Polymer (ASP) Slug and its use in Enhanced Oil Recovery. Petroleum Science and Technology, 2009;27:1926-42.

[6] Mandal A. Chemical Flood Enhanced Oil Recovery: A Review. International Journal of Oil, Gas and Coal Technology 2015;9(3):24.

[7] Kumar S, Mandal A. Studies on Interfacial Behavior ond Wettability Change Phenomena Byionic ond Nonionic Surfactants in Presence of Alkalis and Salt for Enhanced Oil Recovery. Applied Surface Science 2016;372:42-51.

[8] Cao M, Gu Y. Oil Recovery Mechanisms and Asphaltene Precipitation Phenomenon in Immiscible and Miscible CO_2 Flooding Processes. Fuel 2013;109:157-66.

[9] Andrianov A, Farajzadeh R, Nick MM, Talanana M, Zitha PLJ. Immiscible Foam for Enhancing Oil Recovery: Bulk and Porous Media Experiments. Industrial & Engineering Chemistry Research 2012;51:2214-26.

[10] Sheng JJ. A Comprehensive Review of Alkaline-Surfactant-Polymer (ASP) Flooding. *SPE Western Regional & AAPG Pacific Section Meeting 2013 Joint Technical Conference.* Monterey, California, USA: Society of Petroleum Engineers; 2013:20.

[11] R.K.Srivastava, S.S.Huang, M.Dong. Laboratory Investigation of Weyburn CO_2 Miscible Flooding. Journal of Canadian Petroleum Technology 2000;39(2):41-51.

[12] Gogoi SB. Carbon-dioxide for EOR in Upper Assam Basin. In: Hou MZ, Xie H, Were P, editors. Clean Energy Systems in the Subsurface: Production, Storage and Conversion. Springer; 2013, p. 13.

[13] Patel J, Borgohain S, Kumar M, Rangarajan V, Somasundaran P, Sen R. Recent Developments in Microbial Enhanced Oil Recovery. Renewable and Sustainable Energy Reviews 2015;52:1539-58.

[14] Lazar I, Petrisor IG, Yen TF. Microbial Enhanced Oil Recovery (MEOR). Petroleum Science and Technology 2007;25(11):1353-66.

[15] Pourafshary P, Moradpour N. Hybrid EOR Methods Utilizing Low-Salinity Water. IntechOpen; 2019.

[16] Azim RA, Sara Faiz SR, Elbagir A, Obaidi NA. Numerical Study of Low Salinity Water Flooding in Naturally Fractured Oil Reservoirs. Recent Insights in Petroleum Science and Engineering. IntechOpen; 2017.

[17] Olajire AA. Review of ASP EOR (Alkaline Surfactant Polymer Enhanced Oil Recovery) Technology in the Petroleum Industry: Prospects and Challenges. Energy 2014;77:20.

[18] Ahmed T. Reservoir Engineering Handbook. Elsevier; 2006.

[19] Mazzullo SJ, Rieke HH, Chilingarian GV. Carbonate Reservoir Characterization: A Geologic-Engineering Analysis. Elsevier; 1996.

[20] Green DW, Willhite GP. Enhanced Oil Recovery. Richardson, Texas: Society of Petroleum Engineers; 1998.

[21] Amili P, Yortsos YC. Darcian Dynamics: A New Approach to the Mobilization of a Trapped Phase in Porous Media. Transport in Porous Media 2006;64(1):25-49.

[22] Yongmao H, Zenggui W, Yueming JBC, Xiangjie L. Laboratory Investigation of CO_2 Flooding. SPE 2004;88883:6.

[23] Karmakar GP. Carbon Dioxide Sequestration During Enhanced Oil Recovery: Operational and Economical Aspects. Journal of Indian Geophysics Union 2016;1:5-12.

[24] Gogoi SB, Kakoty M. A Study of CO_2 Flooding on Wave Velocities in the Naharkatiya Oil Reservoir of Upper Assam Basin. Resource-Efficient Technologies 2017;3(1):101-12.

[25] Stocker TF, Qin D, Plattner GK, Tignor M, Allen SK, Boschung J, et al. Climate Change 2013: The Physical Science Basis. *Contribution of Working Group I to the Fifth Assessment Report of the Intergovernmental Panel on Climate Change*. 2018.

[26] Council NR, Studies DEL, Resources BES, Geodynamics CS, Engineering CGG, Resources CE, et al. Induced Seismicity Potential in Energy Technologies. National Academies Press; 2013.

[27] Gogoi SB. Carbon-dioxide for EOR in Upper Assam Basin. Berlin, Heidelberg: Springer Berlin Heidelberg; 2013:157-69.

[28] Verma MK. Fundamentals of Carbon Dioxide-Enhanced Oil Recovery (CO_2-EOR)—A Supporting Document of the Assessment Methodology for Hydrocarbon Recovery Using CO_2-EOR Associated with Carbon Sequestration U.S. Geological Survey; 2015:24.

[29] Satter A, Iqbal G, Buchwalter J. Practical Enhanced Reservoir Engineering: Assisted With Simulation Softwar. PennWell Corporation; 2007.

[30] Jarrell PM. Practical Aspects of CO_2 Flooding (SPE Monograph Series, Vol. 22). Society of Petroleum Engineers (U.S.); 2002.

[31] Fath AH, Pouranfard A-R. Evaluation of Miscible and Immiscible CO_2 Injection in One of the Iranian Oil Fields. Egyptian Journal of Petroleum 2014;23(3):255-70.

[32] Bagci AS. Immiscible CO_2 Flooding Through Horizontal Wells. Energy Sources, Part A 2007;29:85-95.

[33] Mangalsingh D, T.Jagai. A Laboratory Investigation of the Carbon Dioxide Immiscible Process. *Society of Petroleum Engineers.* SPE 36134. Port of Spain, Trinidad & Tobago: Society of Petroleum Engineers; 1996:11.

[34] Li S, Li B, Zhang Q, Li Z, Yang D. Effect of CO_2 on Heavy Oil Recovery and Physical Properties in Huff-n-Puff Processes Under Reservoir Conditions. Journal of Energy Resources Technology 2018;140:10.

[35] Song Z, Zhu W, Wang X, Guo S. 2-D Pore-Scale Experimental Investigations of Asphaltene Deposition and Heavy Oil Recovery by CO_2 Flooding. Energy & Fuels 2018;32:3194-201.

[36] Zhang N, Wei M, Bai B. Comprehensive Review of Worldwide CO_2 Immiscible Flooding. *SPE Improved Oil Recovery Conference* Oklahoma, USA: Society of Petroleum Engineers; 2018:14.

[37] Qin J, Han H, Liu X. Application and Enlightenment of Carbon Dioxide Flooding in the United States of America. Petroleum Exploration and Development 2015;42(2):232-40.

[38] Spivak A, Karaoguz D, Issever K, Nolen JS. Simulation of Immiscible CO_2 Injection in a Fractured Carbonate Reservoir, Bati Raman Field, Turkey. *SPE California Regional Meeting.* California: Society of Petroleum Engineers; 1989.

[39] Sahin S, Kalfa U, Celebioglu D. Bati Raman Field Immiscible CO_2 Application: Status Quo and Future Plans. *2007 SPE Latin American and Caribbean Petroleum*

Engineering Conference Buenos Aires, Argentina: Society of Petroleum Engineers; 2007.

[40] Godec ML. Global Technology Roadmap for CCS in Industry Sectoral Assessment CO_2 Enhanced Oil Recovery. USA: United Nations Industrial Development Organization 2011.

[41] Perera MSA, Gamage RP, Rathnaweera TD, Ranathunga AS, Koay A, Choi X. A Review of CO_2-Enhanced Oil Recovery with a Simulated Sensitivity Analysis. Energies 2016;9(481):22.

[42] Zhang, P.Luo, S H. Improved Heavy Oil Recovery by CO_2 Injection Augumented with Chemicals. *CPS/SPE International Oil & Gas Conference and Exhibition* Beijing, China: Society of Petroleum Engineers; 2010:21.

[43] Kumar B, Mani D. India's Energy Future and Carbon Management. *27th Oil Shale Symposium.* Colorado School of Mines; 2007:7.

[44] Viebahn P. Prospects of Carbon Capture and Storage Technologies (CCS) in Emerging Economies. Wuppertal Institute for Climate, Environment and Energy; 2012.

[45] Enick RM, Olsen DK. Mobility and Conformance Control for Carbon Dioxide Enhanced Oil Recovery (CO2-EOR) via Thickeners, Foams, and Gels – A Detailed Literature Review of 40 Years of Research. In: Ammer J, ed. DOE/NETL-2012/1540. National Energy Technology Laboratory; 2012:267.

[46] Ghedan S. Global Laboratory Experience of CO_2-EOR Flooding. *SPE/EAGE Reservoir Characterization and Simulation Conference held* Abu Dhabi, UAE: SPE; 2009.

[47] Srivastava RK, S.S.Huang. Aphaltene Deposition During CO_2 Flooding: A Laboratory Assessment. *SPE Production Operations Symposium* 37468. Oklahoma: SPE; 1997.

[48] Bon J, Sarma HK. A Technical Evaluation of a CO_2 Flood for EOR Benefits in the Cooper Basin, South Australia. *SPE Asia PacificOil and Gas Conference and Exhibition* 88451. Perth, Australia: SPE; 2004.

[49] Leontaritis KJ, Mansoori GA. Asphaltene Flocculation During Oil Production and Processing: A Thermodynamic Colloidal Model. *SPE international Symposium on Oilfield Chemistry.* 16258. Texas SPE; 1987.

[50] Bahadori A. Fundamentals of Enhanced Oil and Gas Recovery from Conventional and Unconventional Reservoirs. Gulf Professional Publishing; 2018.

[51] Elwy M, Zekri AY, Almehaideb RA, Al-Attar HH. Optimization of CO2 WAG Processes in Carbonate Reservoirs-An Experimental Approach. *Abu Dhabi International Petroleum Conference and Exhibition.* SPE-161782-MS. Abu Dhabi, UAE: Society of Petroleum Engineers; 2012:12.

[52] Christensen JR, Stenby EH, Skauge A. Review of WAG Field Experience. SPE Reservoir Evaluation & Engineering 2001;4(02):10.

[53] Rahimi V, Bidarigh M, Bahrami P. Experimental Study and Performance Investigation of Miscible Water-Alternating-CO_2 Flooding for Enhancing Oil Recovery in the Sarvak Formation. Oil & Gas Science and Technology 2017;72(35):12.

[54] Andrei M. Study Confirms Underground Injections of Carbon Dioxide Triggered a Series of Earthquakes in Texas. ZME Science; 2013.

[55] AlSumaiti AM, Hashmet MR, AlAmeri WS, Anto-Darkwah E. Laboratory Study of CO2 Foam Flooding in High Temperature, High Salinity Carbonate Reservoirs Using Co-injection Technique. Energy & Fuels 2018;32(2):1416-22.

[56] Dixit A, Tsau JS, Heller JP. Laboratory Study on Surfactant-Based Selective Mobility Control. *Permian Basin Oil and Gas Recovery Conference.* Midland, Texas: Society of Petroleum Engineers; 1994:9.

[57] Talebian SH, Masoudi R, M.Tan I, Zitha PLJ. Foam assisted CO2-EOR; Concepts, Challenges and Applications. *SPE Enhanced Oil Recovery Conference* SPE 165280. Kuala Lumpur, Malaysia: Society of Petroleum Engineers; 2013:14.

[58] Pu W, Wei P, Sun L, Wang S. Stability, CO2 sensitivity, oil tolerance and displacement efficiency of polymer enhanced foam. RSC Advances 2017;7(11):6251-8.

[59] Skauge A, Stensen JA. Review of WAG Field Experience. *Oil Recovery – 2003, 1st International Conference and Exhibition Modern Challenges in Oil Recovery.* Russia, Moscow; 2003:11.

[60] Kulkarni MM, Rao DN. Experimental Investigation of Miscible and Immiscible Water-Alternating-Gas (WAG) Process Performance. Journal of Petroleum Science and Engineering 2005;48:1-20.

[61] Majidaie S, Onur M, Tan IM. An Experimental and Numerical Study of Chemically Enhanced Water Alternating Gas Injection. Petroleum Science 2015;12:13.

[62] Kumar S, Mandal A. A Comprehensive Review on Chemically Enhanced Water Alternating Gas/CO_2 (CEWAG) Injection for Enhanced Oil Recovery. Journal of Petroleum Science and Engineering 2017;157:20.

[63] Memon MK, Elraies KA, Al-Mossawy MI. Impact of New Foam Surfactant Blend with Water Alternating Gas Injection on Residual Oil Recovery. Journal of Petroleum Exploration and Production Technology 2017;7(3):843-51.

[64] Kibodeaux KR, Rossen WR. Coreflood Study of Surfactant-Alternating-Gas Foam Processes: Implications for Field Design. *SPE Western Regional Meeting.* SPE-38318-MS. Long Beach, California: Society of Petroleum Engineers; 1997:11.

[65] Gandomkar A, Honarvar B, Kazemzadeh Y, Derikvand Z. An Experimental Study of Surfactant Alternating CO_2 Injection for Enhanced Oil Recovery of Carbonated Reservoir. Iranian Journal of Oil and Gas Science and Technology 2016;5(4):01-17.

[66] Salehi MM, Safarzadeh MA, Sahraei E, Nejad SAT. Comparison of Oil Removal in Surfactant Alternating Gas with Wateralternating Gas, Water Flooding and Gas Flooding in Secondary Oil Recovery Process. Journal of Petroleum Science and Engineering 2014;120:8.

[67] Yaghoobi H, Tsau JS, Grigg RB. Effect of Foam on CO_2 Breakthrough: Is This Favorable to Oil Recovery? *SPE Permian Basin Oil and Gas Recovery Conference.* Midland, Texas: Society of Petroleum Engineers; 1998:8.

[68] Aghdam KA, Moghaddas JS, Moradi B. An Investigation of the Effect of Using Foam in WAG Injection in an Iranian Oil Reservoir. Petroleum Science and Technology 2013;31(21):2228-36.

[69] Bernard GG, Jacobs WL. Effect of Foam on Trapped Gas Saturation and on Permeability of Porous Media to Water. Society of Petroleum Engineers Journal 1965;5(04):6.

[70] Gandomkar A, Kharrat R, Motealleh M, Khanamiri HH, Nematzadeh M, Ghazanfari MH. An Experimental Investigation of Foam for Gas Mobility Control in a Low-Temperature Fractured Carbonate Reservoir. Petroleum Science and Technology 2012;30(10):976–85.

[71] Telmadarreie A, Trivedi JJ. Static and Dynamic Performance of Wet Foam and Polymer-Enhanced Foam in the Presence of Heavy Oil. Colloids and Interfaces 2018;2(38):18.

[72] Leeftink TN, Latooij CA, Rossen WR. Injectivity Errors in Simulation of Foam EOR. Journal of Petroleum Science and Engineering 2015;126:26-34.

[73] Shi J-X, Rossen WR. Improved Surfactant-Alternating-Gas Foam Process to Control Gravity Override. *SPE/DOE Improved Oil Recovery Symposium.* Tulsa, Oklahoma: Society of Petroleum Engineers; 1988:8.

[74] Samanta A, A.Bera, K.Ojha, A.Mandal. Comparative Studies on Enhanced Oil Recovery by Alkali–Surfactant and Polymer Flooding. Journal of Petroleum Exploration & Production Technology 2012;2:8.

[75] ShamsiJazeyi H, Hirasaki GJ, Verduzco R. Sacrificial Agent for Reducing Adsorption of Anionic Surfactants. *SPE International Symposium on Oilfield Chemistry.* The Woodlands, Texas, USA: Society of Petroleum Engineers; 2013:16.

[76] M.Srivastava, Zhang J, Nguyen QP, Pope GA. A Systematic Study of Alkaline-Surfactant-Gas Injection as an EOR Technique. SPE 2009;124752:15.

[77] Guo H, Zitha PLJ, Faber R, Buijse. A Novel Alkaline/Surfactant/Foam Enhanced Oil Recovery Process. SPE Journal 2012;SPE 145043:10.

[78] Srivastava JP, D.S.Negi, K.Jain A, A.K.Dhawan. Surfactant-Alternate-Gas (SAG) Injection Process as a Novel EOR Technique-- A Laboratory Investigation. *2nd South Asain Geoscience Conference and Exhibition, GEOIndia2011.* New Delhi, India: Geo India; 2011:7.

[79] Cottin C, Morel D, Levitt D, Cordelier P, Pope G. Alkali Surfactant Gas Injection - Attractive Laboratory Results in Carbonates under Harsh Salinity and High Temperature. *Abu Dhabi International Petroleum Exhibition & Conference* SPE 161727. Abu Dhabi, UAE: Society of Petroleum Engineers; 2012:13.

[80] Lashgari HR, Sepehrnoori K, Delshad M. Modeling of Low-Tension Surfactant-Gas Flooding Process in a Four-Phase Flow Simulator. *SPE Annual Technical Conference and Exhibition.* SPE-175134-MS. Houston, Texas, USA: Society Of Petroleum Engineers; 2015:21.

[81] Nasab SMH, Zitha PLJ. Investigation of Certain Physical–Chemical Features of Oil Recovery by an Optimized Alkali–Surfactant–Foam (ASF) System. Colloid and Polymer Science 2017;295:1873-86.

[82] Afzali S, Rezaei N, Zendehboudi S. A Comprehensive Review on Enhanced Oil Recovery by Water Alternating Gas (WAG) Injection. Fuel 2018;227:218-46.

[83] Srivastava, Zhang J, Nguyen QP, Pope GA. A Systematic Study of Alkaline-Surfactant-Gas Injection as an EOR Technique. *SPE Annual Technical Conference and Exhibition.* SPE 124752. New Orleans, Louisiana, USA: Society of Petroleum Engineers; 2009:15.

[84] Jong S, Nguyen NM, Eberle CM, Long X. Nghiem, Nguyen QP. Low Tension Gas Flooding as a Novel EOR Method: An Experimental and Theoretical Investigation. *SPE Improved Oil Recovery Conference*. Tulsa, Oklahoma, USA: Society of Petroleum Engineers; 2016:25.

[85] Srivastava M. Foam Assisted Low Interfacial Tension Enhanced Oil Recovery. PhD. The University of Texas at Austin; 2010.

[86] Carcoana A. Applied Enhanced Oil Recovery. Prentice-Hall Inc, New Jersey; 1992.

[87] Liu S. Alkaline Surfactant Polymer Enhanced Oil Recovery Process. PhD. Rice University; 2007.

[88] Lyons WC. Chapter 5 - Enhanced Oil Recovery Methods. In: Lyons WC, editor Working Guide to Reservoir Engineering. Boston: Gulf Professional Publishing; 2010, p. 279-310.

[89] Castor TP, Somerton WH, Kelly JF. 1981. Surface Phenomena in Enhanced Oil Recovery. Springer, Boston, MA, p. 249-91.

[90] Sheng JJ. Status of Alkaline Flooding Technology. Journal of Petroleum Engineering & Technology 2015;5(1):44-50.

[91] Speight JG. Chapter 4 - Nonthermal Recovery of Heavy Oil. In: Speight JG, editor Heavy Oil Production Processes. Boston: Gulf Professional Publishing; 2013, p. 63-92.

[92] Ramirez-Corredores MM. Chapter 4 - Acidity in Crude Oils: Naphthenic Acids and Naphthenates. In: Ramirez-Corredores MM, editor The Science and Technology of Unconventional Oils. Amsterdam: Academic Press; 2017, p. 295-385.

[93] Sheng JJ. Investigation of Alkaline-Crude Oil Reaction. Petroleum 2015;1(1):31-9.

[94] Kumar S, Yen TF, Chilingarian GV, Donaldson EC. Chapter 9 Alkaline Flooding. In: Donaldson EC, Chilingarian GV, Yen TF, editors. Developments in Petroleum Science. Elsevier; 1989, p. 219-54.

[95] Leach RO, Wagner OR, Wood HW, Harpke CF. A Laboratory and Field Study of Wettability Adjustment in Water Flooding. Journal of Petroleum Technology 1962;14(02):206-12.

[96] Thomas NC, Ghosh B, AlAmeri WS, Kilybay A. Alkali and Hybrid-Alkali Flooding as a Tertiary Oil Recovery Mode: Prospects and Challenges. International Journal of Petroleum and Petrochemical Engineering 2016;2(2):22-31.

[97] Cheng KH. Chemical Consumption During Alkaline Flooding: A Comparative Evaluation. *SPE Enhanced Oil Recovery Symposium.* Tulsa, Oklahoma: Society of Petroleum Engineers; 1986:14.

[98] Burk JH. Comparison of Sodium Carbonate, Sodium Hydroxide, and Sodium Orthosilicate for EOR. SPE Reservoir Engineering 1987;2(01):9-16.

[99] deZabala EF, Vislocky JM, Rubin E, Radke CJ. A Chemical Theory for Linear Alkaline Flooding. Society of Petroleum Engineers Journal 1982;22(02):245-58.

[100] Sekhar G, Borgohain GS. Review on Microfluidic Studies for EOR Application. Journal of Petroleum Exploration and Production Technology 2019;9(3):2263-77.

[101] Abbas AH, Sulaiman WRW, Jaafar MZ, Gbadamosi AO, Ebrahimi SS, Elrufai A. Numerical Study for Continuous Surfactant Flooding Considering Adsorption in Heterogeneous Reservoir. Journal of King Saud University - Engineering Sciences 2018.

[102] Sheng JJ. Status of Surfactant EOR Technology. Petroleum 2015;1:97-105.

[103] Sandersen SB. Enhanced Oil Recovery with Surfactant Flooding. *Chemical and Biochemical Engineering.* PhD. Technical University of Denmark; 2012.

[104] Bera A, Mandal A. Microemulsions: A Novel Approach to Enhanced Oil Recovery: A Review. Journal of Petroleum Exploration and Production Technology 2015;5(3):255-68.

[105] Lake LW, Johns R, Rossen B, Pope G. Fundamentals of Enhanced Oil Recovery Society of Petroleum Engineers; 2014.

[106] Hirasaki GJ, Domselaar HRV, Nelson RC. Evaluation of the Salinity Gradient Concept in Surfactant Flooding. Society of Petroleum Engineers Journal 1983(June):486-500.

[107] Salehi M, Johnson SJ, Liang J-T. Mechanistic Study of Wettability Alteration Using Surfactants with Applications in Naturally Fractured Reservoirs. Langmuir 2008;24(24):14099-107.

[108] Kumar A, Mandal A. Synthesis and Physiochemical Characterization of Zwitterionic Surfactant for Application in Enhanced Oil Recovery. Journal of Molecular Liquids 2017;243:61-71.

[109] Schramm LL, Wassmuth F. Foams: Fundamentals and Applications in the Petroleum Industry. Americal Chemcial Society; 1994.

[110] Prud'homme R. Foams: Theory: Measurements: Applications. Routledge; 2017.

[111] Kovscek AR, Radke CJ. Fundamentals of Foam Transport in Porous Media. Bartlesville, OK: U.S. Department of Energy; 1993:78.

[112] Ransohoff TC, Radke CJ. Mechanisms of Foam Generation in Glass-Bead Packs. SPE Reservoir Engineering 1988;3(2):573-85.

[113] Sheng J. Enhanced Oil Recovery Field Case Studies. Gulf Professional Publishing; 2013.

[114] Osei-Bonsua K, Shokria N, Grassiab P. Foam stability in the presence and absence of hydrocarbons: From bubble- to bulk-scale. Colloids and Surfaces A: Physicochemical and Engineering Aspects 2015;481:13.

[115] Bond DC, Holbrook OC. Gas Drive Oil Recovery Process. In: Patents U, ed. US; 1956.

[116] Kamal M, Marsden SS. Displacement of a Miscellar Slug Foam in Unconsolidated Porous Media. *48th Annual Fall Meeting of the Society of Petroleum Engineers of AIME*. SPE 4584. Las Vegas: Society of Petroleum Engineers; 1973:7.

[117] Bernard GG, Holm LW, Harvey CP. Use of Surfactant to Reduce CO_2 Mobility in Oil Displacement. Society of Petroleum Engineers Journal 1980;August 1980.

[118] Julio SSD, Emanuel AS. Laboratory Study of Foaming Surfactant for CO_2 Mobility Control. SPE Reservoir Engineering 1989;4(2):136-42.

[119] Lawson JB, Reisberg J. Alternate Slug of Gas and Diute Surfactant for Mobility Control During Chemical Flooding. *First Joint SPE/DOE Symposium on Enhanced Oil Recovery* SPE 8839. Tulsa, Oklahoma: Society of Petroleum Engineers; 1980.

[120] Demin W, Jiecheng C, Qun L, Junzheng W, Wenxiang W, Yanqi Z. First Ultra-Low Interfacial Tension Foam Flood Field Test Is Successful. *2001 SPE Annual Technical Conference and Exhibition.* SPE 71491. New Orleans, Louisiana: Society of Petroleum Engineers; 2001.

[121] Srivastava JP, D.S.Negi, K.Jain A, Dr.A.K.Dhawan. Surfactant-Alternate-Gas (SAG) Injection Process as a Novel EOR Technique-- A Laboratory Investigation. *2nd South Asain Geoscience Conference and Exhibition,GEOIndia2011*. New Delhi, India; 2011:7.

[122] Pei HH, Zhang GC, Ge JJ. Laboratory Investigation of Enhanced Heavy Oil Recovery by Foam Flooding with Low Gas–Liquid Ratio. Petroleum Science and Technology 2011;29:12.

[123] Guo H, Zitha PLJ, Faber R, Buijse M. A Novel Alkaline/Surfactant/Foam Enhanced Oil Recovery Process. SPE Journal 2012;SPE 145043:10.

[124] Luo P, Zhang Y, Huang S. A Promising Chemical-Augmented WAG Process for Enhanced Heavy Oil Recovery. Fuel 2013;104:333-41.

[125] Zhang S, Jiang G-C, Wang L, Guo H-T, Tang X-g, Bai D-G. Foam Flooding with Ultra-Low Interfacial Tension to Enhance Heavy Oil Recovery. Journal of Dispersion Science and Technology 2014;35(3):403-10.

[126] C.Cottin, D.Morel, D.Levitt, P.Cordelier, G.Pope. Alkali Surfactant Gas Injection: Attractive Laboratory Results Under the Harsh Salinity and Temperature Conditions of Middle East Carbonates. *Abu Dhabi International Petroleum Exhibition & Conference*. SPE 161727. Abu Dhabi, UAE: Society of Petroleum Engineers; 2012:13.

[127] Guo H, Zitha PLJ, Faber R, Marten Buijse. A Novel Alkaline/Surfactant/Foam Enhanced Oil Recovery Process. SPE Journal 2012;17(04):10.

[128] Majidaie S, Onur M, Tan IM. An experimental and numerical study of chemically enhanced water alternating gas injection. Petroleum Science 2015(12):13.

[129] Antunes CdMMO, Kakitani C, Marcelino Neto MA, Morales REM, Sum AK. An Examination of the Prediction of Hydrate Formation Conditions in the Presence of Thermodynamic Inhibitors. Brazilian Journal of Chemical Engineering 2018;35:265-74.

[130] Oseghale CI, Ebhodaghe FO. Asphaltene Deposition and Remediation in Crude Oil Production: Solubility Technique. Journal of Engineering and Applied Sciences 2011;6(4):258-61.

[131] Taber JJ, Martin FD, Seright RS. EOR Screening Criteria Revisited-Part 1 : Introduction to Screening Criteria and Enhanced Recovery Field Projects. SPE Reservoir Engineering 1997(August):189-98.

[132] Taber JJ, Martin FD, Seright RS. EOR Screening Criteria Revisited-Part 2: Applications and Impact of Oil Prices. SPE Reservoir Engineering 1997(August):199-205.

[133] Adasani AA, Bai B. Analysis of EOR projects and updated screening criteria. Journal of Petroleum Science and Engineering 2011;79:10-24.

[134] Kamari A, Mohammadi AH. Screening of Enhanced Oil Recovery Methods. In: Ambrosio J, editor Handbook on Oil Production Research. Nova Science Publishers, Inc.; 2014, p. 285-95.

[135] Akanji L, Sandrea R. A Neuro-Fuzzy Approach to Screening Reservoir Candidates for EOR. Advances in Petroleum Exploration and Development 2016;12(1):1-14.

[136] Aladasani A. Updated EOR Screening Criteria and Modeling the Impacts of Water Salinity Changes on Oil Recovery. *Petroleum Engineering.* PhD. Missouri University of Science and Technology; 2012:260.

[137] Manrique E, Calderon G, Mayo L, Stirpe MT. Water-Alternating-Gas Flooding in Venezuela: Selection of Candidates Based on Screening Criteria of International Field Experiences. *European Petroleum Conference.* The Hague, Netherlands: Society of Petroleum Engineers; 1998:9.

[138] Sheng JJ. Status of Alkaline-Surfactant Flooding. Polymer Sciences 2015;1(16):7.

[139] Chang HL, Zhang ZQ, Wang QM, Xu ZS, Guo ZD, Sun HQ, et al. Advances in Polymer Flooding and Alkaline/Surfactant/Polymer Processes as Developed and Applied in the People's Republic of China. Journal of Petroleum Technology 2006;58(02):84-91.

[140] Shedid SA. Experimental Investigation of Alkaline/Surfactant/Polymer (ASP) Flooding in Low Permeability Heterogeneous Carbonate Reservoirs. *SPE North Africa Technical Conference and Exhibition.* Cairo, Egypt: Society of Petroleum Engineers; 2015:16.

[141] F.M. Orr J, Heller JP, Taber JJ. Carbon Dioxide Flooding for Enhanced Oil Recovery: Promise and Problems. *Annual !-leeting of the American Oil Chemists Society*. Toronto; 1982:28.

[142] Gogoi SB. Effluent as Surfactant for Enhanced Oil Recovery. Innovative Energy & Research 2014;3(1).

[143] Amyx JW, Daniel M.Bass J, Whiting RL. Petroleum Reservoir Engineering. Physical Properties. New York : McGraw-Hill Book Co.; 1960.

[144] Klinkenberg LJ. The Permeability Of Porous Media To Liquids And Gases *Eleventh Mid-Year Meeting.* Tulsa, OK; 1942.

[145] IP Standards For Petroleum And Its Products. Part I Methods for Analysis and Testing. The Institute of Petroleum; 1972.

[146] Bon J. Laboratory and Modelling Studies on the Effects of Injection Gas Composition on CO_2-Rich Flooding in Cooper Basin, South Australia. *Australian School of Petroleum Faculty of Engineering, Computer and Mathematical Sciences.* PhD. The University of Adelaide, Australia; 2009:227.

[147] Hubbard RL, Stanfield KE. Determination of Asphaltenes, Oils, and Resins in Asphalt. Analytical Chemistry 1948;20(5):460-5.

[148] Rehan M, Nizami A-S, Taylan O, Al-Sasi BO, Demirbas A. Determination of wax content in crude oil. Petroleum Science and Technology 2016;34(9):799-804.

[149] Belhaij A, Al-Mahdy O. Foamability and Foam Stability of Several Surfactants Solutions: The Role of Screening and Flooding. Petroleum & Environmental Biotechnology 2015;6(4):6.

[150] Bera A, Ojha K, Mandal A. Synergistic Effect of Mixed Surfactant Systems on Foam Behavior and Surface Tension. Journal of Surfactants and Detergents 2013;16:10.

[151] Farzaneh SA, Sohrabi M. Experimental Investigation of CO_2-Foam Stability Improvement by Alkaline in the Presence of Crude Oil. Chemical Engineering Research and Design 2015;94:15.

[152] Vonnegut B. Rotating Bubble Method for the Determination of Surface and Interfacial Tensions. Review of Scientific Instruments 1942;13(1):6-9.

[153] Ahmed S, Elraies KA. Microemulsion in Enhanced Oil Recovery. Science and Technology Behind Nanoemulsions. IntechOpen; 2018, p. 145-65.

[154] Bera A, Ojha K, Kumar T, Mandal A. Phase Behavior and Physicochemical Properties of (Sodium Dodecyl Sulfate + Brine + Propan-1-ol + Heptane) Microemulsions. Journal of Chemical and Engineering data 2012;57:7.

[155] Sarmah S, Gogoi SB, Xianfeng F, Baruah AA. Characterization and Identification of the Most Appropriate Nonionic Surfactant for Enhanced Oil Recovery. Journal of Petroleum Exploration and Production Technology 2019.

[156] Huh C. Interfacial Tensions and Solubilizing Ability of a Microemulsion Phase that Coexists With Oil and Brine. Journal of Colloid And Interface Science 1979;71(2):408-26.

[157] Bera A, Kumar T, Ojha K, Mandal A. Adsorption of Surfactants on Sand Surface in Enhanced Oil Recovery: Isotherms, Kinetics and Thermodynamic Studies. Applied Surface Science 2013;284:87-99.

[158] Arand M, Friedberg T, Oesch F. Colorimetric Quantitation of Trace Amounts of Sodium Lauryl Sulfate in the Presence of Nucleic Acids and Proteins. Analytical Biochemistry 1992;207(1):73-5.

[159] Gogoi SB. Adsorption–Desorption of Surfactant for Enhanced Oil Recovery. Transport in Porous Media 2011;90:589-604.

[160] Ahmadi MA, Shadizadeh SR. Experimental Investigation of a Natural Surfactant Adsorption on Shale-Sandstone Reservoir Rocks: Static and Dynamic Conditions. Fuel 2015;159:15-26.

[161] Kennedy M. Chapter 3 - Core and Other Real Rock Measurements. In: Kennedy M, editor Developments in Petroleum Science. Elsevier; 2015, p. 73-88.

[162] Talukdar P, Gogoi SB. A Study on the Role of Pre-Gelatinized Starch (PGS) in the Non Damaging Drilling Fluid (NDDF) for the Tipam Sand of Geleki Oilfield of Upper Assam Basin. International Journal of Applied Sciences and Biotechnology 2015;3(2):291-300.

[163] Nelson PH, Bird KJ. Porosity-Depth Trends and Regional Uplift Calculated from Sonic Logs, National Petroleum Reserve in Alaska. *Scientific Investigations Report 2005*. USA: U.S. Department of the Interior & U.S. Geological Survey; 2005.

[164] M.Ramm KB. Porosity/depth Trends in Reservoir Sandstones: Assessing the Quantative Effects of Varying Pore-pressure, Temerature History & Mineralogy, Norwegian Shelf Data. Clay Minerals 1994;29:16.

[165] Tiab D, Donaldson EC. Chapter 3 - Porosity and Permeability. In: Tiab D, Donaldson EC, editors. Petrophysics (Second Edition). Burlington: Gulf Professional Publishing; 2004, p. 87-202.

[166] Ma S, Morrow NR. Relationships Between Porosity and Permeability for Porous Rocks. *International Symposium of the Society of Core Analyst.* Montpelier, France; 1996:12.

[167] Nind TEW. Principles of Oil Well Production. McGraw-Hill; 1964.

[168] Al-Bazzaz WH, Gupta A. Reservoir Characterization and Data Integration of Complex Mauddud-Burgan Carbonate Reservoir. *SPE Europec/EAGE Annual Conference and Exhibition.* Vienna, Austria: Society of Petroleum Engineers; 2006:14.

[169] Kamal MS, Hussein IA, Sultan AS. Review on Surfactant Flooding: Phase Behavior, Retention, IFT, and Field Applications. Energy & Fuels 2017;31:7701-20.

[170] Welton JE. SEM Petrology Atlas. Oklahoma: The American Association of Petroleum Geologists; 2003.

[171] AH A, WR WS, M Z, A A. Anionic Surfactant Adsorption: Insight for Enhanced Oil Recovery. Recent Advances in Petrochemical Science 2017;1(5):4.

[172] Wilson L, Wilson MJ, Green J, Patey I. The Influence of Clay Mineralogy on Formation Damage in North Sea Reservoir Sandstones: A Review with Illustrative Examples. Earth-Science Reviews 2014;134:70-80.

[173] Julius P, Ananthanarayanan PN, Srinivasan V. Investigation of Enhanced Oil Recovery (EOR) Surfactants on Clay Mixed Sandstone Reservoirs for Adsorption. Indian Journal of Science and Technology 2015;8(14):4.

[174] Menon ES. Liquid Pipeline Hydraulics. USA: MArcel Dekker, Inc.; 2004.

[175] ASTM. Petroleum Measurements Tables. 2004.

[176] Jafarinejad S. Petroleum Waste Treatment and Pollution Control. Elsevier Science; 2016.

[177] Fozao KF, Gabsia B, Alferov F, Yossa MT. Mount Cameroon Oil Seeps and their Rheological Properties. International Journal Of Engineering Research And Development 2019;15(1):67-78.

[178] Manual on Hydrocarbon Analysis. American Society for Testing and Materials; 1963.

[179] Kandwal VC, Agrawal KM, Nautiyal SP, Khan HU. Paraffin Deposition and Viscosity Temperature Behaviour Of Assam Crude Oil. Petroleum Science and Technology 2007;18:15.

[180] Ramirez-Corredores MM. The Science and Technology of Unconventional Oils: Finding Refining Opportunities. Academic Press, 2017; 2017.

[181] Aske N, Kallevik H, Sjöblom J. Determination of Saturate, Aromatic, Resin, and Asphaltenic (SARA) Components in Crude Oils by Means of Infrared and Near-Infrared Spectroscopy. Energy & Fuels 2001;15(5):1304-12.

[182] Samanta A, Ojha K, Mandal A. Interactions between Acidic Crude Oil and Alkali and Their Effects on Enhanced Oil Recovery. Energy & Fuels 2011;25(4):1642-9.

[183] Renpu W. Chapter 1 - Basis of Well Completion Engineering. In: Renpu W, editor Advanced Well Completion Engineering (Third Edition). Gulf Professional Publishing; 2011, p. 1-74.

[184] Burcik EJ. Properties of Petroleum Reservoir Fluids. Wiley; 1957.

[185] Sheng JJ. Enhanced Oil Recovery Field Case Studies. Gulf Professional Publishing; 2013.

[186] Belhaij A, Al-Mahdy O. Foamability and Foam Stability of Several Surfactants Solutions: The Role of Screening and Flooding. Journal of Petroleum & Environmental Biotechnology 2015;6(4):6.

[187] L.Schramm L, J.Novosad J. The Destabilization of Foams for Improved Oil Recovery by Crude Oils: Effect of the Nature of the Oil. Journal of Petroleum Science and Engineering 1992;7:77-90.

[188] Mannhard K, Novosad JJ, Schramm LL. Foam/Oil Interations at Reservoir Conditions. *SPE/DOE Improved Oil Recovery Symposium.* Tulsa, Oklahoma: Society of Petroleum Engineers; 1998:14.

[189] Simjoo M, Rezaei T, Andrianov A, Zitha PLJ. Foam Stability in the Presence of Oil: Effect of Surfactant Concentration and Oil Type. Colloids and Surfaces A: Physicochemical and Engineering Aspects 2013;438:11.

[190] Farajzadeh R, Krastev R, Zitha PLJ. Foam films stabilized with alpha olefin sulfonate (AOS). Colloids and Surfaces A: Physicochemical and Engineering Aspects 2008;324(1):35-40.

[191] Asari M, Hormozi F. Effects of Surfactant on Bubble Size Distribution and Gas Hold-Up in a Bubble Column. American Journal of Chemical Engineering 2013;1(2):50-8.

[192] Xu X. A Novel CO_2 Flooding Based EOR for Sandstone Reservoirs. *Petroleum Engineering.* PhD. Curtin University; 2016:165.

[193] Pu W, Pang S, Wang C. Experimental Investigation of Foam Performance in the Presence of Crude Oil. Journal of Surfactants and Detergents 2017;20:9.

[194] Wang J, Cao Y, Li G, Deng L, Li S. Effect of CTAB Concentration on Foam Properties and Discussion Based on Liquid Content and Bubble Size in the Foam. International Journal of Oil, Gas and Coal Engineering 2018;6(1):18-24.

[195] Kalekar MS, Bhagwat SS. Dynamic Behavior of Surfactants in Solution. Journal of Dispersion Science and Technolog 2006;27:1027-34.

[196] Azdarpour A, Junin R, Manan M, Hamidi H, Rafati R. The Effects Of Controlling Parameters On Polymer Enhanced Foam (PEF) Stability. Jurnal Teknologi (Sciences & Engineering) 2015;73(1):53-9.

[197] Wang H, Guo W, Zheng C, Wang D, Zhan H. Effect of Temperature on Foaming Ability and Foam Stability of Typical Surfactants Used for Foaming Agent. Journal of Surfactants and Detergents 2017;20:8.

[198] Kamal MS. A Novel Approach to Stabilize Foam Using Fluorinated Surfactants. Energies 2019;12:12.

[199] Yin D, Zhao D, Gao J, Gai J. Experimental Study of Enhancing Oil Recovery with Weak Base Alkaline/Surfactant/Polymer. International Journal of Polymer Science 2017:7.

[200] Al-Sahhaf T, Elkamel A, Ahmed AS, A.R.Khan. The Influence of Temperature, Pressure, Salinity, and Surfactant Concentration on the Interfacial Tension of the N-Octane-Water System. Chemical Engineering Communications 2005;192:667-84.

[201] Salehi MM, Omidvar P, Naeim F. Salinity of Injection Water and its Impact on Oil Recovery Absolute Permeability, Residual Oil Saturation, Interfacial Tension and Capillary Pressure. Egyptian Journal of Petroleum 2017;26:301-12.

[202] Ruckenstein E, Rao IV. Interfacial Tension of Oil-Brine Systems in the Presence of Surfactant and Cosurfactant. Journal of Colloid and Interface Science 1987;Vol. 117(1):104-19.

[203] Phan TT, Attaphong C, Sabatini DA. Effect of Extended Surfactant Structure on Interfacial Tension and Microemulsion Formation with Triglycerides. Journal of American Oil Chemists Society 2011;88:1223-8.

[204] Healy RN, Reed RL. Immiscible Microemulsion Flooding. Society of Petroleum Engineers 1976:32.

[205] Lv W, Bazin B, Ma D, Liu Q, Han D, Wu K. Static and Dynamic Adsorption of Anionic and Amphoteric Surfactants with and without the Presence of Alkali. Journal of Petroleum Science and Engineering 2011;77:10.

[206] Seethepalli A, Adibhatla B, Mohanty KK. Wettability Alteration During Surfactant Flooding of Carbonate Reservoirs. *SPE/DOE Symposium on Improved Oil Recovery*. Tulsa, Oklahoma: Society of Petroleum Engineers; 2004:10.

[207] Krumrine PH, Falcone JS, Jr., Campbell TC. Surfactant Flooding 1: The Effect of Alkaline Additives on IFT, Surfactant Adsorption, and Recovery Efficiency. Society of Petroleum Engineers Journal 1982;22(04):503-13.

[208] Elraies KA, Ahmed S. A New Strategy for Minimizing Precipitations during ASP Flooding in Carbonate Reservoirs International Journal of Chemical and Molecular Engineering 2012;6(12):1186-8.

[209] Ghosh P. Study of Alternating Anionic Surfactant and Gas Injection in Carbonate Cores. MS. The University of Texas at Austin; 2016.

[210] Hong SA, Bae JH. Field Experiment of Lignosulfonate Preflushing for Surfactant Adsorption Reduction. SPE Reservoir Engineering 1990;November 1990:8.

[211] J.Novosad. Laboratory Evaluation of Lignosulfonates as Sacrificial Adsorbates in Surfactant Flooding. Journal of Canadian Petroleum Technology 1984:24-8.

[212] Syahputra AE, Tsau J-S, B.Grigg R. Laboratory Evaluation of Using Lignosulfonate and Surfactant Mixture in CO_2 Flooding. *2000 SPE/DOE Improved Oil Recovery Symposium* SPE 59368. Tulsa, Oklahoma: Society of Petroleum Engineers; 2000:9.

[213] Tsau J-S, Syahputra AE, Yaghoobi H, Grigg RB. Use of Sacrificial Agents in CO_2 Foam Flooding Application. *1999 SPE Annual Technical Conference and Exhibition* SPE 56609. Houston, Texas: Society of Petroleum Engineers; 1999.

[214] Kronberg B, Holmberg K, Lindman B. Surface Chemistry of Surfactants and Polymers. Wiley Online Library; 2014.

[215] Bagci AS. Immiscible CO2 Flooding through Horizontal Wells. Energy Sources 2007;29:85-95.

[216] Goos E, Riedel U, Zhao L, Blum L. Phase diagrams of CO_2 and CO_2 -N_2 gas mixtures and their application in compression processes. Energy Procedia 2011;4:3778-85.

[217] Bagheri SR. Experimental and Simulation Study of the Steam−Foam Process. Part 2: The Effect of Oil on Foam Generation. Energy & Fuels 2017;31:2687-96.

[218] Memon MK, Elraies KA, Al-Mossawy MI. Impact of new foam surfactant blend with water alternating gas injection on residual oil recovery. Journal of Petroleum Exploration and Production Technology 2017;7:9.

[219] Rao D. Gas Injection EOR- A New Meaning in the New Millennium. Journal of Canadian Petroleum Technology 2001;40(02):8.

[220] Hollebone B. Chapter 4 - Measurement of Oil Physical Properties. In: Fingas M, editor Oil Spill Science and Technology. Boston: Gulf Professional Publishing; 2011, p. 63-86.

[221] Kamal MS, Hussein IA, Sultan AS. Review on Surfactant Flooding: Phase Behavior, Retention, IFT, and Field Applications. Energy & Fuels 2017;31(8):7701-20.

[222] Mandal ABA. Microemulsions: a novel approach to enhanced oil recovery: a review. Petrol Explor Prod Technol 2015:14.

[223] Moayedi M, James LA, Mahmoodi M. An Experimental Study on Optimization of SAG Process Utilizing Nonionic Surfactants and Sodium Lignosulfonate. *International Symposium of the Society of Core Analysts.* Avignon, France; 2014:6.

[224] Kumar R, Dao EK, Mohanty KK. Emulsion Flooding of Heavy Oil. *SPE Improved Oil Recovery Symposium.* Tulsa, Oklahoma, USA: Society of Petroleum Engineers; 2010:13.

[225] Han L, Gu Y. Optimization of Miscible CO_2 Water-Alternating-Gas Injection in the Bakken Formation. Energy & Fuels 2014;28:6811-9.

[226] Anuar NABM, Yunan MH, Sagala F, Katende A. The Effect of WAG Ratio and Oil Density on Oil Recovery by Immiscible Water Alternating Gas Flooding. American Journal of Science and Technology 2017;4(5):80-90.

[227] Amin ME, Zekri AY, Almehaideb R, Al-Attar H. Optimization of CO_2 WAG Processes in a Selected Carbonate Reservoir: An Experimental Approach. International Journal of Engineering Research and Science & Technology 2013;2(2):16.

[228] Zekri AY, Nasr MS, AlShobakyh A. Evaluation of Oil Recovery by Water Alternating Gas (WAG) Injection - Oil-Wet & Water-Wet Systems. *SPE Enhanced Oil Recovery Conference.* Kuala Lumpur, Malaysia: Society of Petroleum Engineers; 2011:8.

[229] Chen B, Reynolds AC. Ensemble-Based Optimization of the WAG Injection Process. *SPE Reservoir Simulation Symposium.* Houston, Texas,: Society of Petroleum Engineers; 2015.

[230] Hussain AAA, Amin A, Vincent-Bonnieu S, Farajzadeh R, Andrianov A, Hamid PA, et al. Effect of Oil on Gravity Segregation in SAG Foam Flooding. *19th European Symposium on Improved Oil Recovery.* Stavanger, Norway: EAGE IOR NORWAY 2017; 2017:14.

[231] Li J, Gao Y, Jiang H, Liu Y, Dong H. Pore-Scale Imaging of the Oil Cluster Dynamic during Drainage and Imbibition Using In Situ X-Ray Microtomography. Geofluids 2018;2018:13.

[232] Hatchell DC. Gravity-Assisted Inniscible CO_2 for Enahnced Oil Recovery and Storage. *Department of Energy Resources Engineering.* Master of Science. Stanford University; 2017.

[233] Safarzadeh MA, Nejad SAT, Sahraei E. Experimental Investigation of the Effect of Calcium Lignosulfonate on Adsorption Phenomenon in Surfactant Alternative Gas Injection. Journal of Chemical and Petroleum Engineering 2011;45(2):141-51.

[234] Azzolina NA, Gorecki CD, Ayash SC, Peck WD, Melzer LS, Chatterjee LS. Statistical Analysis of CO_2 EOR Production and Injection Data to Examine Ongoing

and Ultimate CO_2 EOR Incidental Storage. *13th Annual Carbon Capture, Utilization & Storage Conference.* Pittsburgh, Pennsylvania; 2014.

[235] Khan MY, Kohata A, Patel H, Syed FI, Al Sowaidi AK. Water Alternating Gas WAG Optimization Using Tapered WAG Technique for a Giant Offshore Middle East Oil Field. *Abu Dhabi International Petroleum Exhibition & Conference.* Abu Dhabi, UAE: Society of Petroleum Engineers; 2016:12.

[236] J.P.Srivastava, Mahli L. Water-Alternating-Gas (WAG) Injection a Novel EOR Technique for Mature Light Oil Fields - A Laboratory Investigation for GS-5C sand of Gandhar Field. *9th Biennial International Conference and Exposition on Petroleum Geophysics.* Hyderabad, India; 2012.

[237] Srivastava JP, Mahli L. Water-Alternating-Gas (WAG) Injection a Novel EOR Technique for Mature Light Oil Fields - A Laboratory Investigation for GS-5C sand of Gandhar Field. *9th Biennial International COnference and Exposium on Petroleum Geophysics.* Hyderabad, India; 2012:7.

[238] Tovar FD. Experimental Investigation on the use of Water Soluble Polyacrylamides as Thickeners during CO_2 WAG EOR. MS. Texas A&M University; 2014.

[239] Tsau J-S, Heller JP. Evaluation of Surfactants for CO_2-Foam Mobility Control. *Permian Basin Oil and Gas Recovery Conference.* Midland, Texas: Society of Petroleum Engineers; 1992:9.

[240] Hanssen JE, Holt T, Surguchev LM. Foam Processes: An Assessment of Their Potential in North Sea Reservoirs Based on a Critical Evaluation of Current Field Experience. *SPE/DOE Improved Oil Recovery Symposium.* Tulsa, Oklahoma: Society of Petroleum Engineers; 1994:16.

[241] Ghoodjani E, H.Bolouri S. Prediction of Water-Flooding Performance in Core Scale: Comparison of Numerical Simulator, Neural Network and Correlation. Brazilian Journal of Petroleum and Gas 2011;5(4):209-16.

[242] Hosseini-Nasab SM, Padalkar C, Battistutta E, Zitha PLJ. Mechanistic Modeling of the Alkaline/Surfactant/Polymer Flooding Process under Sub-optimum Salinity Conditions for Enhanced Oil Recovery. Industrial & Engineering Chemistry Research 2016(22):6875-88.

[243] Spildo K, Sun L, Djurhuus K, Skauge A. A Strategy for Low Cost, Effective Surfactant Injection. Journal of Petroleum Science and Engineering 2014;117:8-14.

[244] Glover CJ, Puerto MC, Maerker JM, Sandvik EL. Surfactant Phase Behavior and Retention in Porous Media. Society of Petroleum Engineers Journal 1979;19(03):11.

[245] Hong SA, Bae JH, Lewis GR. An Evaluation of Lignosulfonate as a Sacrificial Adsorbate in Surfactant Flooding. SPE Reservoir Engineering 1987;February 1987:11.

[246] Syahputra AE. Experimental Evaluation of Lignosulfonate as a Sacrificial Agent in CO_2-Foam Flooding. *Department of Petroleum Engineering*. MS. Socorro, New Mexico: New Mexico Institute of Mining and Technology; 1999:122.

[247] Tsau J-S, Syahputra AE, Grigg RB. Economic Evaluation of Surfactant Adsorption in CO_2 Foam Application. *SPE/DOE Improved Oil Recovery Symposium.* SPE 59365. Tulsa, Oklahoma: Society of Petroleum Engineers; 2000:9.